2018

SELF-SENSING CONCRETE FOR STRUCTURAL HEALTH MONITORING OF SMART INFRASTRUCTURES

Kay Christian Ackermann
University of Rhode Island, kay_ackermann@my.uri.edu

SELF-SENSING CONCRETE FOR STRUCTURAL HEALTH MONITORING OF SMART INFRASTRUCTURES

BY

KAY CHRISTIAN ACKERMANN

A THESIS SUBMITTED IN PARTIAL FULFILLMENT OF THE REQUIREMENTS FOR THE DEGREE OF MASTER OF SCIENCE

IN

CIVIL ENGINEERING

UNIVERSITY OF RHODE ISLAND

2018

MASTER OF SCIENCE THESIS

OF

KAY CHRISTIAN ACKERMANN

APPROVED:

Thesis Committee:

Major Professor Sumanta Das

George Tsiatas

Arun Shukla

Nasser H. Zawia
DEAN OF THE GRADUATE SCHOOL

UNIVERSITY OF RHODE ISLAND
2018

ABSTRACT

The self-sensing ability of cementitious materials with conductive particles for Structural Health Monitoring (SHM) gained a lot of interest in the last few decades. Based on previous literature it is known, that various materials and sensors have been developed, but still are not commonly used in practice, since the materials used for the conductive phase can be extremely costly and difficult to disperse within the cementitious matrix, which especially accounts for nanoscale materials such as carbon nanotubes (CNTs). Recently, a new approach of creating a conductive and self-sensing concrete containing latex-CNTs thin film-coated aggregates has been developed and investigated with experimental methods. This method enables a less costly and less complex dispersion of the CNTs by spray-painting the coating on coarse and fine aggregates.

The objective of this thesis was to develop a numerical method to predict the piezoresistive behavior of the developed cementitious composite. Nowadays, to avoid costly and time-consuming experiments, numerical simulations are an important tool to address such problems. Within a first step, significant parameter for creating a representative microstructure and numerical finite element model had to be identified. The electro-mechanical simulations were conducted for cementitious composites in the mortar-scale by applying a tensile strain to the microstructure. After generation a random microstructure and performing preliminary simulations for a coupled mechanical-electrical physics it was realized, that interfacial debonding must be applied to achieve a fractural change in resistivity (FCR), which is an indicator for the strain-sensing ability of a cement-based composite. Afterwards, the numerical simulation was

validated with experimental data, which showed an extremely high correlation of the FCR of both studies.

Finally, a parameter study was performed, where the effect of variation of the volume fraction of the conductive coated aggregates, the coating thickness and electrical conductivity on the FCR was investigated. First results showed, that the electrical resistivity of the composite was significantly reduced compared to the plane mortar. The result provided by the parameter study showed, that the change of volume fraction of aggregates and coating thickness has the largest impact on the FCR and sensing ability of the composite. The change of the initial electrical conductivity of the coating does not lead to a considerable FCR. This was traced back to the large difference in conductivity between cement matrix and coating and the high volume fraction of conductive material, which is well above the percolation threshold of nanoscale conductive materials.

ACKNOWLEDGMENTS

I would like to express my utmost gratitude and regards to my supervisor Professor Sumanta Das, who guided, supported and motivated me during the time of my research and I'm thankful, that he gave me the opportunity to work in his research group. Besides my research for this thesis, he was also a supporting mentor and helped me with tough decisions for my academic career at the University of Rhode Island.

Special thanks to Dr.-Ing. Kaja Boxheimer and Prof. Dr.-Ing. Jens Schneider from the Technical University of Darmstadt, who gave me the opportunity to take part in the international exchange program with URI and supported me during my time in Germany and abroad to achieve the degree Master of Science at both universities.

I also express my gratitude to my officemate Sumeru, who supported and helped me with his knowledge during the simulation processes.

Finally, I wish to express my warm and sincere thanks to my beloved family and friends in Germany and USA who supported me mentally with their love and enabled me to complete this work.

TABLE OF CONTENTS

LIST OF TABLES

LIST OF FIGURES

1. INTRODUCTION INTO STRUCTURAL-HEALTH-MONITORING

In the age of technology, the interest in monitoring and evaluate the state of structures in civil infrastructure is raising. Additionally, due to the increasing amount of traffic on highways it is very important to know the state of the structures such as bridges. Many bridges, which were built in the late 20th century, were not constructed for the initial demand or are in need of repair, because of aging processes in consequence of internal and external impacts. This could cause issues such as reduced capacity of a bridge or even road closures. Already, in the state of Rhode Island 22 % of all 1,162 bridges are structurally deficient. Accordingly, in the field of Civil Engineering research in Structural Health Monitoring (SHM) is getting constantly more ("State of Rhode Island: Rhode Island Department of Transportation").

SHM describes the technology to continuously monitor the state of a structure to prevent failure by detecting the development of flaws (Kuang, Quek, Koh, Cantwell, & Scully, 2009). One of the most promising approaches is an early damage detection system, which can be applied to the load bearing structure. The biggest advantage is, that the assessment of a detected flaw can be performed early, and the damage can be remedied, if it is necessary. A further intention of this procedure is to prevent the growth of damage before it affects larger areas. If the affected area is small, the reconstruction can be accomplished much faster and cheaper. So, with this method not just the safety factor will be covered, but also the economical point of view (Azhari, 2008).

Civil engineering infrastructure is one of the most expensive investments in any country. These structures have long service life compared with other commercial products. To maintain structures like bridges or high-rise buildings it takes a lot of time

and a vast amount of financial resources. Nowadays, the state of a structure is determined by either destructive or non-destructive methods. This thesis will focus on non-destructive methods. Non-destructive methods include on-site investigations by mounting external gauges or run complex and expensive measurements. A drawback of current methods is, that these tests just give an idea about the surface not the inner integrity of a structure. This problem addresses SHM, which aims to develop automated systems for continuously monitoring, inspection and damage detection of structures with minimum labour involvement (Sun, Staszewski, & Swamy, 2010). Another issue with on-site investigations is, that typically just a small area of a whole structure will be inspected with the possibility to miss a critical damage. The major goal of SHM is to observe the entire system of a structure or at least the most important elements like columns, girders, decks and other load bearing parts.

Especially the monitoring of concrete structures gains high interest, since concrete is the most extensively used construction material. Due to the fact, that concrete has an extremely high pressure-resistance it is widely used for bridge elements such as abutments or pillars. Whereas, it is unfavourable to use for tensile loaded elements, due to the low tensile strength (Al-Dahawi, Yıldırım, Öztürk, & Şahmaran, 2017). As a result of environmental and mechanical impacts such as changing temperatures, wind or traffic, structures tend to degrade with extended service-life. Specifically bridges for civil infrastructures suffer under increasing volume of traffic, which leads to a faster deterioration.

Due to the quasi-brittle structure of concrete, the extremely random and uncontrolled crack propagation and venerable to the effects of the environment, it is

quite important to apply SHM to concrete structures. Another drawback of structural elements made of concrete is the ability to collapse abruptly without notice. By using SHM systems, occurring damages can be detected and prevented from further propagating to assure safe conditions. So, investigations in SHM for concrete structures have an immense benefit for civil infrastructure.

Many methods to monitor structures by measuring mechanical properties such as stress, strain, displacement, vibration or chemical properties such as hydration of concrete, carbonatization and temperature have already been developed. Some methods are conventionally used by mounting sensors externally (strain gauges) or embedding internally of a structural element (plastic fiber-optic sensors). Unfortunately, most of these sensors have a short service life or degrade much faster due to the rough mechanical and chemical environment of concrete.

In the last few decades, scientists search for alternatives to create a more resistant sensing material for SHM systems of concrete structures. One of the biggest achievements are cement-based composite sensors. Cement-based composite means, that these sensors consist of cementitious materials as a host matrix which contains different additional phases, such as cement aggregates and conductive materials. The cementitious matrix is created by commonly used concrete materials such as Portland cement. Conductive materials can be conductive fibers or particles, that crate a conductive phase, to obtain a low resistivity. Without the conductive phase, the conduction of an electric potential would not be possible, due to the high electrical resistivity of the concrete. By adding small steel or carbon fibers, the resistivity of the concrete mixture significantly decreases, which obtains a self-sensing concrete. In this

thesis self-sensing composites for strain sensing and damage detection are of higher interest, which implies a further investigation of the piezoresistive effect of cement-based composites. This effect defines the change of resistivity of a composite element upon a deformation which can be converted into strain or stress (Azhari & Banthia, 2012). These sensors are mainly embedded into concrete structures, where they work as part of a load bearing element but additionally sense stress, strain or other effects. Chapter 3 will discuss the principles, properties, advantages and disadvantages of self-sensing piezoresitive cementitious materials and sensors.

To accurately monitor the structural integrity and safety, a SHM system includes three major components. SHM systems contain a sensory system, a data processing system and a health evaluation system. This thesis will principally deal with the sensory system for SHM. Many researchers are working in health evaluation, for example to determine criterions of how to evaluate deficiencies on the substance of a structure. Nevertheless, a well applied and excellent working SHM system can ensure a real time or on demand assessment of a structure. This will lead to an early detection of local anomalies and an adequate course of actions can be taken so that the optimum maintenance can be carried out (Azhari, 2008).

2. CONVENTIONAL SENSORS IN SHM

In the last few decades a various number of sensors for civil infrastructure purposes have been invented and are already conventionally in use. These sensors can be split in two groups. One group includes all sensors, which are mounted externally to a structural element to create a non-intrinsic self-sensing concrete for SHM. The other group includes integrated sensors, which are embedded into a load bearing part of a structure, to from an intrinsic self-sensing concrete. Compared to non-intrinsic concrete, intrinsic concrete is fabricated by adding conductive inclusions, such as steel or carbon particles, to the matrix, which gives the concrete the ability to function as a self-sensing composite without the need of other external sensors (Han, Wang et al., 2015). Intrinsic self-sensing concretes will be discussed in Chapter 4.

To achieve useful data for the determination of the health of a structure, multiple non-intrinsic sensors must be placed at different positions on or in a structural element. Moreover, it must be considered, that all types of sensors have different abilities to measure physical and chemical parameters, such as conventional strain gauges are only able to sense strain, whereas fiber-optic sensors are able to sense strain and moisture. Dependent on the purpose of conducting a measurement for SHM, the correct sensor must be selected and applied to the structure. But a much more important factor, which simultaneously is a major issue of all sensors, is the durability, reliability and the long-term stability in the sensing capability over the service life of a structure (Sun et al., 2010). Some of these aspects will be discussed for selected sensors for civil infrastructure, in the next few paragraphs.

2.1. EXTERNAL SENSORS

External sensors are usually mounted onto the surface of a structural element. They can be applied to a structure at any time for several purposes in SHM. Mostly they are used to measure the displacement, acceleration or strain. In the following paragraphs, electric resistance strain gauges and wireless sensors will be shortly discussed.

2.1.1. ELECTRICAL RESISTANCE STRAIN GAUGE

Electrical resistance strain gauges or also known as strain gauges are the most mature and widely used sensors in research. The functionality of strain gauges is very simple and reliable. The sensor is set under a continuous electrical current. With an applied force or deformation on the sensor the electrical resistance changes. By detecting these changes, it is possible to measure the strain of the specimen, where the sensor is embedded on. Strain gauges are mostly attached on a surface but can also embedded into concrete or installed on reinforcement bars of concrete structures. The testing parameter of strain gauges is only the strain (Han, Wang et al., 2015).

The reasons why strain gauges are widely used for strain measuring purposes are, that they are easy to install, having lower cost and excellent reproducibility of sensing property. They also show a very good correspondence between measured and estimated strains. But the sensitivity, also expressed by the gauge factor (see Chapter 3.1.4), is very low by ranging from 2 to 5. Additionally, strain gauges are easily affected by electromagnetic interference. Further disadvantages are the prone to drift and the high sensitivity to moisture and humidity, which making the sensors less durable and unsuitable for long-term monitoring. In case of large specimens, strain gauges will not cover all possible fracture positions, which could lead to and unforeseen sudden fracture

(Muto et al., 2001). Some of these aspects are insignificant for laboratory tests, but have an extremely high relevance for SHM, which makes strain gauges useless for long-time health monitoring purposes.

2.1.2. WIRELESS SENSOR NETWORKS

An SHM system contains a huge network of sensory devices measuring parameters such as strain and displacement, but also temperature, acceleration, humidity. This leads to an extensive amount of wires from the sensor to the data processing system (DPS). Furthermore, with an increasing distance between the sensor and the DPS, data become less reliable, due to electrical interferences and resistance of the wires.

To prevent a decrease of accuracy and reduce the amount of wires, researchers developed wireless smart sensors. These sensor nodes can measure three-axes acceleration for global response monitoring, strain for local response monitoring and temperature for SHM. Lately invented modules can communicate with the DPS at distances of up to 1 km.

Each node has an on-board microprocessor that can be used for digital signal processing, self-diagnosing, self-calibration and self-identification of anomalies in the collected data. The network of sensors can communicate with each other to estimate the bridge's physical state or detect failures even faster. For example, the monitoring system is able to measure the acceleration of a system at different points and extract the modal properties such as natural frequencies, mode shapes and modal damping ratios. This data can be used to the numerical model to determine the structural performance and find possible locations.

To use wireless sensor networks more commonly in SHM, some improvements have to be developed. Issues with the fidelity of data acquisition, reliable communication, power management and data management have to be solved to achieve a reliable assessment of the structure. Some researchers are working on next-generation wireless smart sensor platforms to improve the capability of these sensors (Spencer, Park, Mechitov, Jo, & Agha, 2017).

2.2. INTEGRATED SENSORS

The following sensors are usually incorporated into a concrete structure. In some cases, these sensors can also be mounted onto a surface of an existing element for subsequent examinations or monitoring. The following integrated sensors define also non-intrinsic self-sensing concrete for SHM. In the last few decades, a wide range of sensors and materials have been invented, that mostly do not fulfill just one purpose. They are able to determine a number of commonly monitored parameters. Some of these parameters are strain, stress, displacement, temperature, moisture, corrosion and presence of cracks and damage inside of a structural element. Some of the developed integrated sensors or materials are Fiber Optical Sensors (FOSs), Piezoelectric materials, Shape Memory Alloy (SMAs) and Self-Diagnosing Polymer Composites (Han, Wang et al., 2015). Due to a wide area of application, FOSs and Piezoelectric Materials will be further discussed in the next few paragraphs.

2.2.1. FIBER OPTIC SENSORS

Fiber Optic Sensors (FOSs) are multi-functional as they are sensitive for measuring strain, displacement, moisture-content, corrosion, temperature and detect cracks in the concrete microstructure. It was proven, that installed FOSs into a prestressed concrete

girder, the relaxation behavior of the prestressing tendons from the combined effects of distressing, concrete creep and shrinkage was able to evaluate (Sun et al., 2010). The sensing is possible through measuring changes in light intensity, phase-angle, polarization, wavelength or transit time of light inside the fiber (Han, Wang et al., 2015). In general, there are two methods of classifying FOS. The first method is based on the light characteristics modulated by the parameters to be sensed. The second method groups the so-called intensity-based FOS in two further classes. Here, a sensor can be intrinsic or non-intrinsic. Intrinsic sensors get a direct result of the physical change in the optical fiber in response to some measurands. So, the light in the sensing segment is modified inside the fiber. In non-intrinsic FOS, the signal modulation takes place outside of the optical fiber, which is less reliable for SHM systems. Another factor for the reliability and durability is the choice of the fiber material. Some of the most common materials are polymethylmethacrylate (PMMA), polycarbonate (PA) or polystyrene (PS). These materials are cheaper and have a better fracture resistance and flexibility compared to glass fibers. In the harsh engineering environment, plastic optical fibers are more appropriate to rough handling. Furthermore, standard glass fibers react corrosive in appearance of concrete, due to the interaction with the extremely alkaline environment. Moisture can also weaken the glass core and accelerates crack growth in the fiber (Kuang et al., 2009).

Researchers embedded FOSs into concrete structures, which made it possible to measure the strain accurately in different locations along a structure and provide information about debonding or microcrack failure. The embedded FOS were more sensitive to the surface crack of concrete and physical condition change and had a much

better signal-to-noise ratio than commonly used strain gauges. Moreover, the higher sensitivity and better signal-to-noise ratio is required for a better analyzation of the response of dynamic loading. Also, the fast completion of one measurement with FOS, by measuring a strain distribution in seconds, makes it applicable for dynamic signal measurements (Sun et al., 2010).

FOS have a lot of advantages compared to strain gauges or other external sensors or materials. They are insensitive to electromagnetic radiation, nonconductive, lightweight and suitable for embedding into structures. Furthermore, the sensors can work in the harsh environment and have a large sensing scope. In general, FOS are more promising for SHM of civil engineering structures than other smart sensors, that are conventionally in use. But as of now, the sensors are not fully elaborated. The long-term sensing ability due to aging has to be further investigated and a damage on a fiber is still difficult to repair when embedded. Another weakness of the sensors is the connection part between the optical fiber and the outer data recording system, which could lead to false alarm or malfunctions in the data processing (Han, Wang et al., 2015).

2.2.2. PIEZOELECTRIC EFFECT AND SENSORS

Piezoelectric sensors are based on an active sensing method, whereby the sensing ability is resulting from the piezoelectric effect. The piezoelectric effect requires a stored energy inside of a solid object, which creates an internal polarization. Consequently, two specific phenomena can be deduced. The first phenomenon is known as the direct effect, which implies a generated surface charge, due to a change in the internal polarization, in response to an implied mechanical strain or stress. The second phenomenon appears conversely, whereas with an applied electric field a mechanical

strain is produced (Han, Wang et al., 2015). To conclude, piezoelectric materials can be actuators and sensors and can be classified further into three categories, piezoelectric ceramics (PZT), piezoelectric polymers and piezoelectric composites. For civil infrastructure, PZT as the sensor material is most commonly used, because these sensors are easy to embed into concrete structures.

With PZT sensors it is possible to detect strain/stress, temperature, cracks and damages and local debonding between concrete and reinforcement bars. Strain sensing is straight forward. By applying an external force or displacement, the sensor will be deformed. This will cause a change in the electrical impedance response, which can be measured. The change of the electrical impedance can be converted into the present strain. A crack or damage in the concrete structure causes a change of the mechanical dynamic response, which also affects the electrical impedance response.

Piezoelectric materials are extremely sensitive in detecting strain and damage. But since various types of damage such as cracks, corrosion or delamination affect the mechanical impedance similarly, the distinction between each type of damage is very difficult. Further techniques are necessary to determine the exact nature of a damage (Sun et al., 2010). Moreover, piezoelectric materials are more likely for time-varying sensing applications. So, they can only produce electrical response to dynamic mechanics. Due to the disturbing effect of small DC leakage currents, these materials cannot be used for quasi-static measurements, which makes piezoelectric sensors uninteresting for many SHM applications. Further disadvantages are an unfavorable compatibility and a poor durability with the concrete structure (Han, Wang et al., 2015).

3. INTRODUCTION INTO SELF-SENSING MATERIALS

This chapter deals with self-sensing piezoresitive materials like smart composites and self-sensing concrete. First of all, some important terms, regarding to self-sensing materials, will be explained. To get an idea of, how smart composites perform their sensing abilities, the most common materials will be discussed. To conclude this chapter, a short abstract of the state of art for cement-based piezoresistive composites and sensors will be given.

3.1. TERMINOLOGY FOR SMART COMPOSITES

To understand how smart composites like self-sensing concrete work, it is important to be clear about the terminology. In the next few paragraphs, the most important terms in smart composite technology will be discussed.

3.1.1. OHM'S LAW

Ohm's law describes the relationship between the flow of electrical current through a material, its voltage and the materials resistance. Ohm's law can be described with Equation (1). For strain-sensing composites, the resistance of a material is one of the most important values and outlines a major role in conductive cement composites. The resistance states as a constant of proportionality, which describes how strong a material influences the flow of electrical current, when it crosses the material. Also, it does not change over various ranges of voltage. At a constant temperature, the amount of a steady current is directly proportional to the potential difference or voltage. A low resistance characterizes a material, where the current can more easily pass the conductor than with a material of high resistance. Furthermore, the resistance depends on the shape and length of the conductor.

$$R = \frac{V}{I} \tag{1}$$

Where R is the electrical resistance in ohms (Ω), V the voltage measured in volts (V) and I the current in amperes (A). By applying a direct current (DC) onto a material, resistance is the only opposing parameter of concern. To describe the flow in an electrical circuit with an alternating current (AC), Ohm's law has to be modified, since the opposition of the electrical flow is now defined as impedance (Z). The impedance also defines the relationship between voltage and current in an AC circuit, but contains resistance and reactance (X), which is generally described by using a complex notation (Equation (2)).

$$Z = \frac{V}{I} = R + iX \tag{2}$$

The real part of the complex impedance is defined as the resistance and the imaginary part of impedance is known as reactance. In an AC circuit the ohmic resistance is described by Equation (3) and ohmic reactance by Equation (4), whereas θ implies the phase angle between the alternating current and voltage.

$$R = |Z| \cdot cos\theta \tag{3}$$

$$X = |Z| \cdot sin\theta \tag{4}$$

Reactance can be further characterized into inductive (X_L) and capacitive (X_C) reactance. If the reactance is positive ($X > 0$) it is more inductive, whereas a negative reactance ($X < 0$) defines a more capacitive reactance. In the case of a reactance equal to zero ($X = 0$), no reactance is present, and the impedance is equal to the resistance, which occurs when the phase angle is zero.

To evaluate the sensing ability in a conductive material, alternating current flows between two electrodes through the conductor. By using an Electrical Impedance

Spectrometer (EIS) the resistivity of a conductor can be measured which can be converted to electrical conductivity and resistivity.

3.1.2. ELECTRICAL RESISTIVITY AND CONDUCTIVITY

As in Chapter 3.1.1 already mentioned, resistance does not just depend on the material and its electrical properties. It is also influenced by the shape and length of a conductor or specimen. To achieve comparability of the electrical resistance between different materials independent on their geometry, this coherence is represented by the electrical resistivity ρ (Ωm). Electrical resistivity is used as an indicator to unify the electrical performance of a material, such as cement-based composite, to make it more comparable with other materials, based on their ability to conduct electricity. Equivalent to resistance, a low resistivity indicates a material, that allows a higher flow of electric current through a conductor compared to a material with a high resistivity. The resistivity can be calculated with Equation (5) as resistance per unit length (Lee, You, Zi, & Yoo, 2017).

$$\rho = R \cdot \frac{A}{l} \tag{5}$$

Where A (m²) is the cross-section area and l (m) the length of a conductor or l as the distance between two voltage electrodes. In conclusion, resistivity is an intrinsic property of resistance. The electrical conductivity σ (S/m) or specific conductance is basically the reciprocal of electrical resistivity and measures the ability of a material to conduct an electric current. In relation to resistivity, the conductivity can be described by Equation (6).

$$\sigma = R \cdot \frac{l}{A} = \frac{1}{\rho} \tag{6}$$

Equations (5) and (6) are valid for resistors and conductors with a uniform cross-section, where a uniform electric current exists. A more general approach for the definition of electrical resistivity and conductivity is to take account of the ration between an electric field and the density of the current, that it creates (Equation (7)) (Yang, Chowdhury, & Neithalath, 2018).

$$\rho = \frac{E}{J} \tag{7}$$

Where E (V/m) is the electric field and J (A/m²) the current density of a conductor with an applied electric current. This case applies for any non-uniform cross-section and inhomogeneous materials such as cement composites.

3.1.3. PIEZORESISTIVITY

The electrical phenomenon of piezoresistivity can be described as the change of electrical resistivity with an applied deformation. This effect is being used to measure the strain in cementitious self-sensing composites. The principal method is to measure the change of electrical resistance in a conductor or specimen and determine the strain in the material, which means that the specimen has the ability to work as a self-sensing strain-sensor (Chung, 2016). For cement-based self-sensing materials, this effect will be further discussed in Chapter 3.2. Compared to the aforementioned piezoelectricity, in piezoresistive materials no stored energy is present due to polarization, which means the piezoresistive effect can only be used for passive sensing of strain (Azhari, 2008).

In general, piezoresistivity is affected by many aspects. The highest influence on piezoresistivity has the type and the amount of the conductive material. It gives a non-conductive or low-conductive material the property to conduct electrical current and

lastly sense strain. Dependent on the materials resistance, the resistance of the host material or matrix will be significantly reduced.

Regarding cement-based piezoresistive sensors further aspects are the effect of curing, effect of temperature, effect of moisture content, effect of microstructure and pore-structure and the type of current (DC or AC), that is applied to a specimen (Chapter 3.1.5). Some of these aspects will be further discussed in detail in Chapter 3.2.

3.1.4. FRACTIONAL CHANGE IN RESISTIVITY

Compared to a commonly used strain gauges, piezoresistive sensors do not display the actual strain. As in the previous chapter described, the change in resistance is measured to describe the behavior of strain. The strain value in a piezoresistive sensor is represented by calculating the fractional change in resistivity (FCR). The FCR is defined as the ratio between the change in electrical resistivity and the initial electrical resistivity (Equation (8)).

$$FCR = \frac{\rho_I - \rho_0}{\rho_0} = \frac{\Delta\rho}{\rho_0} = \frac{\Delta R}{R} \tag{8}$$

Where $\Delta\rho$ is the change in resistivity, ρ_I the resistivity after applying a stress/strain and ρ_0 the initial resistivity. Accordingly, the FCR is used as an indicator of strain-sensing since its response is proportional and reversible to the actual strain measured with a strain sensor (Lee et al., 2017).

If a longitudinal compressive stress is applied, the electrical resistance is reduced. Upon tension, the effect acts conversely, which means an increase on the resistance will be measured. Additionally, these effects are reversible in the elastic range of the material or sensor. A damage can be detected, when the material reaches its plastic range, which

can be noticed as an irreversible change on the electrical resistivity (Baeza, Galao, Zornoza, & Garcés, 2013).

To achieve good results from a piezoresistive measuring, which is as accurate as a measuring with a commonly used strain gauge, the sensitivity of the piezoresistive material must be considerably higher than the plain material. To evaluate the sensitivity of a strain sensor, the gauge factor (GF) has to be calculated. Accordingly, the GF is one of the most important parameters in self-sensing materials and is defined as the fractional change of electrical resistivity per unit strain (Lee et al., 2017). The GF can be calculated in accordance with Equation (9).

$$GF = \frac{FCR}{\varepsilon} = \frac{\Delta\rho/\rho_0}{\varepsilon} \tag{9}$$

Where $\Delta\rho$ is the change of resistivity, ρ_0 the initial resistivity and ε the measured longitudinal strain. A low GF describes a strain sensor with a low sensitivity, which means the sensor does not give a good response of strain to an applied load. The higher the sensitivity of a sensor, the more accurate is the representation of the actual strain in a sensor. Theoretically, the GF is fixed for a sensor of a specific material and size. In many cases dealing with cement-based composites, the GF varies upon tension and compression. It was realized, that the GF upon compression is lower than under tension. For mortar the GF for compression is about 10 times smaller than for tension. This is due to small cracks in the microstructure of the composite that appear much earlier under tension, at about 0.2 ‰ of strain, than under compression, at about 2 ‰ of strain.

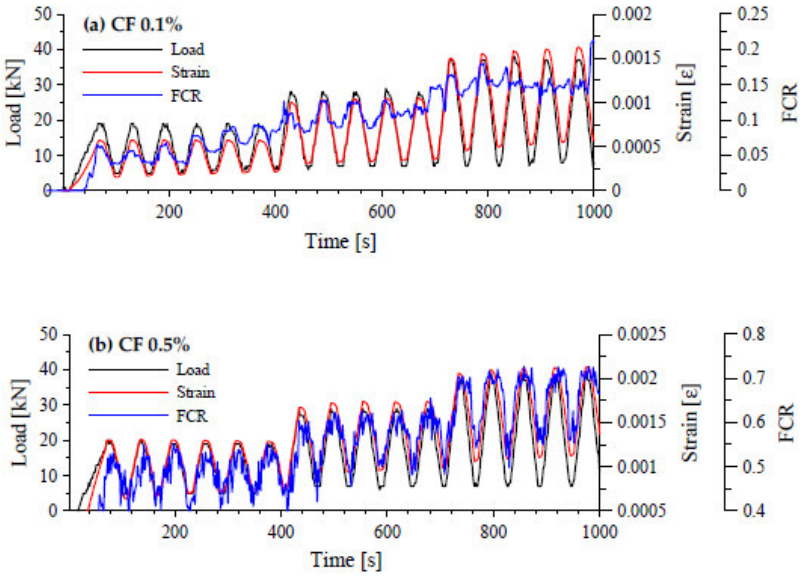

Figure 1 Response of cement-based composites under cyclic compression

This phenomenon should be illustrated by Figure 1 (Lee et al., 2017), which shows that a cement-based composite with a higher volume fraction of conductive particles (CF) has a better sensitivity to an applied load. With 0.1 vol.% CFs the response of the FCR is rather linear and does not represent the actual strain, which is critical, because strain peaks are not recognized. The specimen with 0.5 vol.% CF shows a much better accordance to the applied load and the actual strain. Concludingly, the GF of the sensor with 0.1 vol.% CF would be much lower than the one with 0.5 vol.% CF. For SHM purposes, it is desirable to implement sensors with a high sensitivity for a better and more accurate real-time monitoring of a structure.

3.1.5. POLARIZATION IN AC AND DC CIRCUITS

Since this work specifically deals with cement-based composites containing conductive particles, the influence of DC and AC electrical circuit on a cement-based sensor will be discussed in more detail. To identify the resistivity of a resistor or sensor, the resistance has to be measured. As aforementioned in Chapter 3.1.1, the resistance of

a DC circuit can be extracted directly by using Ohm's law. Consequently, it is favorable to apply DC circuit to a system. Since, reactance is mostly present in an AC circuit, the identification of the resistivity is more complicated.

A huge drawback of a DC circuit is, that cement-based sensors with conductive particles tend to electrically charge itself when a direct current is applied to the sensory system. This is due to the fact, that cement-based composites perform rather capacitive than inductive (Azhari, 2008). This phenomenon makes the measurement of the electrically resistance, especially under cyclic loading, technically difficult (Azhari & Banthia, 2012). Furthermore, due to this charging ability, polarization of the cement-based material occurs, but mostly when it contains carbon particles.

The effect of polarization affects the measurement of resistance by giving a non-linear response of the initial value. By applying a direct current, the resistance increases, because the sensor charges itself. From the time the sensor reaches its maximum electrical capacity, the polarization is stable, and the resistance will be constant (Wen & Chung, 2001).

For measuring the resistance in consequence of an applied static load, the polarization is rather negligible or can be eliminated, because the response of the resistance will be a constant value. By applying a dynamic load, which is common for SHM systems, the polarization has a huge influence on the response of the electric resistance. Since, the increase and decrease of polarization is extremely inertial, due to slow charge and discharge processes of the capacitor, the fast-changing strain cannot be reflected by the resistance measurement. Therefore, measures must be taken, to reduce

the effect of polarization and allow a quicker response from the materials (Al-Dahawi et al., 2017).

By applying an alternating current to a conductor, the effect of polarization can be reduced to a minimum. By increasing the frequency of the AC signal, the effect of polarization still exists, but is rather negligible. By choosing frequencies of 100 kHz or higher, polarization is narrowed to a tolerable range and the response of resistance is very accurate. This also implies a better illustration of the resistivity and a more direct behavior for strain-sensing.

3.1.6. PERCOLATION THRESHOLD

By dealing with conductive particles such as carbon fibers or carbon nanotubes, the electrical conductivity and resistivity is highly dependent on the volume fraction of the particle content. The conductivity increases by adding more conductive particles to a non-conductive phase. When the concentration of conductive particles reaches a critical value the changes in conductivity increases marginally. This critical value is called percolation threshold. The theory behind this phenomenon is called the percolation theory (Azhari & Banthia, 2012).

The percolation theory describes the relationship between conductivity and connectivity of the conductive particles. In a composite or region with a very low fiber concentration the particles are distributed very homogeneously in the non-conductive matrix. There is no contact between adjacent fibers. By adding particle content, these will form agglomerates or clusters, which have a higher conductivity. Up to a certain amount, these clusters are separated. By increasing the amount of particles, adjacent clusters get in contact and will form a network through the entire matrix. This can be

measured by an increase in conductivity. When a conductive network is formed, the conductivity increases slowly with increasing the fiber content. This is due to the fact, that an increase of particulates just slightly improves the connectivity of the conductive network. The increase of conductivity almost stops when the amount of fiber does not improve the conductive network. This relationship between connectivity and conductivity is illustrated in Figure 2 (Xie, Gu, & Beaudoin, 1996).

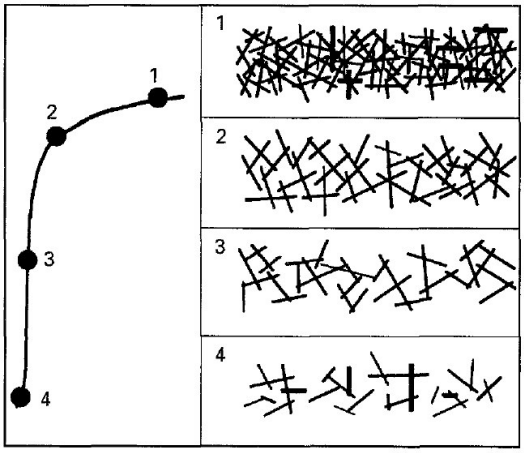

Figure 2 Illustration of the percolation phenomenon

Stage 4 to 1 show the amount of fiber with regard to the connected particles and the forming network. In stage 4 no conductive network has formed. Stages 3 and 2 show a formed network with increased amount of particles. Between stage 2 and 1 the conductivity just slightly increases until the percolation threshold is reached. It should also be mentioned, that the type of conductive particle and the size and shape will also affect the forming conductive network and percolation threshold.

3.2. SELF-SENSING MATERIALS FOR SMART COMPOSITES

In the following paragraphs, some of the most commonly used materials in research and for SHM will be discussed. This thesis specifically deals with carbon-based materials, so the material properties, advantages and disadvantages of carbon fibers,

carbon black and carbon nanotubes will be pointed out. Furthermore, the effect of conductive paint on SHM-sensors will be mentioned.

Carbon-based materials in general show a very good behavior referring to electrical conductivity. They can be used or added to other materials such as cement to improve the electrical behavior of the matrix, such as reducing the resistivity. For SHM purposes, this provides many possibilities, such as strain sensing or damage detection. As described in chapter 3.1.3, the strain sensing behavior is put down to the piezoresistive effect. The effect of carbon-based materials onto the piezoresistivity of cement-based self-sensing materials will also be discussed.

3.2.1. CARBON FIBERS

Carbon fibers are of particular interest for SHM, since their material properties bring many advantages for cement-based strain sensors or damage detectors. In general, the ability of fibers to enhance the material properties on plain concrete is been known for a long time. For example, toughness, fatigue resistance, tensile strength, flexural strength and the reduction of creep and shrinkage are known improved properties of concrete with fiber content.

CFs possess a very small diameter, which is much smaller than the diameter of a human hair. The atomic structure is similar to that of graphite and consists of sheets of carbon atoms arranged in a regular hexagonal pattern. The difference to graphite is the strong non-crystalline interlock between the separate sheets, which gives carbon a very high tensile strength. Carbon fibers are predominantly used in combination with other materials to form and strengthen composite materials. CF composite materials are most commonly used in the field of aerospace in combination with epoxy resin. Therefore,

the fibers are normally long and webbed to a mesh for a better strength in multi-axial directions. Generally, for SHM purposes, short CFs are used for a better distribution in the cement matrix. Figure 3 (Sun, Li, Wang, & Zhang, 2015) shows a Scanning Electron Microscope (SEM) picture of CF distributed in a concrete matrix, which forms a carbon fiber reinforced concrete composite (CFRC).

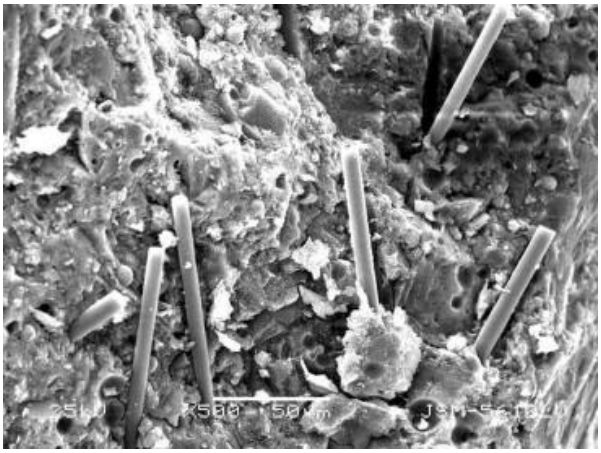

Figure 3 SEM picture of CFs in CFRC

The influence of CFs onto the mechanical and electrical properties of cement paste or concrete are highly dependent on the properties of the fibers itself. The average material properties of commonly used CFs are listed in Table 1. Compared to a steel fiber, CFs show big advantages especially on the size and strength (Chung, 2000).

Table 1: Comparison of Steel and Carbon fiber properties

	Carbon Fiber	Steel Fiber
Fiber diameter [µm]	15 ± 3	≥ 60
Fiber length [mm]	≥ 3	≥ 5
Tensile strength [MPa]	690	250
Young modulus [GPa]	48	21
Electrical resistivity [Ωm]	2.3×10^{-6}	6×10^{-5}
Specific gravity [kg/m³]	1600	7850

Not just the material itself influences the composite properties. There are further parameters that can be changed by selecting another type of fiber, such as shape of the

fiber or fiber treating, which gives the fiber the ability to chemically interact with the matrix.

For SHM purposes, the improvement of mechanical parameters of concrete is basically just a bonus feature despite the main idea to use carbon fibers for improving the electrical behavior of its host matrix. In previous researches CFs are more likely to use for strain sensing, than other materials such as steel fibers. CFs are found to be less costly and have a lower electrical resistivity of around 2.3 x 10^{-6} Ωm compared other fiber materials such as steel fibers with a resistance of 6 x10^{-5} Ωm (Fu & Chung, 1996).

Chen and Chung started investigations with concrete containing short carbon fibers in 1993. It was found, that these composites can form an intrinsically smart concrete that can sense elastic and inelastic deformation (Chen & Chung, 1995). Based on their results, researchers started to work on similar problems to improve the electrical behavior of cement composites even more. Factors of interest are to increase the durability and reliability of the cement-based sensors, to have a measurement repeatability and stability, to increase the sensitivity and resolution of the sensors, to improve the response and to provide a sensitivity to a wide dynamic range of strain.

By taking care of the mentioned factors it must be ensured, that the mechanical properties of the concrete do not decrease. CFs are known to have inert properties regarding to cementitious materials, which means CFs don't react with the cement and water, so that the hydration process is not affected. They rather improve the mechanical properties, by giving the concrete or cement paste a higher tensile strength and modulus. This effect is due to a good cohesive bonding interaction between the fibers and the

cement matrix. The fiber content reduces the amount of crack formation and crack opening, which also improves the durability of the concrete.

One of the aspects with the highest influence on mechanical and electrical properties is the variation of the volume fraction. By increasing the content of CFs, the electrical conductivity of the cement matrix increases, and mechanical properties will be improved. By investigating the conductivity of plain concrete a very low response will be detected, as concrete is known to be a poor electrical conductor, whereas the resistivity is about 6.5 $x10^5$ Ωm (Xie et al., 1996). In comparison, CFs have an about eight times higher conductivity than the concrete, especially under dry conditions. Concludingly, the properties and microstructure of the non-conductive composite do not influence the conductivity of the composite very much. Just the conductive fiber content determines the conductivity of the system.

It is important to mention, that the increase of conductivity by adding more fibers is limited. This phenomenon can be explained with the percolation theory, which was explained in chapter 3.1.6. Figure 4 (Chiarello & Zinno, 2005) shows the increase of electrical conductivity by adding carbon fibers to a non-conductive cement matrix. It can also be recognized, that the increase of conductivity gets less with the amount of fiber content.

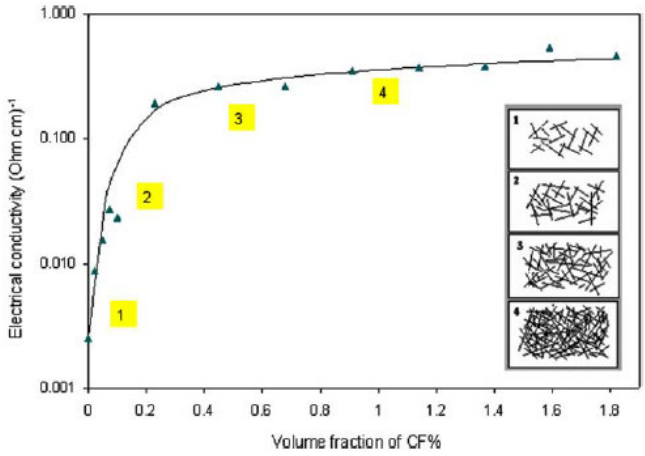

Figure 4 Change in electrical conductivity dependent on the CF volume fraction

In chapter 3.1.6 it was shortly mentioned, that the conductivity of a composite and the percolation threshold is also influenced by the fiber dimensions. Mostly dependent on the fiber length and diameter it was investigated, that the percolation threshold increases with a decreasing fiber length. In exchange, to form a conductive network with shorter fibers, the fiber content must be higher. So, the interrelation between fiber length and the fiber content should be carefully examined. Figure 5 (Chiarello & Zinno, 2005) should illustrate the described behavior.

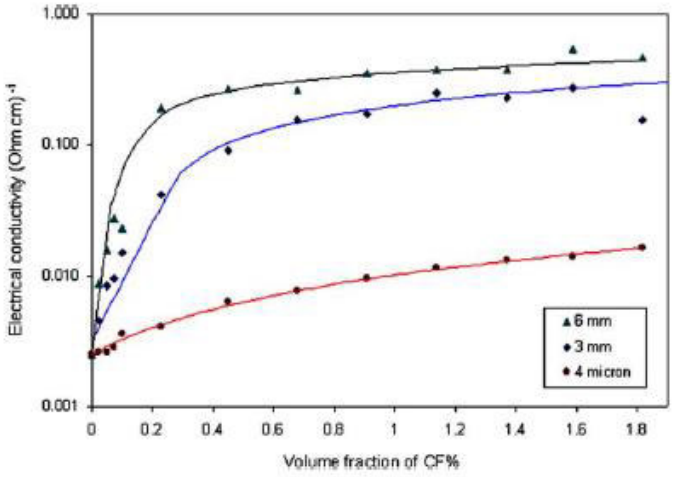

Figure 5 Effect of CF length on percolation threshold and conductivity

In previous research projects, also the effect of hydration or curing time on the electrical conductivity of CFRC was investigated. Before doing the experiments, it was expected, that the formation of new hydrates in the concrete will affect the connectivity of the fibers, so that the fiber-contact may be broken. It could be shown, that the hydration has no effect on the percolation threshold. But it does affect the overall conductivity. Due to the fact of chemically binding the water in the hydrates and curing of the concrete, the conductivity of the CFRC will decrease. The less amount of pore water is present in the concrete, the less conductive is the composite material. But this phenomenon is independent on the amount or shape of the fiber content (Chiarello & Zinno, 2005).

In conclusion, CFs are perceived to be an excellent conductive phase to improve the conductivity of cement and to create cement-based conductive materials. The resistivity can be significantly reduced by adding CFs to a cement paste with a volume fraction around the percolation threshold. Investigations, dealing with CFs to create self-sensing concrete, have been practiced since the early 1990th. CFs can not only be used for strain sensing, but also for damage detection under impact stress, evaluation of the fatigue life under cyclic flexural loading and even more (Han, Wang et al., 2015). During the last two decades several more conductive materials have been invented to improve the electrical conductivity of concrete, such as carbon black materials or carbon nanotubes, which will be discussed in the next paragraphs.

3.2.2. CARBON BLACK

Carbon black (CB) is a form of para-crystalline carbon, that consists of nearly spherical primary particles. The particles have an extremely small diameter in the

nanometer-range and a small specific surface area. These two properties predominantly affect mechanical, electrical and optical properties of composite materials containing CB. CB has primarily been used as filler in elastomers to improve the heat conduction of automobile tires but also to enhance the electrical conductivity of polymers (Pantea, Darmstadt, Kaliaguine, & Roy, 2003).

Since the early 2000, scientists are investigating the electrical behavior of CB as conductive filler in cement-based composites. It was found, that CB as conductive filler can significantly enhance the electrical behavior, such as decreasing the resistivity and improving the piezoresistivity of cement-based sensors. The main effect of conducting electrical current through a sensor was traced back to the tunneling effect of electrons, which will be further discussed in chapter 3.2.3. Cement-based sensors containing CB were first developed by (Li, Xiao, & Ou, 2006), who investigated the electrical behavior of sensors containing huge amounts with up to 25 % by weight of cement.

It was shown, that cement-based sensors containing CB possess a very good sensing behavior. The fractional change in resistivity showed good response to the measured strain. Similar to CFs, the conductivity of sensors with CB are very dependent on the volume fraction and the percolation threshold. Above the percolation threshold the tunneling effect plays a critical role in conductivity (Li et al., 2006). Furthermore, the sensors show a better repeatability and sensitivity in the elastic range than sensors only containing CFs. The combination of CFs and CB was also investigated. In this scenario, CB was used as an even smaller filler between the carbon fiber to provide an even better sensibility (Azhari, 2008).

3.2.3. CARBON NANOTUBES

In the past ten years, nanoscale carbon materials gained a lot of interest in SHM. Many researchers investigated the effect of nanoscale materials on various material properties of quasi brittle cementitious materials, and achieved distinct results, which show the positive behavior onto cementitious materials. Some of the most common nanocarbon materials are carbon nanotubes (CNT) and carbon nanofibers (CNF).

CNTs and CNFs are quasi-one-dimensional and very small in the cross-section diameter. CNTs specifically have a hollowly cylindrical nanostructure and are a few nanometers in diameter and several microns in length. CNFs compared are solid and their diameter is in the range between CNTs and CFs (Han, Sun et al., 2015). In the following paragraphs some material properties and positive effects on the mechanical and electrical properties of cementitious nanocomposites containing CNTs will be discussed.

3.2.3.1. MATERIAL PROPERTIES

CNTs are known to be highly effective in terms of mechanical and electrical behavior onto cementitious materials. Nanotechnology and especially CNTs allow to improve the atomic structure of concrete. More specifically, CNTs affect the calcium-silicate-hydrate (CSH) structure, which is a product of the hydration process of cement. By intervening the CSH atomic structure on a very small scale, CNTs have a powerful lever to develop the micromechanics of cementitious materials (Safiuddin, Gonzalez, Cao, & Tighe, 2014).

Depending on the manufacturing process, different types of CNTs can be generated. In general, CNTs can be characterized as a modified form of graphite, where

one or multiple sheets of graphite are rolled up into a tube structure (Azhari, 2008). The first type is defined as single-walled CNTs (SWCNT), the second type is defined as multi-walled CNTs (MWCNT). SWCNTs tend to possess much better material properties than MWCNTs, such as a higher tensile strength or elastic modulus. A disadvantage of SWCNTs are the manufacturing process and costs. MWCNTs are less expensive and more readily available. Therefore, MWCNTs are used rather than SWCNTs (Safiuddin et al., 2014). Figure 6 illustrates a rendering of the atomic structure of a SWCNT and a MWCNT.

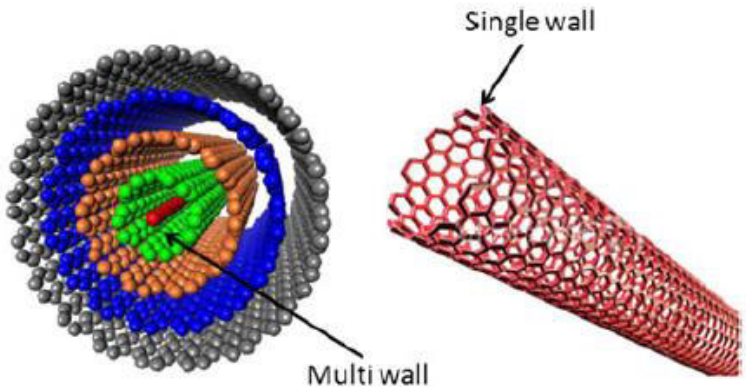

Figure 6 Atomic structure of single-walled and multi-walled CNT

As aforementioned, MWCNTs have outstanding mechanical and electrical properties. The nanoscale dimensions and very high aspect ratio improves the microstructure of unhardened and hydrated cementitious composites. Table 2 (García-Macías, D'Alessandro, Castro-Triguero, Pérez-Mira, & Ubertini, 2017) shows some of the most important material properties of MWCNTs in comparison to SWCNTs. It has to be noted, that fiber length and diameter is varying. The given material properties stand for a specific type of fibers.

Table 2 Comparison of MWCNTs and SWCNTs

	MWCNT	SWCNT
Fiber diameter [nm]	8 – 15	0.75 – 3
Fiber length [µm]	1 – 50	1 – 50
Tensile strength [GPa]	~ 150	50 – 500
Young modulus [TPa]	0.3 – 1	1
Electrical resistivity [Ωm]	up to 1 $x10^{-7}$	n.a.
Electrical permittivity	6.5	n.a.
Specific gravity [kg/m³]	50 – 150	n.a.
Surface area [m^2/g]	100 – 250	n.a.

Moreover, another important mechanical parameter of CNTs is the Poisson's ratio, which is very complicated to determine for MWCNTs, since the size of the fibers is very small. In previous researches, the Poisson's ratio was discovered to be in the range of other common textile fibers and varies around $\nu = 0.269$ (Miao, McDonnell, Vuckovic, & Hawkins, 2010).

Comparable to other conductive particles, MWCNTs achieve their highest effect in a composite, when the volume fraction of the fiber content is around the percolation threshold. By reaching the percolation threshold CNTs begin to form conductive networks, which reduces the resistivity of the matrix. This is also due to the fact, that electron hopping between the CNTs tends to be easier. The percolation threshold of MWCNTs in general is extremely low, with a concentration of about 0.695 vol. %. It can be deduced, that the low percolation threshold is a consequence of the very high aspect ratio of the CNTs, which can also be considered to be infinite (García-Macías et al., 2017). García-Macías et al. also investigated the overall behavior of MWCNTs on the percolation threshold. They found out, that the percolation threshold varies marginally, which can be traced back on the non-straightness of the fibers and the distribution in the matrix. It was discovered, that the threshold increases for compressive

and tensile strains according to a change in tunneling resistance and the tendency of nanoscale inclusions to agglomerate in clusters. The problem of agglomeration of CNTs to form clusters will be further discussed in the next paragraph, which deals with fiber dispersion.

3.2.3.2. FIBER DISPERSION

The fiber dispersion of CNTs is a very important step to create a cement-based self-sensing composite. The CNTs must be homogeneously distributed in the cement matrix to form a conductive network and to inherently reduce the resistivity of the non-conductive matrix. The agglomeration of CNTs is a result of the large surface area, high aspect ratio and strong Van der Waals attraction forces, which leads to a decrease in the positive effect of CNTs (Liew, Kai, & Zhang, 2016).

Several methods to properly disperse CNTs have been developed in the last couple of years. These methods can be divided into physical and chemical methods. Physical methods include sonication, ball milling and mechanical stirring, whereas chemical methods include the use of different surfactants to disperse CNTs.

Sonication breaks agglomerations of CNTs by providing energy to overcome Van der Waals (VdW) interactions. Thereby, voltage is transferred into pressure waves to form a cavitation field and produce micro bubbles. these will break the bonding between the fibers. Ball milling and mechanical steering or shear mixing will break the VdW interactions but cannot properly disperse CNTs. These methods are usually used as a preliminary treatment or in combination with sonication.

With chemical methods, covalent or noncovalent bonds are added to improve the wettability of the CNTs surface. A common approach to modify the surface of CNTs is

to form covalent bonds by adding polar functionalized groups such as carboxyl (COOH). Another method is to grow polymer chains from the surfaces of CNTs, which keeps the CNTs in distance and improve the wettability. These polymer chains can be created by using surfactants to disperse CNTs. In the current experimental research also combinations of the mentioned methods are practiced to disperse CNTs, such as combining ultrasonication and surfactants (Liew et al., 2016). In the following illustration Figure 7, a scheme of how the mixing process would take place by using surfactants, a magnetic stirrer and ultrasonication to disperse CNTs properly.

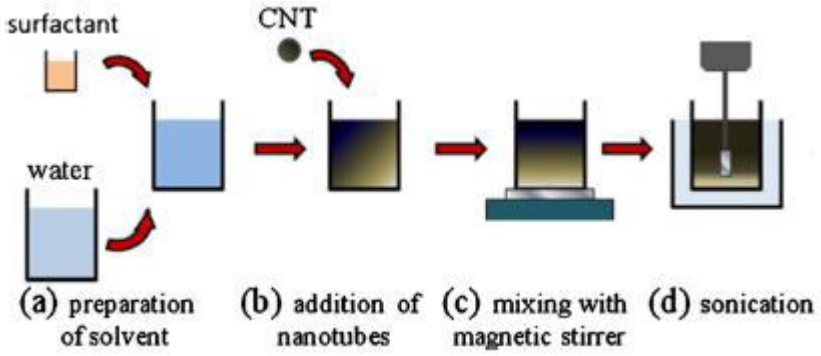

Figure 7 Mixing procedure to disperse CNTs in water

First surfactant such as superplasticizer is added to water. To this solvent, pure CNTs are poured into the liquid solution. The surfactant already helps to disperse the CNTs, but with mixing the solution with a magnetic stirrer and additionally sonication, the fibers will be dispersed very homogeneously.

In the following, the use of surfactants will be further discussed. CNTs absorb the hydrophobic part of the added surfactant at the side walls through VdW forces, while aqueous solubility and electrostatic repulsion ensure to distribute the fibers. The range and strength of the electrostatic repulsion depends on the density of polymers on the CNT's surface. The optimal mass ratio of surfactant/CNTs varies with the type of

surfactant and CNT. Since surfactants react with the cement hydrates, it is recommended not to use surfactants that have a negative effect in the hydration process. Surfactants such as superplasticizers or with a similar structure are rather recommended, since superplasticizers are already widely used in the cement industry. It must be noted, that the amount of water and superplasticizer has to be slightly increased, because of the extremely high specific surface area of MWCNTs (Azhari & Banthia, 2012). It is recognized that the amount of superplasticizer was 0.023 – 0.14 % by the weight of water in a mixture to achieve good results for the dispersion of MWCNTs (Liew et al., 2016). In a well dispersed manner, CNTs show an extremely good behavior on the mechanical and electrical properties of cement-based composites.

3.2.3.3. EFFECTS ON MECHANICAL PROPERTIES

It has been reported, that CNTs show many improvements of the mechanical properties of fresh or hydrated cementitious composites. In general, CNTs have a strong effect on the hydration process and hardness of cementitious composites. In fresh conditions, it was reported, that MWCNTs could increase the viscosity of the fresh concrete. In hardened conditions the nanoscale materials act as fillers, which reduces the pore size and distribution in the matrix. This also decreases the porosity of the composite, which helps to retain crack growth and propagation. This enhances the Youngs modulus and the stiffness of the composite (Konsta-Gdoutos, Metaxa, & Shah, 2010).

A further aspect of improving the microstructure is the strong bond between CNTs and the matrix, because of the interaction of CNTs and the hydrates, and the improved particle packing, which reinforces the quasi brittle cementitious material on a nanoscale.

This reduces early autogenous shrinkage of at least 30 % after 96 h and strength the composite material. From previous investigations, it is known, that CNTs can improve the tensile strength, tensile modulus, compressive strength, flexural strength, fracture toughness and the Youngs modulus by 34 %, 70 %, 200 %, 269 %, 149 % and 227 % respectively (Liew et al., 2016).

Several reinforcing mechanisms have been developed to describe the mechanical behavior of CNTs on cement-based composites. The primary mechanism is named as the crack bridging mechanism. It describes the ability of CNTs to bridge nanoscale cracks and pores in the range of $10 - 10^3$ nm. This effect provides an efficient load transfer and is simultaneously a cause for the electrical sensitivity, which will be discussed in the next chapter. The crack growth of nanoscale pores will be delayed, because of the high strength of the CNTs and the strong bond. This will also hinder the formation of micro cracks, that can turn into macro cracks (Chowdhury, Haque, Okabe, & Gillespie Jr., 2012).

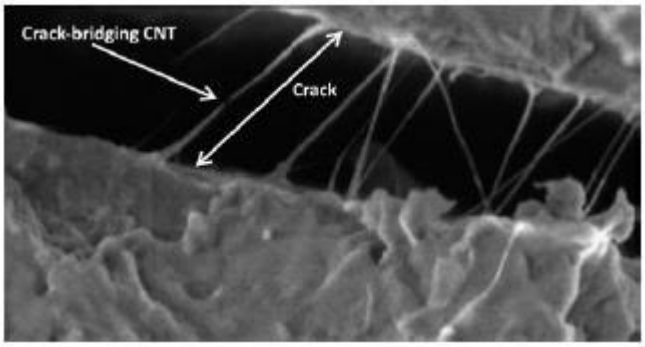

Figure 8 SEM picture of crack bridging CNTs

Figure 8 (Safiuddin et al., 2014) shows a SEM picture of a crack in a cementitious composite containing CNTs. The opened crack is reinforced by the CNTs, so that the crack propagation is slowed down, which automatically gives the composite a higher tensile strength. The crack bridging effect is present, until the strength capabilities of

the CNTs come to a limit and the fibers break. Other failure mechanisms are the fiber pull-out or fiber debonding between the CNTs and the matrix.

Further reinforcing mechanisms are the aforementioned capability of filling nanoscale pores and gaps of the matrix, the modification of the microstructure of hydration products and the role of CNTs as nucleating agents for CSH gel, because of the hydrophobic nature of the CNT structure, which allows them to absorb water (Liew et al., 2016).

3.2.3.4. EFFECTS ON ELECTRICAL PROPERTIES

In many publications it has been reported, that the electrical properties of CNTs itself are outstanding. The most important parameters are listed in Table 2. In combination with cement-based materials with an almost insulating electrical behavior, CNTs can achieve piezoresistive self-sensing properties. CNTs decrease the electrical resistivity of cement-based composites dramatically to nearly 1 Ωcm and increases the electrical conductivity. Comparable to the mechanical properties, electrical properties are also highly dependent on the CNT concentration and dispersion. Agglomerates of CNTs will cause anomalies in the conductive network, which will reduce the effect of piezoresistivity of the composite (Han, Sun et al., 2015).

To achieve a low resistance and a high sensitivity of a cement-based composite for strain sensing, the CNTs content should be around the percolation threshold. If the CNTs concentration is around the percolation threshold and the fibers are well dispersed, several conduction mechanisms go into action. With applying a deformation to a piezoresistive cement-based composite, a change in the intrinsic resistance applies. This means, also the resistance of each CNT changes, but because of the small size and

the high Young's modulus, this factor is rather negligible regarding to the piezoresistive sensing of the whole composite.

Another factor of conducting electrical current through a cement-based composite is the change in contact resistance between the CNTs. Due to the tension and compression, fibers will be moved together or apart, which has a considerable impact on the sensing behavior. The closer the fiber content is to the percolation threshold and the better fibers are dispersed, the better is the sensitivity. The change of tunneling distance comes close with the change in contact resistance. This mechanism describes the behavior of electron hopping between CNTs dependent on their distance. Figure 9 (Han, Sun et al., 2015) should illustrate this mechanism.

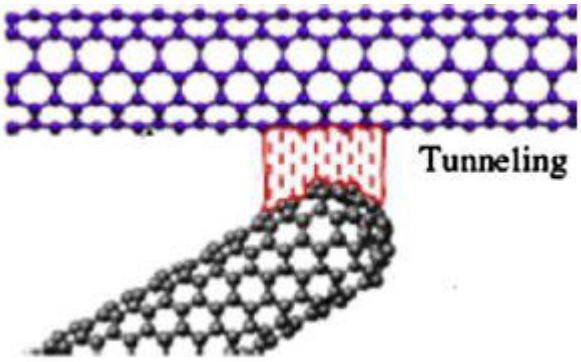

Figure 9 Illustration of the tunneling effect between two adjacent CNTs

Obviously, the jump of electrons between adjacent CNTs is easier, which implies a lower resistance, when the fibers are closer together, than when they are further apart. Another factor of influencing the sensitivity is the change in bonding between the CNTs and the matrix. It should also be mentioned, that all conduction mechanisms work together for the contribution of the sensing properties (Han, Yu, & Ou, 2011).

4. CEMENT-BASED SENSORS IN CIVIL INFRASTRUCTURE

Sensors to measure strain, deflection or temperature have been used in civil infrastructure for many decades. A new approach of measuring different states of structures has been made recently, where researchers added steel fibers and carbon fibers to a cement matrix to reduce the resistivity of the matrix and develop a piezoresistive composite. This means, no external sensor has to be externally attached to a cement sample or structure. Instead the cement composite can sense its own strain or many other parameters.

In the past two decades, many investigations on improving the sensitivity and repeatability of self-sensing cement-based sensors have been done. Different materials, such as steel fibers/particles, carbon fibers, carbon black particles or carbon nanotubes, and different ways to apply the conductive phase into the cementitious matrix are used to achieve better results and an easier way to apply these kinds of sensors to structures.

In the following paragraphs the principal function of cement-based sensors, the effect of the choice of different materials, mixture proportions and effect of testing configurations on the FCR and sensitivity will be reviewed and discussed.

4.1. FUNCTIONING OF CEMENT-BASED SENSORS

The main principle of how cement-based piezoresistive sensors work will be explained in the following. Cement-based sensors are primary developed to sense strain in a structure. Usually they are embedded to structures with a changing deformation, that means a dynamic applied load, which makes the sensitivity in small changes of strain and a high repeatability very important. To enable strain sensing the piezoresistive effect is used, which means by applying a deformation and an electric potential to a

sensor, changes in the conductive network apply, which are expressed as the FCR. This FCR can be converted into a change in strain. Since the electrical conductivity of cement is very low or possesses almost insulating properties, an additional conducting phase is added to reduce the resistivity of the cement. Conductive phases can be some of the aforementioned materials, such as carbon fibers, carbon nanotubes or steel particles.

Besides strain-sensing, different types of cement-based sensors are developed to sense concrete conditions and environmental parameters, such as crack-propagation, damage, temperature and humidity. The main advantage of cement-based sensors is, that they consist of the structural material itself. Further aspects that can be expected are a long service time and an easy installation and maintenance of the sensors, which clearly differentiates them from conventional sensors. From previous research it can be extracted, that successful investigations were made to achieve a high sensitivity of sensing under small deflections of sensors (Han, Wang et al., 2015). The current state of the art requires to investigate methods to make the sensors easier to embed into the structure or develop different ways to apply a sensory system to a civil infrastructure.

4.2. EFFECT OF SETUP CONFIGURATIONS

The effect of the setup configurations has to be carefully considered, since it is essential for measuring the correct values and receive usable results. The setup configuration defines which load state will be applied, or how electrical measurements are performed. These two aspects will be discussed in the next paragraphs.

4.2.1. MECHANICAL SETUP

The most common method to determine FCR or the sensitivity of a cement-based sensor is to load the specimen under compression or tension. These experiments are

necessary to evaluate the sensing behavior of conductive particles in a cement-based composite under pure compression or tension. Since, cement-based sensors should also apply to bending-elements, such as beams or bridge decks, the capability of strain sensing under flexure is also very important. Therefore, usually three-point or four-point bending tests are performed to investigate the sensing behavior under flexural conditions.

Another factor is the type of loading, which is applied to the specimen or sensor. The basic way is to apply a constant load to the sensor and measure the parameters such as conductivity and resistance, while a current is crossing the circuit. This method is applied, to determine the piezoresistive behavior under static loads and the intrinsic material parameters. Another method is to apply an increasing load, until the specimen with an embedded sensor or the sensor itself collapses. This procedure is deployed to investigate the ultimate load behavior and the sensing-behavior until a damage is detected.

The most interesting setup for civil infrastructure is the sensing under a dynamic load state. Since, usual external forces on bridges are very varying, such as traffic and wind, the sensing of dynamic loads and deterioration of the structure is very important. Therefore, sensors must be very sensitive to measure even small changes in strain and be reversible in the elastic range for long term observations of the structure.

The general sensing behavior of cement-based sensors under compression can be explained with the FCR. With an increase in compressive load the resistivity values decrease, which results in a negative FCR. With unloading of the sensor, the FCR increases to its initial value, if stresses did not exceed the elastic range of the composite.

Under tension the FCR is increasing with an decreasing load, which results in a positive FCR and decreases after unloading (Azhari & Banthia, 2012).

The decrease of resistivity under a compressive load can be explained with a slight fiber push-in that accompanies crack closing. Additionally, the distance of conductive particles decreases, which reduces the tunneling distance and contact resistivity of adjacent particles. Inversely, the increase of resistivity under tension follows the fact of slight fiber pull-out that accompanies crack opening. The tunneling distance increases which implies an increase of the contact resistivity (Chung, 2016). These phenomena are very unique and highly dependent of the used materials and mixture proportions, which will be discussed in chapter 4.3.

For the strain sensing of a dynamic load usually several cycles of an increasing and decreasing load are applied. To achieve a long-term durability of cement-based sensors, the aforementioned reversibility plays an important role onto the dynamic sensing behavior. With a low reversibility, the amount of cycles the sensor can undergo is limited. A low reversibility is usually a result of a low fiber content. The small amount of contact pairs in the conductive network break, which increases the resistivity (Chung, 2016). The sensitivity of the cement-based sensor is decreasing from cycle to cycle. To improve the reversibility of a sensor, the conductive particle content should be around the percolation threshold. This gives a high elastic range and reduces the influence of degradation of bonding between the inclusions and the matrix (Al-Dahawi et al., 2017).

If a cement-based sensor reaches the plastic range, changes in the resistivity can be noticed. Due to the irreversibility of the deteriorated conductive network the initial resistance has changed which also can be observed in an irreversible response of the

composite's electrical resistance. At this state a damage in the sensor or the embedded structure can be assumed. It has been reported, that damage that is associated with an irreversible decrease in resistance in the case of flexure, may be due to excessive crack closing (Zhu & Chung, 2007).

4.2.2. ELECTRICAL SETUP

To apply a current to a cement-based piezoresistive sensor, at least one anode and one cathode have to be attached to the sensor. The current enters the sensor through the anode and leaves it through the cathode. The sensor is usually attached to an LCR meter, which is a type of electronic test equipment to measure the inductance L, capacitance C and the resistance R. The LCR meter is used to perform an electrical impedance spectroscopy (EIS) to measure dielectric properties of a medium as a function of frequency, such as the electrical conductivity, resistivity and permittivity (Chiarello & Zinno, 2005). EIS is executed with an applied AC, which involves a resultant impedance instead of the resistance directly. As mentioned in chapter 3.1.5, an AC should be adopted to a cement-based sensor, to almost eliminate the phenomenon of electrode polarization. Due to the polarization in a DC, the electrical resistance varies over time since the sensor/capacitor will be charged and an opposite current is generated (Coppola, Buoso, & Corazza, 2013). In an EIS the electrical impedance is expressed with equation (10).

$$Z = \frac{R}{\sqrt{1 + \omega^2 C^2 R^2}} \tag{10}$$

Where R is the resistance in Ohms (Ω), C the capacity in Faraday (F) and ω the circular frequency with equation (11).

$$\omega = 2\pi f \tag{11}$$

Anticipatory, it is mentioned, that EIS measurements run over a specific frequency range. For measurements with cement-based sensors a frequency range of 0.1-100 kHz. From previous literature it is known, that at 100 Hz the practically constant value of the impedance indicates, that it is close to its real part. The upper limit is chosen as a reference value for the electrical resistance (Chiarello & Zinno, 2005).

Usual EIS measurements are performed with a 2-probe setup testing of the cement-based sensor. Within a 2-probe setup, two electrodes are attached or embedded into the sensor and connected to the electrical source and the testing machine. An alternative would be the 4-probe setup, where four electrodes are attached at specific locations to the sensor. In this kind of setup, the current and voltage paths are separated. So, the outer electrodes are connected to the source of current, whereas the inner electrodes are employed to measure the resultant voltage (Al-Dahawi et al., 2017).

It has been noticed, that the overall resistance of the 2-probe setup was higher than with the 4-probe setup. This can be explained with a higher contact resistance of the 2-probe setup between the electrodes and the piezoresistive cement-based material which is not suitable for resistivity measurements (Ou & Han, 2008). With the 4-probe setup, also the effect of polarization is reduced (Wen & Chung, 2001). Additionally, to minimize the effect of contact resistance, the location of the electrodes and the type of electrode must be considered. Embedding copper plates or a copper mesh into the sensor gives a lower contact resistance than with attached electrodes at the ends of the sensor or copper wires, that are wrapped around the sensor. By attaching the electrodes, a conductive paste, such as silver paint must be used to ensure a good contact with the

sensor. The resistance of the conductive paste must be additionally considered in the electrical circuit. Figure 10 (Chiarello & Zinno, 2005) illustrates different electrode setups.

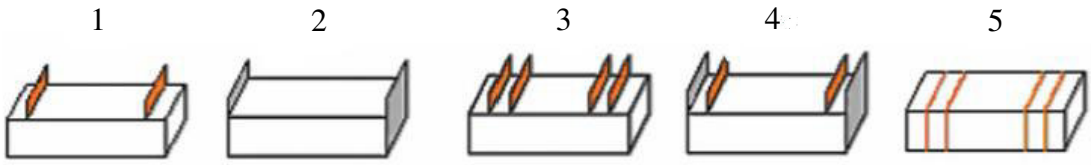

Figure 10 Different types and locations of electrodes in 2-probe and 4-probe setups

The best performing setup shows case 3, followed by case 4. The piezoresistive behavior is very good with a low effect of polarization and contact resistance at the electrodes. Case 5 illustrates a copper wire setup, where the electrodes just wrap up the sensor. Cases 1 and 2 have been proven not to be beneficial for piezoresistive measurements, because of the high contact resistance, but these setups can still show comparable and respective results.

Another aspect of the positioning the electrodes is to minimize and prevent an early localization of micro cracks around an embedded electrode, which weakens the structure, increases the resistance and could give a false alarm in regard to damage sensing. The location is especially critical at flexural testing, where tension and compression appear. An appropriate position for the electrodes, for example in a 3-point bending test, is close to the area of the supports.

4.3. EFFECTS OF MATERIAL TYPE AND MIXTURE PROPORTIONS

The sensing ability and sensitivity of a cement-based sensor is highly dependent on the material of the conductive phase, which provides a higher conductivity of the composite. Many aspects, such as the fiber content and the effect of a specific

conductive material were already discussed in chapter 3.2. This chapter should show the effect of specific mixture proportions onto the mechanical and electrical behavior of cement-based sensors.

In general, good sensing capabilities of cement-based sensors were achieved, if the volume fraction of the conductive phase was around the percolation threshold. Azhari et al. performed resistivity measurements with cement-based sensors containing different volume fractions of CF. The resistivity was significantly decreased, but by reaching a CF content of 20 vol.% the composite seemed to be more brittle. To avoid a brittle structure, the CF content was decreased and replaced with a small content of CNT. Due to the high surface area and the excellent electrical properties, an additional content of 1 vol.% inherently decreased the resistivity. The result of the creation of a hybrid of conductive particles with different sizes and surface areas, such as CF and CNT or CB, is a perfect mix to form a conductive network for an excellent conduction and still equal or improved mechanical properties compared to the plain cementitious material. Especially the use of CNT can bridge the existing pathways between the CF and create a more uniform conduction path. This helps to increase accuracy and repeatability of cement-based sensors (Azhari & Banthia, 2012).

Ou et al. investigated the electrical behavior of cement-based materials containing only 0.38 vol.% CF and a hybrid containing 0.18 vol.% CF and 15 vol.% carbon black particles. The sensors were loaded with a linear increasing compressive load until failure of the sensor. It was shown, that the hybrid had a better reproducibility and linearity of measuring the FCR. This effect was traced back to the enhancement of the contacting and tunneling conduction effect. The direct comparison of the results for a composite

with CF only (a) and a composite hybrid with CF and CB (b) is shown in Figure 11 (Ou & Han, 2008).

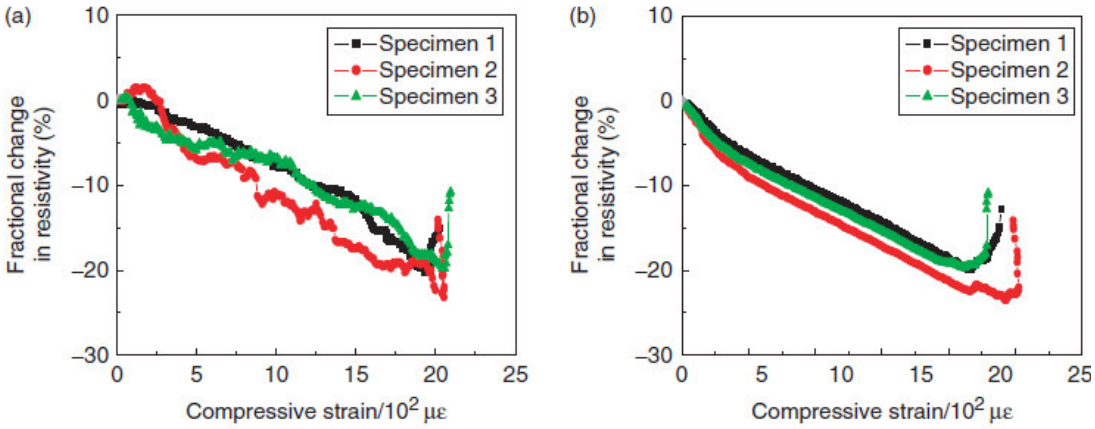

Figure 11 Comparison of the FCR under a compressive load

To run perform the experiment, three specimens with the same mixture proportions were casted to have a better representation of the results. The graphs show, that the sensing of the mixture containing only CF was very unstable and not linear. The sensing ability of the hybrid was less noisy in representing the FCR. It has to be noted, that the maximal measured FCR is almost equal in both mixtures and fail at the same strain level. So, both mixtures can be used for strain sensing, but the hybrid sensor would be more favorable for strain-sensing under a dynamic load.

Azhari et al. also performed piezoresistive measurements with cement-based composite mixtures containing 15 vol.% CF only, which is well above the percolation threshold of CF, and a hybrid mixture containing 15 vol.% CF and 1 vol.% MWCNTs. For dispersion of the MWCNTs superplasticizer with an additional sonication was used before adding the solution to the cement. By comparing the average base-line resistivity of the composites, a 10 % improvement in conductivity was noticed, whereas the CF only sensor had a resistivity of 413 Ωm and the hybrid a resistivity of 371 Ωm. This

decrease is a result of the effective bridging of existing pathway for electrical conduction by the MWCNTs. For the strain-sensing measurements a compressive dynamic load with different load amplitudes was applied. Figure 12 shows the sensing behavior (FCR) of the CF cement-based sensor dependent on the load amplitude of a cyclic compressive load and time (Azhari & Banthia, 2012).

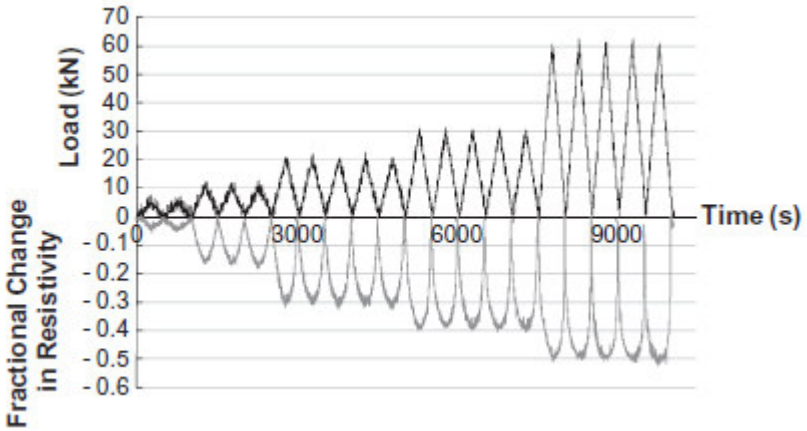

Figure 12 Piezoresistive response of CF cement-based sensor

The plot shows a good sensing behavior, since the signal-to-noise ratio, which is a term for how sensitive and accurate a cement-based sensor is to measure the FCR, is very low. The composites also show a good reversibility upon unloading, which is important for a long durability.

Konsta-Gdoutos et al. investigated the electrical behavior of CNTs and carbon nanofibers (CNF) in cement paste. In the cement composites 0.048, 0.1 and 0.3 wt% (volume percent of cement) CNTs and CNFs were added. First, the resistivity properties of unloaded sensors were evaluated. To achieve accurate and stable results, a specific amplitude of the voltage was validated. A voltage of 20 V appears as the optimum amplitude for measurements of the electrical resistance. The measurements showed, that CNTs achieve a lower resistivity of the cement composite than CNF, especially at higher

volume fractions. This behavior is illustrated in Figure 13 (Konsta-Gdoutos & Aza, 2014).

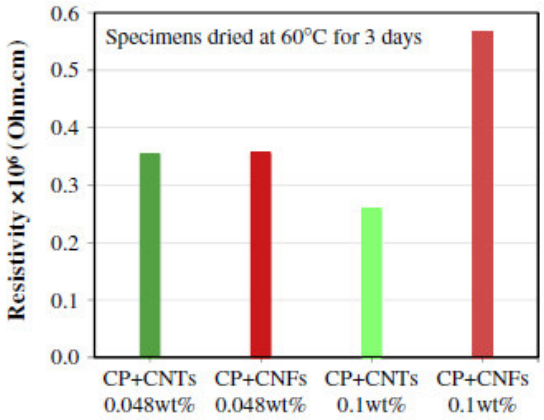

Figure 13 Average resistivity of cement-based composites with CNTs and CNFs

In regard to the piezoresistive behavior, the assembled mixture proportions show a good benefit on the self-sensing behavior. The sensors were set under a cyclic compression load. The FCR displays a reversible behavior within the elastic range. The average FCR of the cement-based composites was estimated to 5 % compared to the plain cement specimen. Hence, the tested sensors were considered to be piezoresistive (Konsta-Gdoutos & Aza, 2014).

Since, CNTs are very costly compared to other carbon materials, such as carbon fibers, it is not favorable to use CNTs as conductive phase only. Due to their size and extremely high aspect ratio, CNTs act perfect as filler in a combination with CF to improve the conductive network and refining the pore size (Azhari & Banthia, 2012). A new approach in using CNTs as conductive phase of coarse aggregates of concrete has been developed, which is less costly and more practical to use. This issue will be further discussed in chapter 4.5.2. Finalized it can be noted, that the sensitivity and the accuracy of the measurements is highly dependent on the conductive particle type and its volume fraction in the composite mixture.

4.4. EFFECT OF CURING

Besides the main factors of influencing the electrical properties of cement-based sensors such as conductive particle content or its material properties, further aspects in regard to sensor resistivity and sensitivity have to be considered. In this paragraph, the effect of curing will be shortly discussed.

The piezoresistive behavior of cement-based sensors containing carbon fibers or particulates is changing with the time of curing. From previous reviewed literature it can be seen, that the electrical conductivity can change with the advance of the hydration process (Azhari, 2008). From Figure 14 shows, that the conductivity decreases with hydration time.

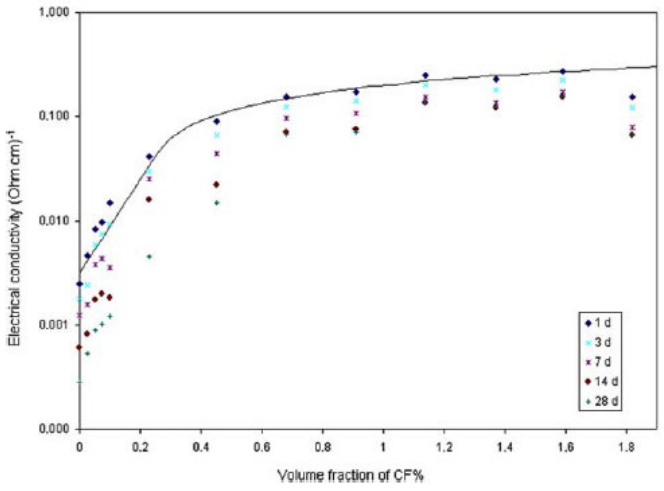

Figure 14 Effect of hydration time on carbon fiber cement-based sensors

This change can be traced back to the fact, that the pore water gets chemically bonded within the hydrates, whereas water is a good conductor of electricity. The microstructure loses moisture, which results in a decreased electron movement between the conductive phase and the matrix. This effect appears predominantly in an early age of the cement-based sensor. Additionally, it has been realized, that a composite with a

high volume fraction is less sensitive to the dehydration, since the conductive network dominates the electron transport.

4.5. APPLICATIONS OF CEMENT-BASED SENSORS

To monitor the structural health of civil infrastructures, cement-based piezo-resistive sensors must be mounted or embedded to the load bearing elements, or parts which are of pronounced interest. In Canada, several SHM systems and methods have been successfully applied to structures, such as bridges. These systems are monitoring the current health state of a structure and furthermore, observe the traffic volume on bridges. The applied systems can even work as earthquake alert systems, since structures react onto small dynamic excitation, which is recognized by the sensory system. Canada is a perfect example of implementing SHM systems to civil infrastructures, but most of the sensors, that are used for strain sensing are electrical sensors, such as fiber optic sensors or piezoelectric sensors. The use of cement-based strain sensors is extremely rare and usually used for research purposes, since an adequate mounting or embedding for practical purposes is not achieved jet. In the following paragraphs some examples for embedded cement-based sensors will be discussed. Furthermore, an alternative method of self-sensing concrete will be introduced.

4.5.1. EMBEDDED CEMENT-BASED SENSORS

Compared to traditional sensors in civil infrastructure, cement-based sensors show a high durability, high sensitivity, low cost and excellent compatibility with concrete structures. Xiao et al. investigated the sensing behavior of embedded sensors containing carbon black. The sensors contain around 9 vol.% CB and showed low resistivity values of around 7.2 Ωm. For the strain sensing, three sensors were embedded at three different

locations in a concrete beam. Since, in such an experiment the Euler beam cannot be assumed, different stress regions are investigated. Two sensors were placed in the mid-span area. One sensor in the compression stress and another sensor in the tension stress zone, to investigate the pure tension and tensile strain sensing. A third sensor was embedded near the loading point, where an additional shear stress is present. Under a cyclic load the sensors in the compressive zone responded good compressive strain sensing properties, which was precise and repeatable. The sensor in the biaxial stress zone had a reduced sensing range, because the maximum compressive strain decreases under biaxial stresses. As the beam yields in the compressive zone under monotonic loading, the sensors were sensing a decrease in strain upon unloading, but did not return to default values, since a small permanent damage occurred. The sensor in the tensile zone of the beam was able to measure the strain, but the capacity was limited, because of the small tensile deformation capacity of cement-based sensors and probably a failure in the bonding between the sensor and the concrete (Xiao, Li, & Ou, 2011). Figure 15 shows the sensing response of the three carbon black cement composites (CBCC) sensors, in direct comparison to strain gauge (SG) measurements. In all cases, the measuring is very accurate, but the sensor in the pure compression zone has the highest accuracy.

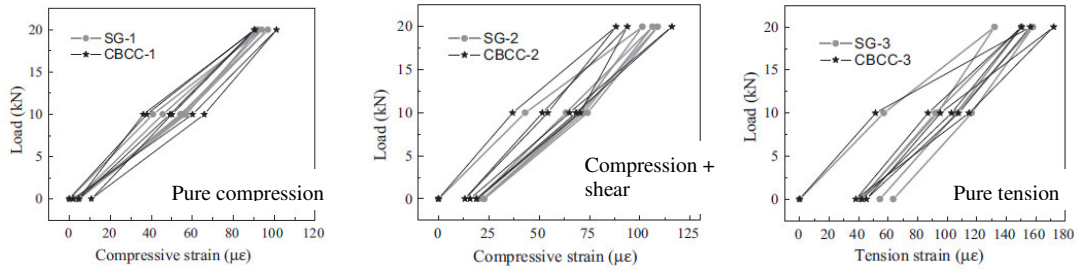

Figure 15 Cement-based sensors in three different strain zones

D'Alessandro et al. performed static and dynamic strain monitoring measurements with cement-based sensors containing 1 % of MWCNTs with respect to cement weight. Since, SHM implies a monitoring of a whole structure, or at least the most important structural elements, various sensors are necessary to extract the structural health. Moreover, it is not expedient to use just one sensor or just a few, because damage can occur at any point of the structure. To achieve a good state of the structure or to find the specific location of a damage, many sensors are necessary or a method, that is called damage mapping has to be applied, which will be shortly discussed in the next chapter. By using a various number of sensors, a proper placement is critical for accurately analyzing the structural performance. A well distributed sensing system increases the probability of finding and characterizing the amount of damage. Accordingly, seven sensors were embedded into the compression zone of a beam for a full-scale experiment. In beforehand, the electrical and mechanical sensor properties were identified. It was mentioned, that each sensor needed to be individually calibrated before embedding. It was reported, that the sensors can be used to accurately monitor in-situ strain conditions due to static and dynamic loading in the range of a few tens of micro strains within full-scale concrete structures (D'Alessandro et al., 2017).

One of the challenges of cement-based sensors is the mounting of the sensors to a structural element. Azhari embedded small 5 mm x 5 mm x 50 mm cement-based sensors containing 15 % CF to the underside, the tension area, of a beam and applied a cyclic load in a flexural four-point bending setup. It was reported, that the values for the measured FCR were measured to be negative for compression instead of positive values for tension, as expected. Furthermore, the sensing in general was very noisy and

inaccurate and after macro cracks appeared, a visible crack line around the sensor appeared. These aberrations were traced back to an insufficient bonding between the sensor and the beam (Azhari, 2008).

Whereas, the sensors are made of the material of the host structure, bonding is still an issue. The sensors are already hardened when they are embedded to the structure and consequently do not form a continuous and homogeneous material. So, under tension gaps or cracks appear between the sensor and the host, which creates problems with the sensing response.

Another issue is that most of the currently developed cement-based sensors do not have the same material structure as the host. Conventional concrete beams contain fine and coarse aggregates for a better load transfer through the material and cement as the binder. Cement-based sensors are made of pure cement paste containing the conductive phase. This creates a big difference in strength and stiffness between the sensor and the host material. This problem addresses the next few paragraphs, which discuss a new method of creating a self-sensing piezoresistive concrete.

4.5.2. USE OF A CONDUCTIVE INTERPHASE

Some applications of cement-based sensors have been realized in several projects for civil infrastructure. But, since the mounting into or on structural elements is still not perfectly achieved, new methods to create a self-sensing concrete have been developed. One of the newly achievements, is a self-sensing concrete, which is enabled by nanoscale composite cement-aggregate interphases.

A common problem, which is especially critical for practical applications, where large quantities of conductive additives are needed, is the dispersion of small nanoscale

conductive particles in the cement, mortar or concrete matrix. As mentioned, an insufficient dispersion can lead to a degradation of the mechanical properties and no significant advantage in the electrical conductivity. Additionally, most of the recent investigations with cement-based sensors deal with plain cement-paste containing a conductive phase, which is not practice-oriented, since in a common concrete material, fine and coarse aggregates are always present.

A new approach to create a conductive network, is to alter the cement-aggregate interface by using a conductive coating, instead of dispersing conductive particles in the cement matrix. Since, in a common concrete mixture fine and coarse aggregates are finely tuned and well distributed to be in close contact and to form a compact structure for a high compressive strength, since the main load transfer in a concrete is achieved by the aggregates, coated aggregates would create a dense conductive network. The cement matrix is necessary to bond the aggregates (Gupta, Gonzalez, & Loh, 2017).

The conductive coating is based on a latex polymer, which contains a specific amount of MWCNTs. An incorporation of CNTs inside of highly viscous polymers can be synthesized by emulsion polymerization such as polystyrene (PS) or polymethylmethacrylate (PMMA) (Yu et al., 2007). The MWCNTs are dispersed in an aqueous solution by ultrasonication before the latex polymer is added to obtain the MWCNT-latex ink. Afterwards, the highly conductive latex ink is spray painted by airbrushing onto the fine and coarse aggregates (Figure 16). The final coating should have a uniform distribution on the aggregates and a thickness of a few microns. It should be noted, that the CNT-based thin films are directly coated onto the surface of the aggregates. After drying of the fresh film-coated aggregates, they are used as is to cast

the final concrete. The embedded thin films are uniformly distributed within the cementitious composite to form a dense network and provide a highly conductive concrete (Gupta et al., 2017).

Figure 16 Spray painting of conductive MWCNT-latex ink onto fine aggregates

Since the CNT-latex ink is a mixture made of MWCNTs and latex polymer, the electrical and mechanical properties of the composite have to be obtained from the homogenized material. By adding a decent amount of CNTs to latex, the mechanical and electrical properties of latex as well, are significantly improved. Whereas, MWCNTs show excellent material properties for strain sensing, such as a very high electrical resistivity of up to $1x10^{-7}$ Ωm (Table 2), latex has very low mechanical and electrical properties, such as tensile strength and electrical conductivity respectively. Yu et al. reported an increase of electrical conductivity of MWCNT thin films from $1x10^{-10}$ S/m to about $1x10^{3}$ S/m (Yu et al., 2007). Further material properties of the conductive ink are shown in Table 3 It has to be noted, that the electrical conductivity varies dependent on the volume fraction of MWCNTs.

Table 3 Material properties of CNT thin films

	CNT thin films
Film thickness [μm]	20 – 100
Young modulus [Pa]	~ 3 x10^9
Poissons ratio	0.4
Specific gravity [kg/m³]	~ 1500
Electrical conductivity [S/m]	~ 1 x10^3
Relative permittivity	6.5

The biggest difference but also advantage of adding a conductive interphase to the concrete aggregates to long-time investigated cement-based sensors containing MWCNTs is, that the final product will be a conductive concrete, instead of a conductive cement paste. Investigations with conductive cement-paste containing fine and coarse aggregates to form a conductive concrete have been reported, but it was mentioned, that this approach did not lead to the expected or required results. Concrete with a conductive cement-paste did not show an increasing conductivity, which can be traced back to a low CNT distribution to form a conductive network. By creating a conductive interphase around the concrete aggregates, a highly conductive network will be present, which creates more flexibilities and opportunities to apply self-sensing cementitious composites to a structure.

A major drawback that has been reported in previous literature is the impact of CNT thin films on the mechanical properties of concrete. It was noticed, that coating the aggregates diminishes strength and bond between the aggregates and the cement matrix. This phenomenon was primary recognized by coating the coarse aggregates. Furthermore, it was mentioned, that the coating could create a smother surface, which would reduce the effectiveness of bonding. Fortunately, by coating sand, no adverse effects seemed to be produced (Gupta et al., 2017).

By creating a conductive concrete, new possibilities for strain-sensing and damage detection systems are given. Whereas, cement-based sensors have to be embedded to multiple locations of a structural element to form a sufficient sensory system and to determine the current health status, the whole element would be conductive with coated aggregates. This gives the opportunity to monitor any part of a structural element and not just one or multiple specific locations. A method, which is called electrical impedance tomography could be enable strain-sensing and spatial damage detection by creating a damage map of the element. To achieve a proper sensing, electrodes have to be placed around a structural element, which enable the flow of a current through a structure. By measuring the resistivity of the concrete between two opposite electrodes a resistivity mesh can be created, which gives information about strain or damage. This method of monitoring the structural health was investigated by Gupta et al., who created conductive concrete plates with drilled holes to study the behavior of this method, when it is applied to concrete containing CNT thin film-coated aggregates. By creating a concrete with coated fine and coarse aggregates they achieved a very exact sensing behavior of the composite. Figure 17 shows one example of a conductive concrete plate with two drilled holes and the correspondent damage map as a change in resistivity (Gupta et al., 2017).

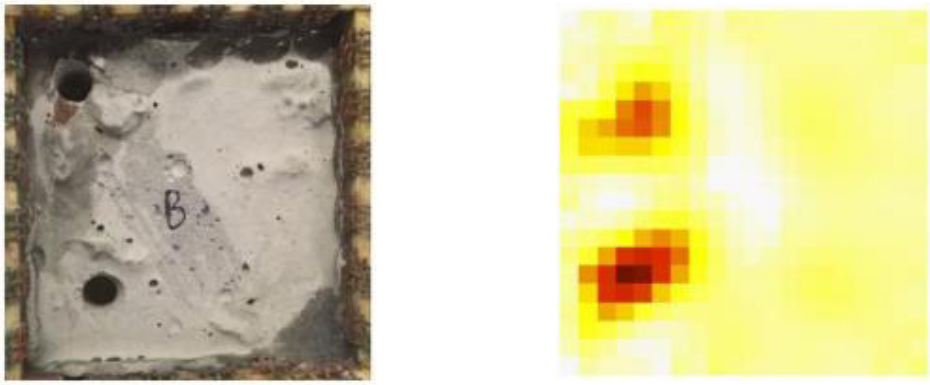

Figure 17 Result of EIT measurement for damage detection of conductive concrete

The shown experiment was conducted just with small specimens, because of a better validation for research purposes, but this method could also enable structural health monitoring of real structural elements, such as concrete bridge decks or beams, since this method is using real structural material, as it is the host material. No further actions have to be performed to embed or attach an external sensor, such as strain gauges or cement-based sensors, which should give a higher accuracy in sensing and predicting damage. In conclusion, since this new method is just in the beginning of its potential, the increase of research in this field is well invested.

5. MICROSTRUCTURE GUIDED NUMERICAL SIMULATION FRAMEWORK AND ANALYSIS

Within this thesis, the electro-mechanical behavior of piezoresistive cement-based composites enabled by adding a conductive interphase in the microscale will be investigated. In a first step the electrical and mechanical behavior will be determined separately until the interaction will be considered. In general, an accurate prediction of effective elastic properties is a challenging task, especially by dealing with highly heterogeneous materials with multiple microstructural phases. A reliable classification and characterization of incorporated phases in terms of its volume fractions, size distribution and default elastic properties are important for a precise analysis. Multiple analytical and numerical analyses have been performed to achieve accurate results in the material property prediction. This thesis specifically deals with a numerical approach of characterizing conductive cementitious materials. Since there have been achieved tremendous improvements in terms of computational efficiency, finite element method (FEM) has become one of the most efficient numerical approaches to calculate the approximate material properties (Das et al., 2016).

This thesis follows a comprehensive microstructure-guided property prediction scheme, whereas the final result does not show exact material properties, it rather demonstrates the piezoresistive behavior of cement-based composites obtained by conductive interphase coated fine cement aggregates. In the following paragraphs, the procedure of the generation of the microstructure and the finite element analysis for these kinds of materials will be explained, to obtain a better understanding of the analysis results.

As of now, it has to be mentioned, that the whole process is based on the homogenization of a composite material in the microscale. This means an area-averaged material property for a composite with multiple phases, that have different material properties, is conducted to show the material property for the whole composite. These homogenized values can be used for further investigations of a macroscale model or as material properties of a material, that is used as matrix within another microstructure. The general process for the homogenization of a random two-dimensional (2D) microstructure is shown in Figure 18.

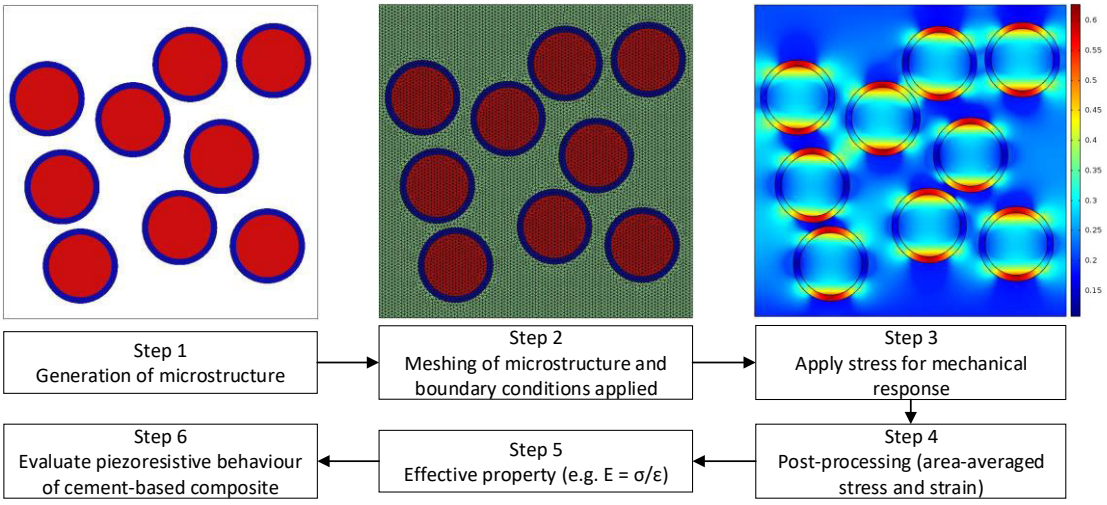

Figure 18 Modeling scheme for a general numerical homogenization

The first step includes the generation of the microstructure, which will be further discussed in chapter 5.1. In the second step of the homogenization, the generated microstructure must be meshed, and all required boundary conditions have to be applied. This step is described in chapter 5.2. After meshing and building the model for the simulation, a deformation or load to the microstructure is applied and the simulation is computed to receive the solutions for the analysis. In a following step, the computed results must be averaged over the area of the microstructure to get an overall value for the response. These values are necessary for the post-processing and to calculate the

effective property of the microstructure. For example, in a mechanical analysis stress and strain could be computed as a response of a mechanical applied strain to the boundary conditions. After averaging the stresses and strains inside of the microstructure, the Youngs modulus of the randomly created composite microstructure can be calculated. Finally, the calculated properties can be used in further analysis. Step 3 to 6 are discussed in more detail in chapter 5.4.

5.1. GENERATION OF MICROSTRUCTURE

The center of interest in a numerical FEM analysis for heterogenous materials is to achieve a precise prediction of the material behavior. Therefore, a microstructure, which adequately represents the material characteristics in the macroscale, must be artificially generated. These microstructural elements are called representative volume elements (RVE). In the understanding of the function of an RVE, it must be clear, that these elements represent the microstructure of a material at a very small random position in a macroscale element, such as a concrete beam. In the macroscale model, the microstructure usually differs in any position, so the RVE just picks one position and averages the material behavior of the whole material in the macroscale. By creating an RVE, one analysis should lead to a convergence in the predicted properties. That is why the inputs, such as phase fraction, distribution, phase properties and the size of the RVE have to be chosen extremely carefully. An RVE, which represents the materials microstructure, can be a 2D or three dimensional (3D) unit cell (Das et al., 2016).

For the generation of the RVE a microstructural stochastic packing algorithm with inputs from actual microstructural features was used. This specific algorithm is called Lubechevsky-Stillinger algorithm, which generates randomly distributed non-over-

lapping disc particles in a 2D square RVE (Lubachevsky & Stillinger, 1990). By giving the algorithm a specific volume fraction and size distribution of the different phases, the desired number of particles are randomly distributed inside of the boundary box. From previous research, it is known, that an RVE size with a length, that is five times larger than the largest particle size, achieves the most accurate results (Das et al., 2016).

Each particle has a random initial velocity and the initial radius of each particle is set as zero at time t = 0. If all particles have the same growth rate, all particles are ending up with the same radius. For a multi-dispersed packing, different growth rates are generated. The random distribution follows, after one particle is fixed, whereas the rest of the particles is placed randomly around the first particle. After positioning the infinitesimal particles, the discs are generated at each node, whereas the radius of i^{th} particle (r_i) is a function of the growth rate (g_i), which is fitted to attain a defined particle size distribution (Equation (12)).

$$\frac{dr_i}{dt} = g_i \tag{12}$$

$i = 1, 2, \ldots$ describes the number of particles. As a result of the growth of particles with time, collisions become possible. The growth rate between two time-increments t^n and t^{n+1} is computed by using a finite difference scheme (Equation (13)).

$$g_i = \frac{(r_i^{n+1} - r_i^n)}{\Delta t} \tag{13}$$

The particle radii are then updated as follows for time t^{n+1} by employing the growth rate and time increment (Δt) (Equation (14)).

$$r_i^{n+1} = r_i^n + g_i \Delta t \tag{14}$$

In addition, the position of each particle i at time t^{n+1} is updated considering a constant velocity (v^n_i) between the time nodes (Equation (15)). While growing occurs, the particles are moving with its initial velocity until the best packing is achieved.

$$x_i^{n+1} = x_i^n + v_i^n \Delta t \tag{15}$$

The branch vector that connects the centers of two particles i and j is obtained by subtracting the position vectors of the two particles (Equation (16)).

$$I_{ij}^{n+1} = x_j^{n+1} - x_i^{n+1} \tag{16}$$

The particles i and j are in contact if the sum of their radii is equal to the length of the connection vector. The time step size can be calculated as Equation (17).

$$\Delta t = \min\left[\frac{-V \pm \sqrt{V^2 - UW}}{U}\right] \tag{17}$$

Where $\Delta t > 0$ and V, U and W are given as Equation (18) – (20).

$$V = I_{ij}^n.[v_j^n - v_i^n] - [r_i^n + r_j^n][g_i + g_j] \tag{18}$$

$$U = [v_j^n - v_i^n]^2 - [g_i + g_j]^2 \tag{19}$$

$$W = [I_{ij}^n]^2 - [r_i^n + r_j^n]^2 \tag{20}$$

The time step calculation (Equation (17)) is performed for each particle pair, that is being able to collide and thus a minimum time step for all the possible collisions is adopted to move forward for the next event. Moreover, checkups for particle contacts and post-contact velocities are performed for every time step. All the particle positions x_i^{n+1} are updated using the forward Euler scheme (Equation (15)) and new search for next collision is started. The post-contact velocities are computed with Equation (21).

$$v_{n_i}^{n+1^+} = \min\{v_{n_i}^{n+1^-}, v_{n_j}^{n+1^-}\} - g_i \quad v_{n_j}^{n+1^+} = \max\{v_{n_i}^{n+1^-}, v_{n_j}^{n+1^-}\} + g_i \tag{21}$$

To find the final geometry, this iterative procedure has to be repeated several times. By repeating all the above-mentioned steps, the particles change their position in the defined boundary square, collide and grow until it reaches the defined volume fraction (Meier, Kuhl, & Steinmann, 2008). To even avoid contact between adjacent discs, the relative or total distance between the discs can be adjusted. The process of particle growth stops before collision appears. The relative distance is set as a ratio dependent on the particle diameter.

For preliminary investigations of the piezoresitive behavior of coated cement aggregates enabled by a conductive paint, a 2D-RVE was selected and set to be a square with equal side length l_{RVE} x l_{RVE}. Sand was chosen to create the fine cement aggregates and was added with a volume fraction of 30 % in the cement matrix, which seemed to be a good starting point for preliminary analysis. Since, no information about the percolation threshold of coated aggregates with conductive paint in cement paste for electrical conductivity was found within a literature review, the system parameters such as volume fraction and coating thickness of the interphase were obtained from research investigations in similar fields to estimate a good sensing behavior for a conductive cementitious material.

The size of the sand grains was fixed to 0.2 mm in diameter, which results in a 1 mm x 1 mm RVE size to obtain the size ratio of 1:5. The coating thickness was set to a relative thickness in respect to the sand aggregates of 0.1. The coated sand aggregates were then randomly distributed in the cement matrix, which created ten inclusions. A minimum relative distance between particles in respect to the inclusion diameter was

set to 0.05 to avoid overlapping of the coatings. The randomly created micro structure is illustrated in Figure 19. The black outline defines the RVE boundaries. The red colored discs represent the fine sand aggregate which are coated with the CNT thin film-ink, which is blue colored.

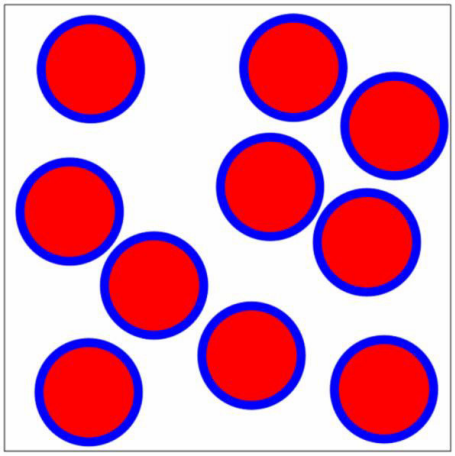

Figure 19 2D microstructure with CNT thin film-coated fine aggregates

After the successful generation of the microstructure, which considers all predefined boundaries, such as particle volume fraction, size and particle distribution, the information are saved as an .iges file to finally obtain a drawing exchange format (.DXF) which can be imported by COMSOL Multiphysics™.

5.2. CONSIDERATION OF BOUNDARY CONDITIONS

To numerically investigate the piezoresistive behavior of a cementitious composite material at the microscale, a 2D FE model was developed by using the software COMSOL Multiphysics™ v. 5.3. To describe the piezoresistive behavior, a mechanical-electrical analysis must be applied to the imported microstructure. The general approach to model this phenomenon was to perform a mechanical analysis, where the simplified 2D microstructure gets deformed by applying a mechanical stress. This deformation results in a change in particle distance. By applying an electrical analysis onto the

deformed structure, the electrical conductivity of the new model can be obtained. By comparing the electrical conductivity of the undeformed and deformed microstructure, an FCR can be measured. In the following, all necessary boundary conditions and tasks to create a model for the numerical analysis will be discussed.

In COMSOL Multiphysics™ physics are added to the model to define the type of analysis and the required properties such as material properties and element type. The physics module solid mechanics was applied to the model, to perform the mechanical part of the analysis. Within the solid mechanics module connections, springs, damper or different constrains can be attached to the model. To represent a uniaxial stress-state inside of the microstructure one fixed constraint at the bottom, two rollers at the left and right side and a prescribed boundary load at the top of the microstructure was applied. The fixed constraint prevents the structure from moving in x- and y-direction and the rollers from moving only in x-direction. To model the deformation in y-direction a negative uniform distributed stress was chosen. At this point, it has to be noted, that a deformation of a microstructure in consequence of an applied constant strain, would be more scientific, but COMSOL Multiphysics™ does not provide this feature.

To predict the electrical response of the undeformed and deformed microstructure an electric current module was employed. With the electric current physics, it is possible to apply different electrical boundary conditions (BC), such as an electric potential, current density, electric insulation or ground. To apply an electrical current to the microstructure, which crosses the RVE in y-direction, an electric potential at the top and a ground BC at the bottom was specified. The sides of the RVE possess electric

insulation BC. The amount of electrical current at the top BC was set to 1 V whereas the ground BC ensures a zero potential.

To finalize the model of the microstructure, the BC between the inclusions and the matrix have to be defined. In a first approach the sand-coating contacts and coating-cement paste contact as well, were assumed to be perfectly bonded. By defining a unified geometry, all elements were created as one part.

5.3. MATERIAL PROPERTIES AND CHARACTERISTICS

To sum up the building of the model, all properties of the incorporated materials were defined. The used values were obtained by previous researches and papers, that deal with cement-based composites and latex-based CNT thin film-coating. The used parameters and properties are shown below in Table 4. Regarding to the existing mechanical properties, the fine sand aggregates show the highest stiffness before the cement paste. The coating has the lowest stiffness, since the host material of the matrix consist of a latex polymer. The Poisson's Ratio and material density of sand and cement paste are in a similar range, whereas the coating shows a high Poisson's ratio and a very low density. In terms of the results of the mechanical analysis, higher stress or strain values and a higher deformation are expected in the coating interphase, because of the soft polymer structure.

Referring to the electrical properties, the CNT-latex coating shows a very high electrical conductivity compared to the sand aggregates and the cement matrix. Accordingly, a low current density in the coating is expected, because of the remarkable conductivity of the coating.

Table 4 Material properties for mechanical and electrical FE analysis

	CNT thin films	Cement matrix	Sand aggregates
Young modulus [Pa]	3×10^9	20×10^9	90×10^9
Poissons ratio	0.4	0.2	0.25
Specific gravity [kg/m³]	1500	3150	2710
Electrical conductivity [S/m]	1×10^3	2×10^{-3}	1×10^{-14}
Relative permittivity	6.5	20	4.5

Cement is a hydraulic-setting binding agent, which hardens as a result of a chemical reaction with water and the cement clinker phases. The main ingredient of cement is Portland-cement-clinker, which contains four different clinker-phases. These clinker-phases are formed, when fine granulated limestone gets fired within a firing process in a rotary kiln at around 1450° - 2000° C. In the reaction with water calcium silicate hydrate phases (CSH phases) are formed, which form a crystalline structure, that provide the concrete strength, density and durability. The four different clinker phases are tricalcium silicate (C_3S), dicalcium silicate (C_2S), tricalcium aluminate (C_3A) and calcium aluminate ferrite ($C_4(A,F)$). The fast strength development contributes to C_3S and C_2S. To slow down the reaction of the cement with water, gypsum is added, which first forms ettringite. Ettringite slows down the reaction between water and C_3S and C_2S. The formed ettringite dissipates after 30 minutes and the cement hydration speeds up. C_3A and $C_4(A,F)$ are responsible for the hardening in a higher age of the concrete, which means that the concrete gains stiffness with the time and also more water is used for these reactions (Kay Ackermann, 2016).

For cement-based piezoresistive composites, this means the older the cement gets the less water contains the cement matrix. Since water is basically the only conductive material in the cement matrix, the conductivity decreases with the time. A good value

for the infinite cement conductivity was obtained from previous literature by (García-Macías et al., 2017).

As aforementioned, the latex-CNT thin film-coating has a lower stiffness, as cementitious materials. This is due to the chemical structure of the latex-polymer. Latex can be described as a stable dispersion of polymer particles in an aqueous medium and can be classified as a thermoplastic elastomer (TPE). The amorph polymer structure of TPE has wide-mesh crosslinked macro-molecules of monomers, with rather weak chemical bindings such as hydrogen bindings and Van der Waals forces (VdWf). These bindings are highly temperature dependent and decisively define the materials mechanical properties. In general, TPE materials show a low density, chemical resistance and low thermal and electrical conductance. Their service temperature usually remains in an entropy-elastic range, which means the material stiffness is highly temperature dependent. With increasing temperatures, stiffness is decreasing (Schneider, Kuntsche, Schula, Schneider, & Wörner, 2016).

In terms of cement-based composites, the temperature dependency could be a problem because of the present hydration temperature inside of the concrete. But an issue of higher relevance is the electrical conductivity of the coating. To provide a conductive behavior, CNTs are added to the latex-polymer. Since, the electrical and mechanical properties as well, of the CNTs are extremely good, they highly affect the material properties of the polymer. The electrical conductivity and mechanical stiffness of the host will get increased. The necessary material properties for the mechanical-electrical analysis were obtained from previous research and reviewed literature (Yu et al., 2007).

Further material properties, such as mechanical properties of sand grains were obtained by Daphalapurkar et al. who performed nanoindentation to determine the stiffness of sand grains (Daphalapurkar, Wang, Fu, Lu, & Komanduri, 2011). The electrical conductivity of sand grains was hard to obtain, so a very low electrical conductivity was assumed, because of an extremely low water content.

5.4. FINITE-ELEMENT-BASED ELECTRO-MECHANICAL SIMULATION

5.4.1. BASICS OF FINITE ELEMENT ANALYSIS

After a successful generation of the model and assigning of all required materials, the next step of the analysis would be the meshing of the microstructure. The model meshing is the key step for an accurate prediction of the composites material parameters. It is very important to understand the function of the meshing, what types of meshes are used and what are the differences between the mesh-types. The general approach to solve structural mechanics problems is called displacement or stiffness method. These methods use the meshing to describe the system properties and perform the analysis. In 2D-systems, such as an RVE, basically two types of meshes are used. These are three-node triangular elements and four-node rectangular quadrilateral elements with corner nodes or higher order elements with intermediate nodes (Figure 20).

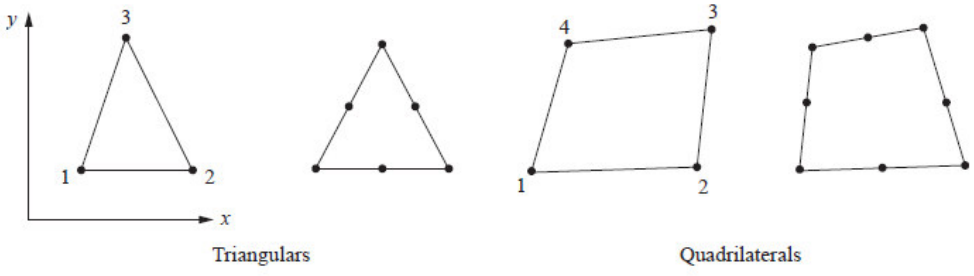

Figure 20 Illustration of two-dimensional elements

These types of elements are usually used for 2D analysis. A structural element or in this case the RVE is divided into many discrete sub-regions of finite size, which are called finite elements, which have a specific type. Dependent on the dimensions of the model, the different types of elements can result in different solutions for the predictions of stress. In cases, where many circular elements are present, triangular mesh elements show a better accuracy than quadratic elements. In other words, triangular elements can more closely approximate boundaries of irregularly shaped bodies.

Each 2D element consists of at least two nodes and a line. The most basic element is defined as a linear element, where the nodes, connected by a straight line, have two degrees of freedom, in x- and y-direction (Figure 21). A triangular element contains three of the basic linear elements, that enclose a specific area. By using the displacement method within a stress analysis, after selecting an element type, the displacements of each node are calculated. Later, these displacements are set in relation to stress and strain.

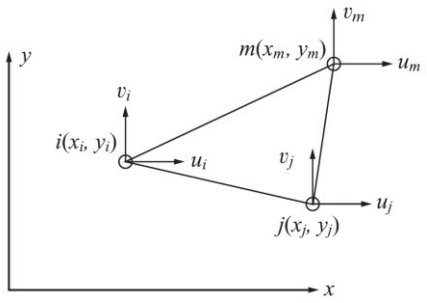

Figure 21 Illustration of a basic triangular element with showing degrees of freedom

The general steps of performing a basic FE analysis are discussed shortly in the following paragraphs. The first step is to discretize the structure and select the element types. By choosing a coarse mesh with big elements, the analysis runs very quick, but the results tend to be inaccurate in predicting the real situation. With a smaller element

size the computing effort and time will increase, but the results show a more realistic prediction. It is up on the user, which effort is put in the meshing and how accurate the results should be. In general, the elements must be made small enough to give usable results. Sometimes, mesh refinements can be applied in areas, where a dense meshing with small elements is required to show the real behavior. In the rest of the structure, the mesh can be rather coarse to minimize the computational effort. The second step involves a selection of a displacement function within each element. Afterwards, the relationship between strain and displacement and stress and strain must be defined. In step four, the element stiffness matrix and equations are derived. The element stiffness matrix includes the material properties of the finite element and describes the stiffness of each element. Accordingly, this matrix is a fixed property and does only change, if initial material parameters or the shape of the elements are changed. Within the next step, the element equations are assembled to obtain the global or total equation to describe the whole structural element. Furthermore, the global nodal equilibrium equations are defined, which set the structures stiffness matrix in relationship to exterior boundary conditions, such as forces and support conditions. This final assembled global equation is shown with equation (22) expressed in matrix form.

$$[F] = [K][d] \tag{22}$$

Whereas, [F] is the vector of global nodal forces, [K] is the structure global stiffness matrix, which is usually square and symmetric and [d] it the vector of known and unknown structure nodal degrees of freedom or generalized displacements. Known displacements are for example structural supports, which have the value zero in the displacement vector. After all forces and known displacements are identified, the

unknown degrees of freedom are calculated by using the algebraic equations (Equation (23).

$$\begin{Bmatrix} F_1 \\ F_2 \\ \vdots \\ F_n \end{Bmatrix} = \begin{bmatrix} K_{11} & K_{12} & \dots & K_{1n} \\ K_{21} & K_{22} & \dots & K_{2n} \\ \vdots & & & \vdots \\ K_{n1} & K_{n2} & \dots & K_{nn} \end{bmatrix} \begin{Bmatrix} d_1 \\ d_2 \\ \vdots \\ d_n \end{Bmatrix} \tag{23}$$

The final step is to solve the equations for the element strain and stresses and interpret the results. Whereas, the unknown displacements are calculated for each element node, stresses are usually assumed to act at the centroid of each element. To receive a field output with a continuous visualization of stress or strain in the structure, the results are interpolated between each element. Sometimes this could still cause jumps between each boundary of adjacent elements, so mostly an average element output is applied (Logan, 2002).

For extremely coarse meshes and simply structures, this procedure could be performed manually. In most cases, structures and especially in the case of analyzing RVEs are very complex with up to several million elements, these calculations are performed by computers. With the increasing computational capacity, systems can get more advanced and complex. The discretization of the models can get more defined with still the same computation time. The explained procedure refers to a structural mechanical analysis, but this principle can be adopted to a numerical electrical analysis, to calculate the electric potential, electric field or current density at any position in the microstructure.

5.4.2. CONTINUOUS UNIFIED STRUCTURE

The basic intention behind performing a FE analysis, is to predict the overall material performance as a result of an applied stress or electric potential expressed as

one overall material parameter. The method behind this procedure is called numerical homogenization and aims to achieve an accurate prediction of composite material parameters. Therefore, the calculated responses of each finite element are summarized or averaged to obtain effective area-averaged RVE responses. These averaged responses represent the new properties of the composite material. This homogenization is conducted for the undeformed and deformed microstructure (Das et al., 2016).

To run a study with the predefined model and applied boundary conditions a FE mesh must be generated. In COMSOL Multiphysics^{TM} a physics-controlled mesh with a free triangular element type and an extremely fine discretization with about 17 500 elements was generated. The generated mesh of the RVE is shown is Figure 22.

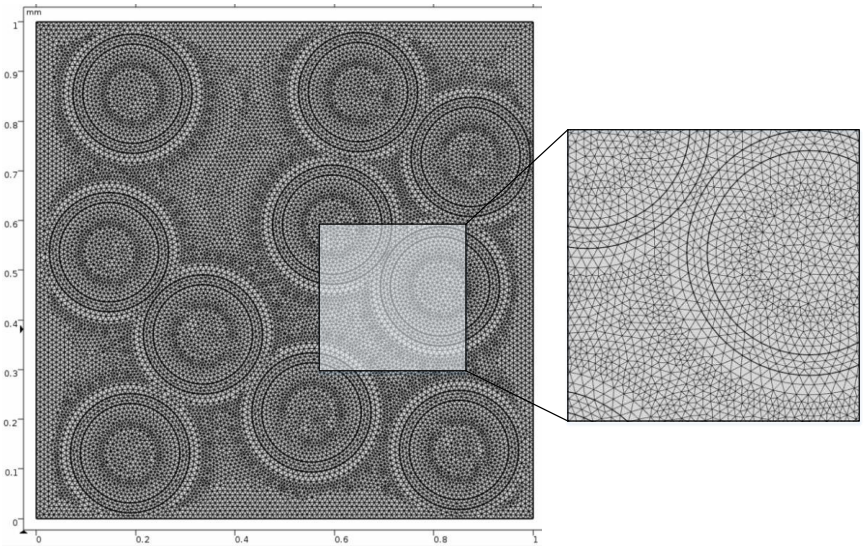

Figure 22 Meshed RVE with a triangular element type

To get the results for the solid mechanics analysis, a stationary study was applied to the meshed model. The stationary study applies a static load, holds it and expresses the results for the displacement, stress and strain response, which are required to calculate the Youngs modulus of the composite material. The next step for the mechanical-electrical analysis to obtain the piezoresistive behavior of the matrix was to

record the deformed geometry and export it as a new geometry for the electrical model, since COMSOL Multiphysics™ does not provide a coupled mechanical-electrical analysis, so two separate analysis had to be applied to the microstructure. Figure 23 illustrates the basic work flow of the mechanical-electrical analysis. Step 1 shows the generated microstructure, which accounts as the RVE for the numerical FE analysis. Step 2 includes the solid mechanics analysis with the application of BC and meshing of the RVE. In step 3, the exported deformed geometry, from the mechanical analysis, is implemented into an electrical analysis as a new geometry.

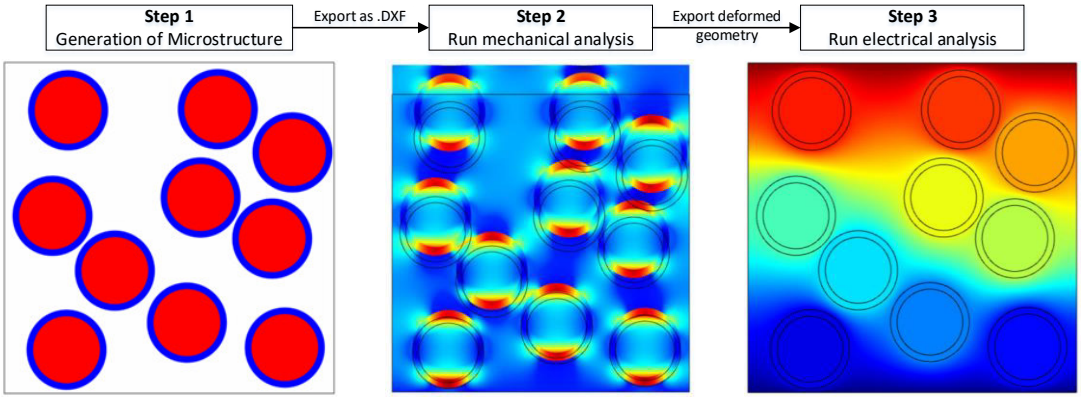

Figure 23 Illustration of the work flow from RVE generation to electrical analysis

After completing the mechanical part of the analysis, the electrical analysis was performed. First, an electrical analysis with the undeformed microstructure was performed to obtain the initial material parameters. The BC for an electrical current analysis were applied and a frequency domain study was conducted. The frequency of the applied alternating current was set to 100 Hz, which was reported to show good results. It was also mentioned, that the conductivity in a composite, comparable to this study, was generally invariant at frequencies greater than 100 Hz (Yang et al., 2018). The desired results for the electrical study were a field-output of the electric potential,

electric field and current density in y-direction, to calculate the electrical conductivity in accordance to equation (24), based on the knowledge from chapter 3.1.2.

$$\sigma = \frac{< J >}{< E >} \tag{24}$$

In this equation J (A/m²) expresses the homogenized or area-averaged current density and E (V/m) the area-averaged electric field. The ratio between these values equals to the area-averaged electrical conductivity σ (S/m). It must be noted, that the frequency domain study with an applied AC circuit shows complex values as results. As mentioned in chapter 3.1.1, the resulting impedance of an AC circuit has a real part, the resistance and an imaginary part the reactance. In this study, only the resistance does matter, so only the real part of the complex impedance is of high interest.

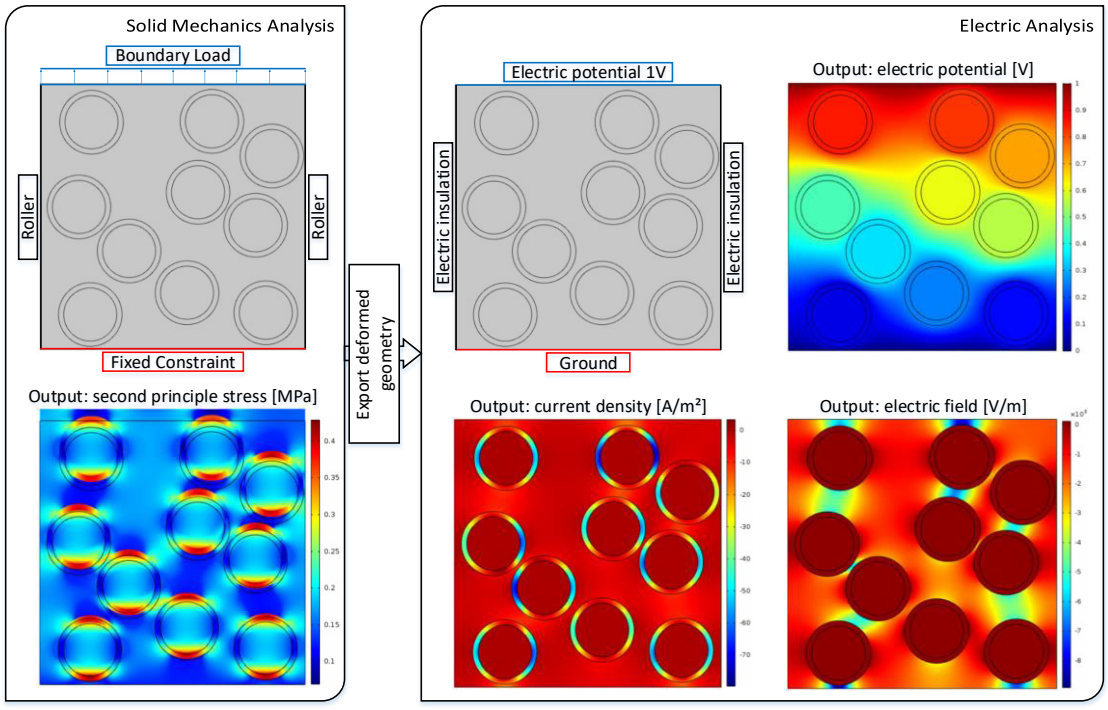

Figure 24 Illustration of the modeling scheme incl. BC and all required field outputs

After computing the initial electrical values for the undeformed RVE, the electrical analysis was performed for the deformed geometry. The exported deformed geometry

from the mechanical analysis was imported as a new geometry in COMSOL Multiphysics™. The electrical physics, such as material properties and boundaries were assigned, and a new triangular mesh was generated. After computing the frequency domain study with an applied frequency of 100 Hz, the results were exported and homogenized to calculate the area-averaged electrical conductivity of the deformed system. Figure 24 shows the complete modeling scheme for the mechanical-electrical analysis. In the left box, the mechanical analysis is illustrated. All required model BC are shown and the field output for the second principle stress in y-direction. From the stress plot it can be seen, that the highest stresses are in the coatings. This is due to the small stiffness of the material, compared to the cement and aggregates. The right box shows the electrical analysis, including the necessary model BC and field outputs for the electrical response in y-direction, respectively. From the plot of the electric field, the current flow through the RVE can be extracted. The light-blue areas in the microstructure show, where the current density is very high, consequently it shows the easiest way for the current to cross the RVE.

The final step of the mechanical-electrical analysis was to calculate the FCR to show the piezoresistive behavior of cement based CNTs thin film-coated cement aggregate composites. Therefore, the area-averaged conductivity was used to calculate the bulk resistance of the RVE by using equation (25).

$$\sigma = \frac{L}{RA} \tag{25}$$

Where L (m) is the length and A (m²) the area of the RVE. Under consideration, that all numerical RVEs have the same cross section area and length, the FCR can directly calculated with equation (26) (Yang et al., 2018).

$$\frac{\Delta R}{R_0} = \frac{\sigma_0}{\sigma_1} - 1 \tag{26}$$

Where σ_0 (V/m) is the area-averaged conductivity of the undeformed RVE and σ_1 (V/m) the area-averaged conductivity of the deformed RVE. Otherwise, the resistivity of the undeformed and deformed geometry has to be calculated and equation (8) must have been used.

To show the variation in FCR and the related strain-sensing ability upon different external loads, different stress states were applied to the RVE, within the mechanical analysis. The different conducted stresses cause a variation in deformation of the RVE, which results in a change in contact distance of the coated aggregates. Because of this change in particle distance, a change in resistivity between different stress states was expected. It has to be noted that the applied stresses were in the range of 0 – 1 MPa to stay within the elastic range of the cement matrix, which is at around 1.4 MPa.

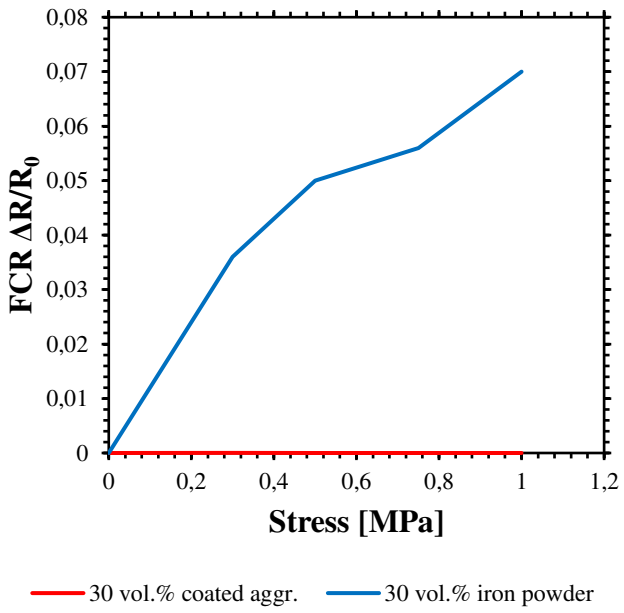

Figure 25 FCR of cement-based composites upon different loading

As a result of the mechanical-electrical analysis with the described microstructure, the measured FCR in consequence of the applied stresses shows extremely low values in the range of 9.3 $x10^{-6}$ to 18.5 $x10^{-6}$ %, whereas the change of the FCR between the different stress states was less than about 3 $x10^{-6}$ %. This means, that basically no strain-sensing takes place. Compared to a piezoresistive analysis of a cement matrix containing 30 vol.% iron powder (IP), where the FCR shows a significant change, the changes in this analysis are rather neglectable. An obvious mismatch in the sensing ability is recognized, independent of the used conductive material in the cement matrix. A first guess for the present behavior is an extremely low change in the contact distance between adjacent aggregates. Since all particles have the same size, the displacement of these particles takes place in an equal manner and is additionally very low. A new approach with a better aggregate size distribution should avoid this phenomenon and should result in a higher, more significant change in resistivity.

5.4.3. SIZE DISTRIBUTION OF AGGREGATES

The second approach of predicting the piezoresistive behavior of a cement-based composite with a numerical FE analysis was, to investigate the change in conductivity by generating a microstructure containing size distributed coated fine and coarse aggregates. The theory behind this approach is from mechanical origin. Due to the substantial difference in the aggregates size, inclusions are displaced differently within the matrix. Bigger particles are less displaced than small particles, because of their bigger surrounded area. This prevents the big inclusions to move within the matrix, when an exterior stress is applied. Theoretically, due to the higher displacement rate of small aggregates in regard to the coarse aggregates, the change in contact distance

between adjacent particles should be larger. Accordingly, a larger FCR is expected within this analysis.

The microstructure generation and the FE analysis follows the same modeling scheme as in the previous chapters. Compared to the first study, two different types of inclusions were generated, to achieve a better size distribution between the fine and coarse aggregates. Fine aggregates represent fine sand with a size distribution from 1 mm to 3.8 mm in diameter and coarse aggregates should represent gravel with a size distribution of 4.75 mm to 19 mm. The volume fraction of the coarse aggregates was set to 40 vol.% and the volume fraction for fine aggregates to 30 vol.% to achieve an overall aggregate volume fraction of 70% in the cement paste matrix. Both types of aggregates were modified with the conductive coating, which was set to a volume fraction of 4 vol.% of the aggregate volume. The generated RVE is shown in Figure 26, whereas the red areas are coarse gravel aggregates, the yellow areas define the fine sand inclusions and the blue areas define the conductive coating of the aggregates.

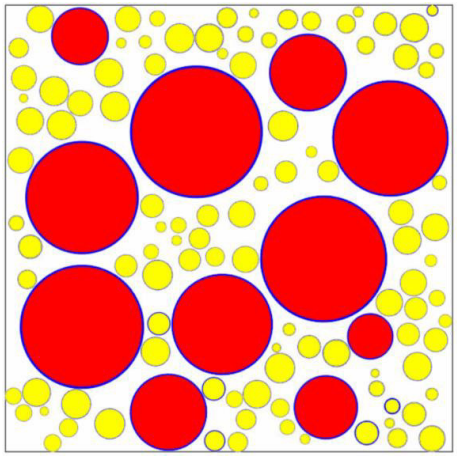

Figure 26 Generated 2D microstructure containing size distributed aggregates

The used material properties were adapted from the previous FE analysis. For the additional phase of gravel, a new material must be assigned.

All required BC are applied to build the FE model and physics are added to compute the study. Also, in this analysis a free triangular mesh was selected to generate the mesh. Due to very thin coatings in regard to the inclusion size the element size of the generated mesh was extremely small, which caused about 320 500 triangular mesh elements. The applied modeling scheme is shown in Figure 27.

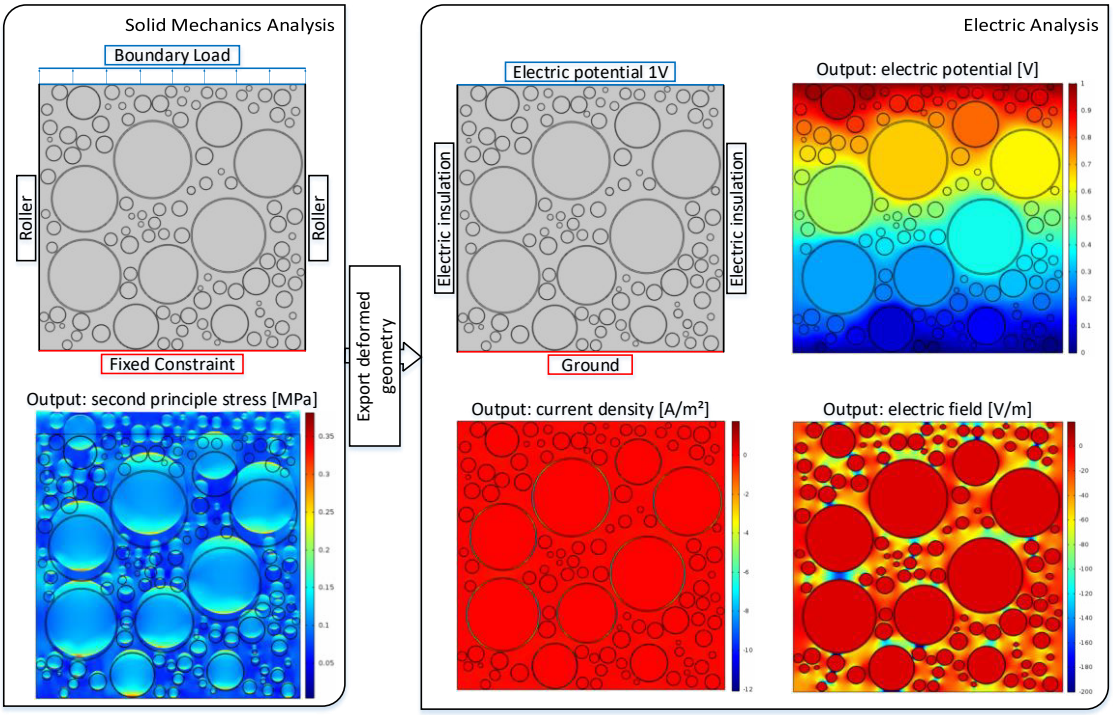

Figure 27 Illustration of the modeling scheme of size distributed cement aggregates

After computing the mechanical and electrical analysis for the undeformed and deformed geometry, the area-averaged conductivity and the FCR were calculated by using the equations (24) and (25), respectively. The final results of the FCR for the mechanical-electrical analysis of the RVE containing size distributed aggregates are shown in Figure 28 in comparison to the piezoresistive analysis with a cement matrix containing 30 vol.% iron powder.

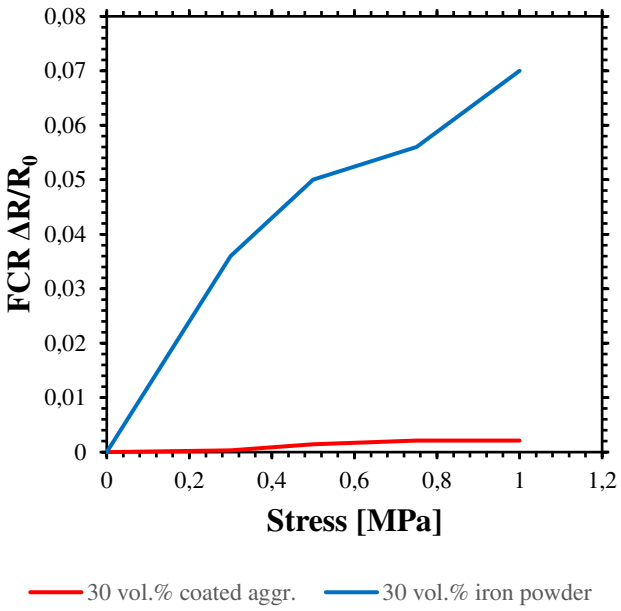

Figure 28 FCR of cement-based composite with size distributed aggregates or IP

The results of this analysis show, that even with size distributed aggregates the piezoresistive behavior is basically not existing. With an FCR in the range of 0.3 x10^{-3} to 2 x10^{-3} % and a change in FCR between the different applied stresses of about 0.7 x10^{-3} % strain-sensing would not be possible. A change in resistivity is visible, but too low to get an exact prediction of the strain state in the composite.

A possible reason for the low values for FCR could be traced back to the high initial conductivity of the cement-based composite with conductive coated aggregates. The changes in resistivity between the deformed and undeformed structure might be similar to previous studies with cement-based composites containing iron powder, but the ratio between ΔR and R_0 is significantly lower in the composite with coated aggregates, because the initial resistivity of the iron powder composite is extremely lower. Hence, the ΔR of the composite containing coated aggregates must be much higher to achieve a significant change. This could be achieved by increasing the conductive coating content to unrealistically high values, which was not further investigated.

From this point of the study it can be deducted, that by simply considering the effect of change in contact distance, the strain sensing behavior of piezoresistive materials cannot be modeled within a numerical FE analysis. Further considerations must be taken in account, to achieve the prediction of strain in a cement-based composite by performing numerical analysis. Yang et al. considered a interfacial debonding between different phases to measure the FCR, which will be further investigated in the next paragraphs (Yang et al., 2018).

5.4.4. CONSIDERATION OF THE EFFECT OF DEBONDING

After investigating, that only the consideration of a change in contact distance between adjacent conductive particles, does not lead to a significant change in resistivity upon an applied stress to the microstructure, a new approach to receive the piezoresistive effect must be applied. Within this approach interfacial debonding will be considered in the numerical FE analysis, which should lead to the desired values in the FCR. Chowdhury mentioned that even at small applied stresses to the microstructure, slight interfacial debonding will take place, due to the large difference of the Youngs modulus and Poisson's ratio between the cement matrix and the conductive coating (Swaptik Chowdhury, 2017). It was realized, that even small discontinuities or changes in the microstructure can influence the electric field and current density, which results in a difference in the predicted electrical response. As discussed in chapter 3.2.3.4, debonding is one of the central phenomena for the electrical strain-sensing ability of cement-based piezoresistive sensors. Accordingly, debonding must be considered in the numerical analysis.

Debonding mostly occurs at areas where different materials are in contact to each other and the continuity of the host matrix is interrupted. It describes a non-linear behavior at material discontinuities, which appears when specific stresses are reached in the microstructure. In the case of fiber incorporated composites, debonding can explained with a slight fiber pullout upon tension, where the adhesive friction bond between the fiber and matrix is overcome. By dealing with coated aggregates in a cement matrix, debonding can rather be understand as a crack opening in the matrix or at the boundary between the coating and the matrix. To numerically analyze this crack opening phenomenon different models can be applied to the microstructure.

The classic approach for solving fracture problems is the linear elastic fracture mechanism (LEFM). It is a useful tool to analyze the fracture of bodies provided with a crack-like notch or an existing flaw. With the LEFM the stress concentration in the peak of a crack can be quantitively described. The mechanism expresses three different modes to describe the crack opening and separation in a material. Mode I characterize a crack separation along the x-z-plane and is also known as symmetrical crack opening. Mode II describes an anti-symmetric separation of the crack surfaces in x-direction. Mode III is similar to Mode II, but shows an anti-symmetric separation in the transverse z-plane of the crack surfaces. All three modes are illustrated in Figure 29. This fracture mechanism follows the hypotheses, that the crack state at the tip of a crack can be explained with stress intensity factors (K-factors). Theses K-factors are seen as a state variable to determine the exposure in the crack-tip-area dependent of the mode (Schneider et al., 2016).

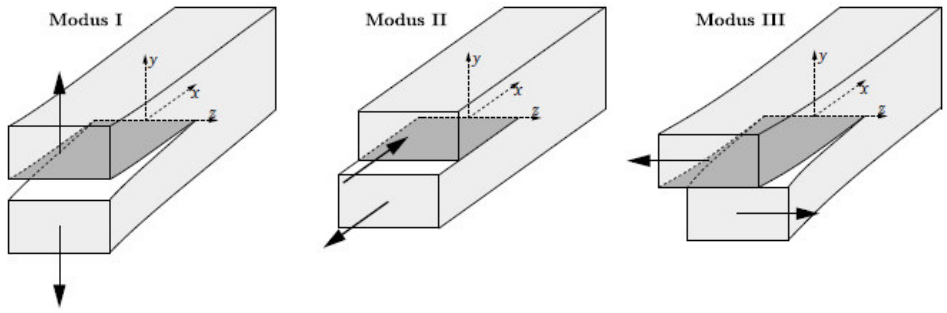

Figure 29 Crack separation modes described in the linear elastic fracture mechanism

The LEFM applies for very brittle materials, such as glass, where the process zone can be lumped into a single point and an initial crack is present. The non-linear zone ahead of the crack tip, which is known as the process zone, is neglectable (Elices, Guinea, Gómez, & Planas, 2002). For concrete materials, the LEFM is unable to predict progressive failure, due to its large non-linear process zone. Within the process zone, the material already starts to redistribute the stresses and changes its material condition. The material behavior can no longer be described as linear-elastic in this area, whereas the main material remains in a linear-elastic manner. Figure 30 should illustrate the process zone (shaded area) and the idealization for numerical simulation purposes, whereas l_p describes the length of the process zone, h_p the height of the process zone, δ the displacement normal to the crack planes and w the relative displacement. In general, the behavior of the crack is defined by the relationship between the stress and the relative displacement w between the upper and lower face of the zone, which is also defined as the cohesive crack width or opening (Elices et al., 2002).

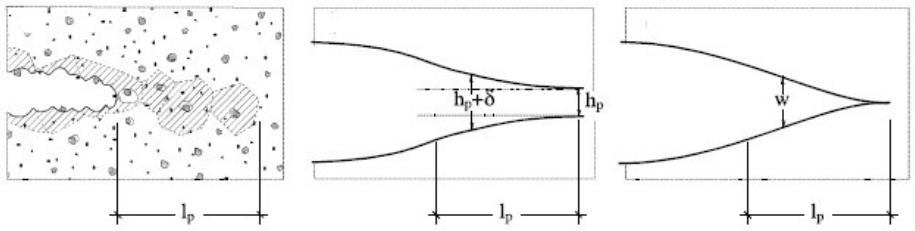

Figure 30 Non-linear process zone and simplification of crack process zone

To consider the non-linear process zone within the fracture mechanism and predict the crack propagation through numerical simulation, an extended cohesive zone model was developed by Hillerborg. This approach considers, that a crack propagates when the stress at the crack tip reaches a specific tensile strength. Particularity come to the point, when the crack opens. The stress in the tip does not fall to zero immediately, but decreases with increasing crack width w. This behavior is described with softening functions (Hillerborg, Modéer, & Petersson, 1976). One of the most common softening function for quasi-brittle materials such as concrete is the bilinear softening function $f(w)$, shown in Figure 31. On the one hand, a bilinear softening function describes the relation between stress and crack opening width across the fracture surface. On the other hand, it is also considered as a material property. Two properties of the softening function are important, to characterize the fracture mechanism of quasi-brittle materials. The first property is the tensile strength f_t, which defines the stress at which the crack is created and starts to open. It is expressed as equation (27) whereas w_{cr} is the relative crack width (Elices et al., 2002).

$$f(w_{cr}) = f_t \tag{27}$$

The second property is the cohesive fracture energy G_F (or tensile energy release rate) that characterizes the external energy supply required to create and break a surface area of a cohesive crack, is given by the area under the softening function and can

expressed with equation (28), whereas w_f is the critical crack opening after which the cohesive stress becomes zero.

$$G_F = \int_0^{w_f} f(w)dw \tag{28}$$

Furthermore, to predict the fracture behavior of quasi-brittle materials with the LEFM model a pre-existing crack is required. By using a traction separation law, such as the cohesive zone model (CSM), only a pre-defined crack path and a penalty stiffness prior to the softening behavior is required. The general CZM can described in four stages, which are implemented into a numerical simulation. The stages are illustrated within Figure 31b. Stage I of the traction separation model defines a general elastic material behavior without separation. The quasi-brittle concrete material can be assumed to be homogeneous and linear elastic. In stage II the initiation of a crack takes place, when a certain criterion, such as the maximum concrete tensile strength for crack opening is reached. In the microstructure analysis of a cement-based composite containing conductive coated cement aggregates the fracture initiation criterion for Mode I fracture (symmetrical crack opening) is assumed to occur when the state of stress reaches the cohesive strength.

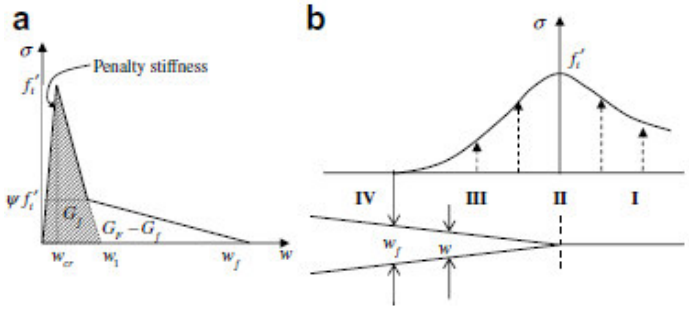

Figure 31 Bilinear softening function for concrete and four stages of CZM

Stage III characterizes the evolution of failure, which is expressed by the cohesive law or the softening function, which was discussed earlier in this chapter. It must be

noted, that the shape of the softening function in the CZM is essential for predicting the fracture behavior of a structure, since it defines the characteristic of the fracture process zone. Stage IV defines local failure when the crack opening width reaches the final crack opening width. Within this final stage, the concrete has no load bearing capacity left (Roesler, Paulino, Park, & Gaedicke, 2007).

To consider debonding at the boundaries between the conductive coating and the cement matrix, a CZM is applied to the numerical microstructure analysis of the piezoresistive cement-based composite in Comsol Multiphysics™. For the modeling, all described setups for the CZM are applied to the solid mechanics simulation with debonding. This means, debonding is considered to occur for the Mode I fracture criterion and a bilinear softening function defines the fracture propagation of the process zone. The input material properties for the softening function of quasi-brittle concrete, tensile strength f_t and tensile energy release rate G_I are shown in Table 5.

Table 5 Material properties for the softening function of concrete

f_t [MPa]	G_I [N/mm]
1.4	25

In comparison to the continuous unified model, some adjustments in the modeling process have to be made. After generating the microstructure and importing it to COMSOL Multiphysics™ as .DXF file the model for the numerical simulation was build. First, the model for the solid mechanics analysis was assembled to generate the deformed geometry including debonding. Therefore, the imported RVE including matrix and conductive coated cement-aggregates are modeled as an assembly, which makes it possible to create contact pairs between the matrix-interphase boundaries. These contact pairs are important to implement the CZM to the microstructure between

the coating and the matrix. For the numerical investigation of the piezoelectric effect with debonding the same microstructure as in chapter 5.1 was used. Figure 32 shows the created contact pairs (purple).

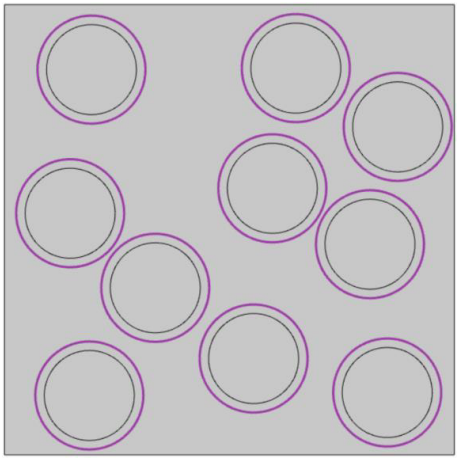

Figure 32 Generated microstructure with created contact pairs

It has to be noted, that between the cement aggregate and conductive coating, the bonding conditions are assumed to be perfectly bonded. Concludingly, no debonding between these two phases takes place upon loading. After creating the model, the material properties were assigned to the different phases. These properties remain to be the same as shown in Table 4.

Within the next step, all boundary conditions were defined. Besides the fixed constraint on the bottom, roller conditions on the sides and the boundary stress on the top of the RVE a special boundary condition for the contact pairs had to be defined. Following the CZM, a bilinear traction-separation law was applied. The required parameter to describe the separation or decohesion, as it is named in COMSOL Multiphysics^{TM}, are given in Table 5. Before computing the simulation, the RVE was meshed with about 32 100 domain elements.

With an applied stress the microstructure was deformed, which created debonded areas (white areas) inside of the microstructure at the predefined contact pairs. The matrix debonded at these areas, where the tensile stress reached the maximum limit that leads to debonding. The deformed microstructure with an applied stress of 1 MPa is shown in Figure 33. The white areas around the coatings are a sign, that the applied stress was high enough to separate the bond between matrix and coating.

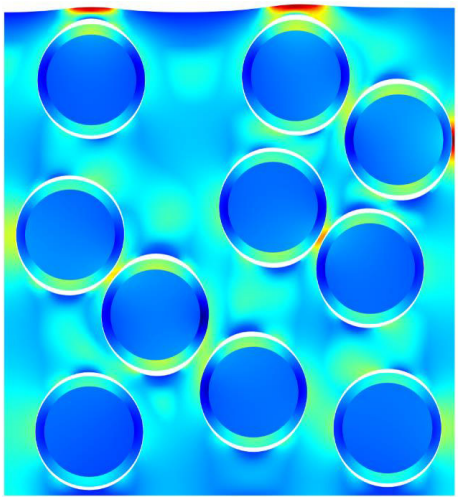

Figure 33 Deformed microstructure with debonding and an applied stress of 1 MPa

After the mechanical analysis, the electrical simulations were performed. The analysis for the initial electrical parameter was simulated with the undeformed geometry to simply homogenize the properties of all phases. The modeling process and boundary conditions to compute the simulation were equal to the analysis in chapter 5.4.2. For the electrical analysis after debonding, the deformed microstructure was imported from the mechanical to the electrical simulation to generate a new geometry. While creating the model for the electrical analysis with the deformed geometry, it was realized, that Comsol Multiphysics^{TM} had troubles to identify the boundaries of each phase, which made it impossible to apply material properties to all phases and furthermore created problems with the meshing of the microstructure. As mentioned in the paper from Yang

et al., the absolute value of the repair tolerance in Comsol Multiphysics™ was set to a very low value of 1 x10^8 mm to prevent a non-debonded or fully debonded interface. But even with the consideration of the repair tolerance, it was not possible to sufficiently import the deformed geometry to the electrical model in COMSOL Multiphysics™.

Another approach by importing the deformed mesh from the mechanical analysis also created issues in the modeling process, since a new model had to be built from the mesh, which lead to the same problems when directly import the deformed geometry.

Accordingly, a different method must be developed to consider the effect of debonding. Chowdury calculated an average debonded area and build a new geometry to consider interfacial debonding, which lead to a change in resistance. The debonded areas were represented as ellipses around the inclusions (Yang et al., 2018). By reproducing this approach, it was noticed, that the debonded areas, for a microstructure containing nano-engineered polymer coatings, are extremely small, which did not show a significant fractural change in resistivity.

With a closer look to the deformed structure, where debonding takes place, it was realized, that the perimeter of debonding around the conductive interphase varies upon different applied stresses. With a smaller applied stress, the debonded surface tend to be smaller. With an increased stress the debonded surface also increases. On behalf of the electrical behavior, a higher conductivity is expected with a smaller debonded surface of the coating, since the surface of the coating in contact with the matrix is larger.

Following to this behavior, another approach, to model and simulate the effect of debonding within a mechanical-electrical analysis, was developed in this thesis, by

considering the debonded length around the coating interphase. The modeling process will be shortly discussed in the following paragraphs.

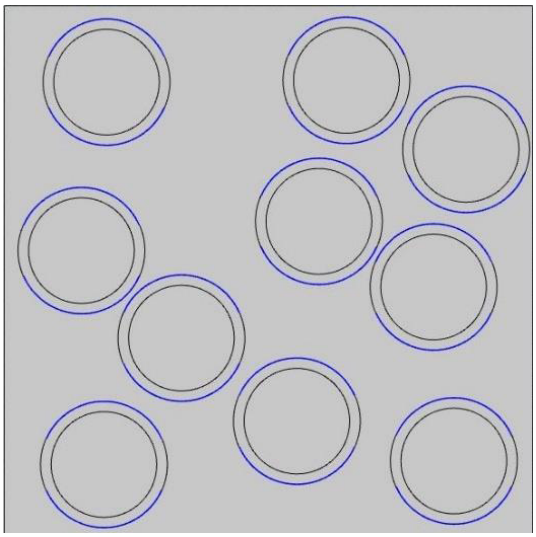

Figure 34 Generated RVE with length averaged predefined debonded perimeter

As in previous simulations, the first step was to perform the mechanical analysis and deform the microstructure that debonding at the coating-matrix interface occurs. This deformed microstructure was exported to determine the length of the debonded perimeter of each inclusion. Afterwards, the applied stress was stepwise increased to find the debonded perimeter for different stress states. To obtain an averaged debonded perimeter that represents the effect of debonding in the electrical analysis, the extracted lengths were separately averaged for each stress. This averaging of the perimeter length was implemented in the process to simplify the modeling process. To achieve a high accuracy for the averaged debonded length, this procedure was repeated for microstructures with different positions of the inclusions and different volume fractions. The observed debonded perimeters are shown in Table 6. It must be noted, that all simulations were performed with a microstructure containing fine aggregates with 2 mm in diameter and a coating thickness of 0.2 mm.

Table 6 Debonded perimeter length after debonding in respect to corr. stress

Stress [MPa]	0.3	0.5	0.75	1
Avg. length [mm]	0.2657	0.2867	0.3052	0.3263

Furthermore, it must be mentioned, that for different thicknesses of the coating or different diameters of the aggregates, the average length must be adjusted, since the overall perimeter of the coating is changing. By not considering this effect an underestimated behavior of interfacial debonding could be produced.

The developed procedure makes it necessary to generate a new geometry, which is implemented in the electrical simulation for the debonded microstructure. The new geometries consider a predefined debonded perimeter (blue line) with the determined averaged length around the coating (Figure 34). This is required to simulate the present separation between the coating and the matrix after tension, which increases the resistivity of the cement-based composite. Within the electrical analysis for the debonded microstructure all material properties and boundary conditions are applied as mentioned in chapter 5.4.2. The applied electrical material properties are shown in Table 4. After remeshing the RVE for the deformed microstructure, which created about 49 000 triangular mesh elements, the electrical analysis was computed.

For post-processing and finalize the simulation, the response of the electric field and current density are area-averaged to homogenize the material properties and to calculate the area-averaged electrical conductivity after debonding with equation (24). Finally, the FCR is calculated with equation (26) for the piezoresistive cement-based composite containing nano-engineered thin-films coated cement aggregates. For a better understanding of the modeling procedure from the microstructure generation to the

calculated FCR, Figure 35 shows the modeling scheme to simulate a piezoresistive behavior of a cement-based composite.

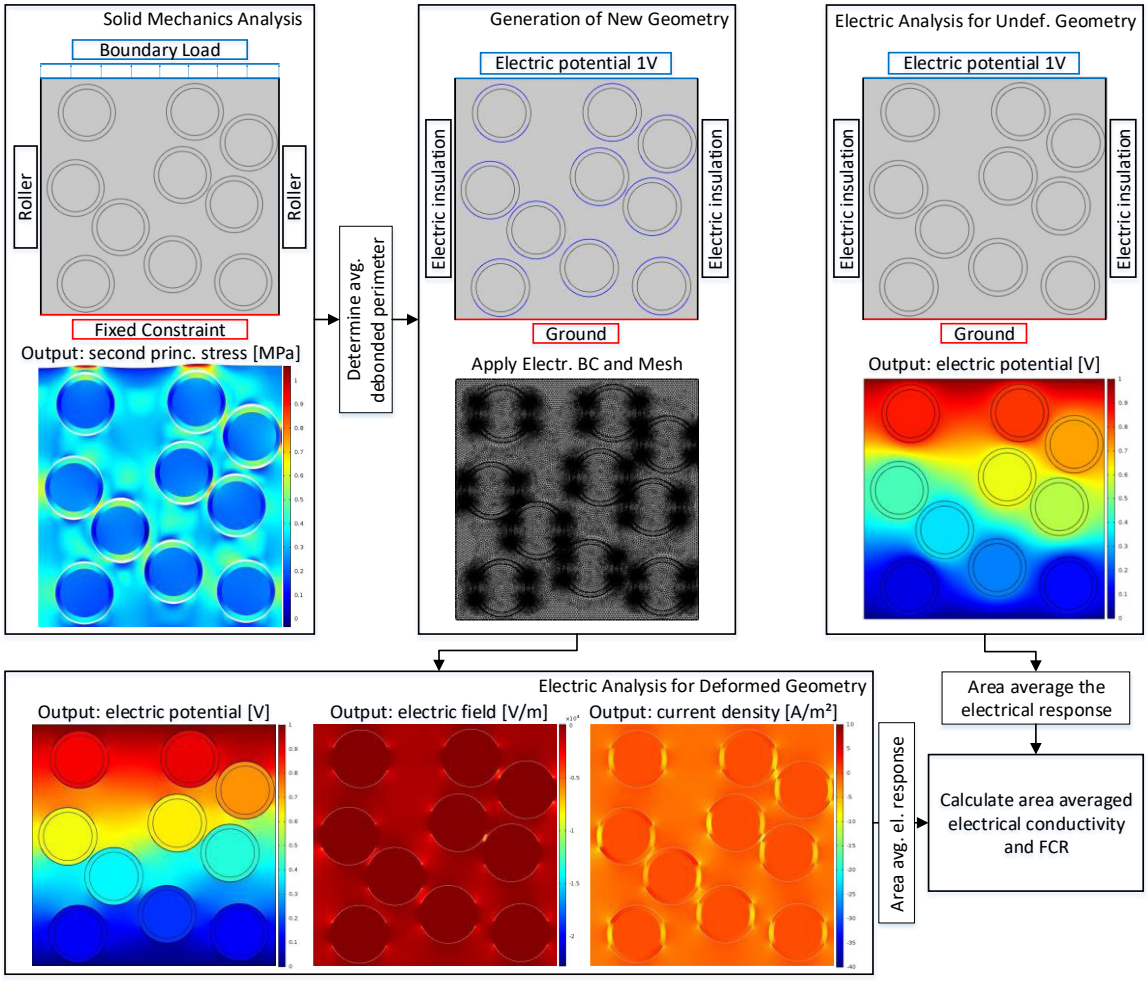

Figure 35 Scheme for electromechanical analysis with interfacial debonding

The graph presented in Figure 36 shows the FCR as a function of stress of a cement-based composite containing 30 % of iron powder and a composite containing 30 % of fine cement aggregates with a CNT thin film-coating and considering debonding in the modeling process. The data for the FCR of iron powder is extracted from a previous research by Yang et al. (Yang et al., 2018). Within this study, the electro mechanical response of a cement mortar with iron powder, which replaces fine cement aggregates, was investigated. The volume fraction of aggregates in the mortar is the same in both

studies, but the actual volume fraction of the conductive phase is relatively lower with the coated aggregates compared to the study by Yang et al., since iron powder is both, conductive phase and cement aggregate.

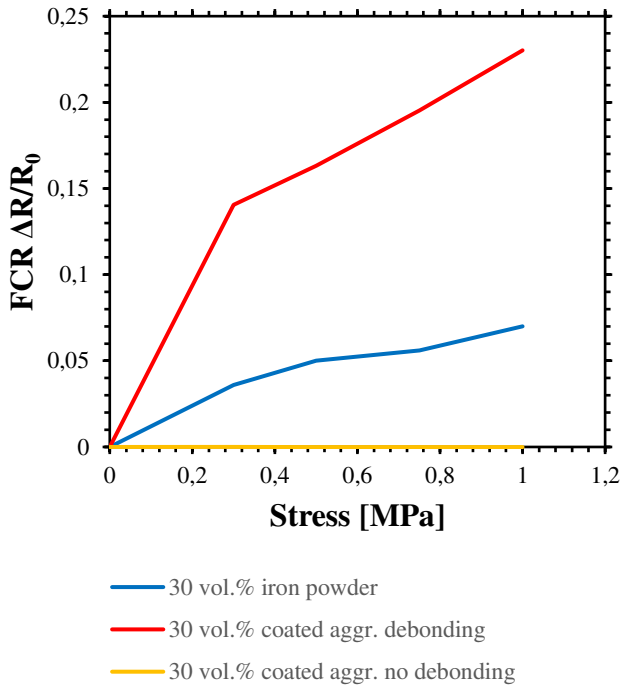

Figure 36 FCR of different cement-based composites considering debonding

Unless, the effective volume fraction of the conductive phase in the composite with coated aggregates is lower than the one with iron powder, the response of the coated aggregates is higher. This behavior can be traced back to the 10 times higher conductivity of the CNT-latex coating, which has a conductivity of around 1000 S/m, whereas the iron powder has a conductivity of 100 S/m. It must be noted, that this graph is no validation for the developed modeling process of the piezoresistive effect of cement-based composites with conductive coated aggregates. It should rather qualitatively compare the effect of debonding on the electro-mechanical behavior of cement-based materials.

In comparison of the studies with coated aggregates it is apparent, that the simulation, which considers interfacial debonding shows a significant change in resistivity, compared to the simulation without debonding. By applying a tensile stress in the range of 0.3 to 1 MPa to the RVE with debonding, the FCR shows a change between 14 to 23 %, whereas the change of FCR between different stress states was about 3 %. In the simulations without debonding it was realized, that no significant change between different stress states was present, whereas in the case of debonding, the FCR shows considerable changes between different tensile stresses. This qualifies the developed procedure to actual respond to different applied tensile stresses and simulate strain-sensing behavior of cement-based sensors.

Concludingly, to simulate the piezoresistive effect of cement-based composites with a numerical approach, the application of interfacial debonding is required to sufficiently explain the physical process in the system, which influences electrical response. In the next chapter, the validation for the numerical simulation of the developed procedure to predict the fractural change in resistivity is performed. Furthermore, the variation of different parameter, such as the volume fraction of the coated cement aggregates, is investigated. This should give a better idea of how the conductive thin film-coating affects the overall electro-mechanical behavior of piezoresistive cement-based composites.

5.5. MODEL VALIDATION

To justify the results from the numerical simulation, a validation must be executed. To achieve a high accuracy in the validation process, it is important to obtain equal material parameter. The most common procedure to validate numerical results, is to

perform laboratory experiments and compare the response or results from the experiment with the results from the simulation. In this thesis, the electro-mechanical response of cement-based composites containing latex CNT thin film-coated cement aggregates was investigated by performing numerical simulations. An experimental part for the validation was planned, but due to the chemically highly sophisticated and complicated fabrication of the latex CNT thin films, an adequate manufacturing of the coated aggregates was not possible.

In chapter 4.5.2 the manufacturing process of a damage sensing concrete, developed by Gupta et al. was shortly discussed. The achievement of Gupta et al. is based on previous research by Loh et al. who performed physical experimental investigations of conducting cement mortar obtained by adding latex CNT thin films-coated fine cement aggregates. Within the experimental procedure, Loh et al. performed electro-mechanical tests on mortar cube specimens (5x5x5 cm^2), which were subjected to compressive cyclic loads, that the piezoresistive sensing response could be characterized. It was reported, that the electrical properties of the designed cementitious composites exhibited extremely high strain sensitivities (Loh & Gonzalez, 2015). The results from this experiment can be used to validate the numerical simulation of this thesis.

A challenging point within the validation is, that the numerical simulations are conducted in the microscale, whereas the experiments are performed in the macroscale. By considering the correct boundary conditions, the microscale model shows similar results as in the experiment, but discrepancies are expected since some effects, such as weakening of local areas in the macroscale cannot be considered in the microscale

simulation. The interface between microscale to macroscale modeling is a relevant problem, which has not been sufficiently solved jet. Since, a microscale model represents only an extremely small area of a macroscale model, the predicted material parameter for the micro-model cannot be used for the whole macro-model. To find a method to deal with this problem is currently state of the art and will not further discussed within this thesis.

As aforementioned, to validate the numeric simulation with results from a physical experiment, the material parameter and properties must agree in both studies. For the numerical part of the validation, the Youngs modulus for the fine sand aggregates was set to 70 GPa and with a median size of d_{50} = 2.5 mm in diameter. The coating thickness was set to 20 % of the aggregate radius. In the experimental part a Portland cement type I/II with type F ground granulated blast furnace slag was used, which was considered with an increased Youngs modulus and a reduced conductivity of the cement paste. All further mechanical and electrical material properties are used from previous reviewed literature (see Table 4). To create a mortar, the average volume fraction of fine aggregates is about 50 %, which was set as criterium for the microstructure generation. The modeling of the microstructure for the mechanical and electrical analysis follows the in chapter 5.4.4 developed procedure.

In the experiment, a cyclic compressive load was applied, which must be considered in the simulation. The boundary load at the top of the generated RVE was changed from a tensile stress to a compressive stress, to simulate compression in the microstructure. The results in the paper from Loh et al. are presented as FCR as a function of strain and the average gauge factor is reported. To validate the results from

the numerical simulation with the experiment, the FCR for an applied compressive stress and gauge factor is calculated and compared with the FCR of the experiments.

Due to the fact, that the FCR is given as a function of strain, whereas the simulation is controlled by applying a stress, the stress states had to be varied to reach the significant strain inside of the microstructure. Therefore, a homogenization of the strain was conducted within the mechanical analysis. For the validation of the FCR between the experiment and simulation, compressive stresses were applied to reach average strains within the range of -0.15 to 0 %. By performing the analysis with compression, it was realized, that no debonding at the interface between aggregate coating and matrix was present. This also means, that the whole microstructure remains in an elastic regime. As a result of compression, the aggregates are displaced into a closer position to adjacent particles, which increases the conductivity of the composite. This means, that the change in contact resistance has a huge impact on the piezoresistive behavior. Reversely to tension, the FCR will be negative, since the resistivity decreases upon compression, that the ΔR gets negative.

After applying a compressive stress to the RVE with the aforementioned material parameter and properties, averaging the strain inside of the RVE, exporting the deformed microstructure and computing the electrical analysis, the homogenized resistivity before and after deformation was calculated to obtain the FCR of the cement-based composite. The graph in Figure 37 shows the FCR for the numerical simulation in comparison to the FCR for the experimental analysis. The plotted red line represents a function where simulation and experiment fully correlate.

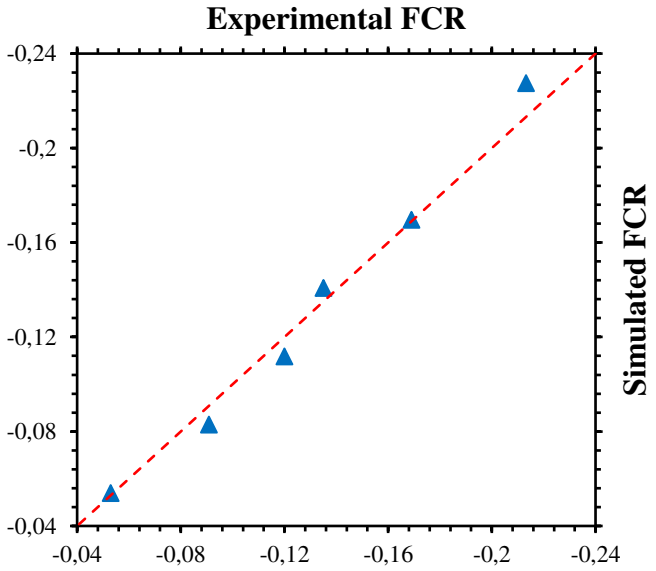

Figure 37 Validation of numerical simulation of cement-based with the FCR

Interpreting the graph in Figure 37 shows, that the computed FCR of the simulation is in good correspondence to the FCR of the experiments. This implies, that the developed procedure, to numerically simulate the piezoresistive behavior of cement-based materials, is successful.

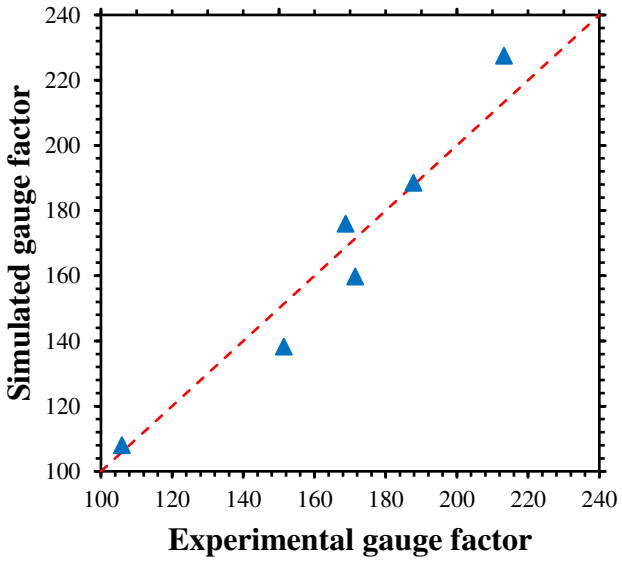

Figure 38 Validation of the strain sensing sensitivity with the gauge factor

Figure 38 should further underline, that the simulation is capable to accurately predict the strain-sensing behavior. The graph shows, that the sensing ability is present, and the sensitivity of the cementitious composite is very high. As aforementioned in chapter 3.1.4 the gauge factor, which expresses the sensitivity of a material or sensor, of a commonly used strain gauge is around 2, whereas the gauge factor of the investigated composite is around 180. Overall, the developed method, to observe the piezoresistive behavior, is applicable for cement-based composites containing conductive coated cement aggregates.

In the next chapter, the variation of some material parameter of the cement-based composites will be performed, to show the influence of the conductive coating on the strain-sensing behavior.

5.6. VARIATION OF MATERIAL PARAMETER

Within this chapter different material parameter of cement-based composites containing CNTs thin-films coated fine aggregates will be further investigated. By varying the aggregate volume fraction, the thickness of the coating and the conductivity of the coating, a change in the conductivity and sensitivity is expected. With this study, it should be observed how strong the influence on the electro-mechanical effect is, when the setup of the cementitious material changes. For the further simulations the same modeling scheme as developed in chapter 5.4.4 is applied. All generated microstructures are applied to a tensile stress in y-direction for the mechanical analysis. The stresses vary in a range of 0.3 to 1 MPa, which is well in the elastic zone of the cement matrix. In the electrical analysis, all RVE are conducted with an electric potential of 1 V and a frequency of 100 Hz. The generated microstructures should represent a cement mortar

with different volume fractions of fine aggregates. For the ease of the modeling all particles are defined to have the same inclusion size. The size of the randomly placed aggregate particles was set to an average value for a 0.125 to 4.5 mm sieve width, that is used to cast cement mortar. All material properties are applied as given in Table 4, since with these values, the validation of the simulation showed a good correlation and are taken from legit sources.

5.6.1. AGGREGATE VOLUME FRACTION

Within the first parameter study, different volume fractions of coated aggregates were applied to the cement mortar. More specifically, three different studies were conducted with 30 vol.%, 25 vol.% and 20 vol.%. For each setup a new geometry was generated, whereas the coating thickness kept constant. With changing the volume fraction of the aggregates, also the fraction of the conductive phase is changing, which should be realized in the response of the FCR. To obtain the FCR the initial resistivity was calculated with the undeformed RVE. After applying the voltage and perform the post-processing with the electrical current density and electric field, the resistivity was calculated. The initial values for the three generated setups are reported in Table 7. It also shows the avg. resistivity for the plain cement matrix. By comparing the resistivity of the cement matrix and the composites, it is realized, that the addition of 30 vol.% coated aggregates can reduce the resistivity of about 70 %.

Table 7 Resistivity of cement composites with different aggregate vol.%

Volume fraction [vol.%]	0	20	25	30
Avg. Resistivity [Ωm]	500	255	168	132

The results for the FCR as a function of stress is plotted in Figure 39. The red line represents the FCR upon different applied stresses for a composite containing 30 vol.%,

the blue line represents 25 vol.% and finally the yellow line the volume fraction of 20 vol.%. Further results are plotted in Appendix A.

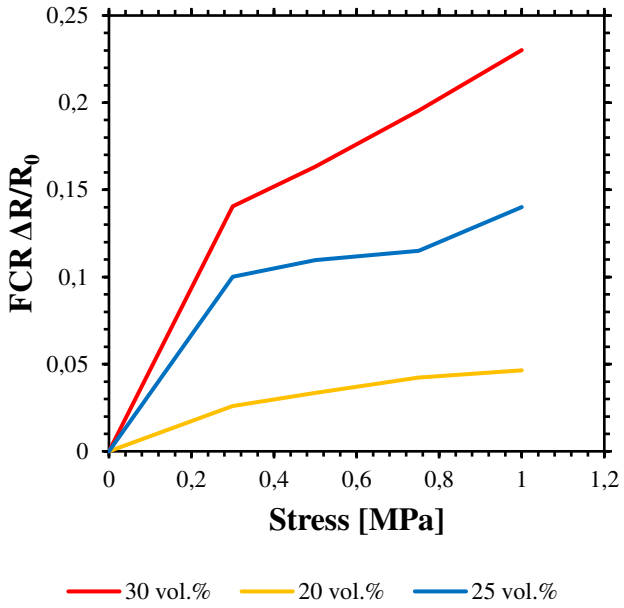

Figure 39 Comparison of FCR dependent on different volume fractions

The graph in Figure 39 confirms, that the variation of the coated aggregate content in the cement matrix has a significant impact on the sensitivity of the cementitious composite. As expected, the RVE with the smallest amount of coated aggregates (20 vol.%) showed the smallest FCR of about 5 % at 1 MPa of tensile stress between the undeformed and deformed microstructure. The RVE with the highest amount of coated aggregates and so with the highest amount of conductive material within the composite shows the largest FCR of about 23 % at 1MPa. The microstructure containing 25 vol.% of coated aggregates has an FCR that is lower than the RVE containing 30 vol.% of aggregates.

It is also noticed, that the different graphs show different slopes, when reaching an applied stress state of 1 MPa. Especially, when comparing the RVE with 30 vol.% and 20 vol.% of coated aggregates. The graph, that represents 20 vol.% has a much

shallower slope, which could be interpreted, that the limit of sensing is reached very early, since no significant change appears after a specific stress level is reached. This could mean, that strain-sensing is less effective for a setup with a volume fraction lower than 20 vol.%. Strain-sensing with a microstructure setup of 30 vol.% or higher of coated aggregates is extremely high, since the differences of the FCR between different stress states are significantly higher.

At a certain point of deformation of the microstructure, debonding does not further propagate due to the boundary effect and transverse contraction. This means, the coated aggregates are always in contact with the surrounding matrix at some areas. Concludingly, the amount of FCR approaches a limit by investigating the behavior in the elastic range. For further increasing of the FCR the plastic range or damage must be considered, which is not part of this study.

It must be noted, that the conductivity of a material or especially of an RVE is also dependent of the position of the coated aggregates. It is possible, that inclusions are positioned to form a conductive path, which increases the conductivity of the material or the inclusions form cluster with larger gaps between adjacent particles apart from the clusters, which lead to a higher resistivity.

5.6.2. THICKNESS OF CONDUCTIVE COATING

In the next study the variation of the coating thickness was investigated. For the simulation the volume fraction of the inclusions was fixed to 25 vol.% and the position of the coated aggregates remains at the same position for each analysis. This makes it possible to just observe the influence of the coating thickness on the electro-mechanical behavior of the cement composite. It has to be noted, that for this analysis, a new

geometry with different positions of the inclusions was generated, which causes slightly different initial resistivities than in the previous analysis.

In general, to achieve a precise coating thickness in experimental research or practical use is hard to obtain, since the latex CNT thin film is manually spray painted on the aggregates. As of now, the behavior of different coating thicknesses on the piezoresistive effect of cement-based composites is difficult to investigate, since the coating thickness is very inconstant. Problems, that are hard to investigate within an experimental procedure, are easier to address with numerical simulations. Within the simulations the coating thickness can be controlled very precisely, so that the material behavior or response can be predicted very accurate, if the modeling process considers a realistic and representative idealization of the microstructure, which can sometimes be very challenging.

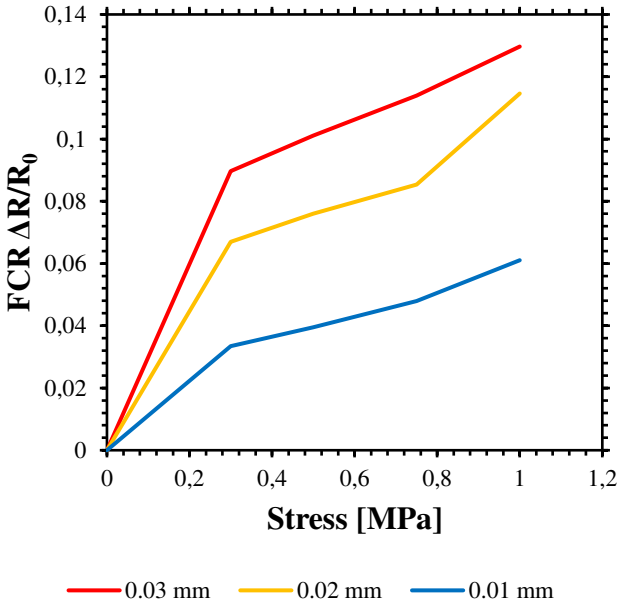

Figure 40 Comparison of FCR dependent on different coating thicknesses

In this study, three different thicknesses of the latex CNTs thin-films coating are investigated. The assessed thicknesses are set to 0.01, 0.02 and 0.03 mm, which

represents a volume fraction of the conductive coating in the microstructure of about 5 vol.%, 11 vol.% and 18 vol.%. After homogenizing the undeformed microstructure, the computed initial electrical resistivity for the composite are reported in Table 8.

Table 8 Resistivity of cement composites with different coating thicknesses

Coating thickness [mm]	0.01	0.02	0.03
Avg. Resistivity [Ωm]	233	194	172

Extracting from the graph in Figure 40 it is found out, that the change of the coating thickness has a significant impact on the electro-mechanical behavior of cement-based composites. Due to the high amount of conductive material at a thickness of 0.03 mm, the FCR shows the highest difference between the initial resistivity and after deforming. By increasing the thickness from 0.02 to 0.03 mm, the sensitivity of the composite could still be increased significantly. The results of this analysis are extremely theoretical, since practically it is not possible to apply an exact coating thickness. This plot just gives a very good idea of how the coating thickness improves the sensitivity of the composite. Additionally, it can be mentioned, that the change of the FCR between different stress states was almost equal of all three observed setups. This could lead to the fact, that by just increasing the thickness, the resistivity gets improved. By comparing the graph from Figure 39 with the one in Figure 40, it can be deducted that the change of the volume fraction of the aggregates has a much bigger impact in the sensitivity of the material. Further results of the electrical and mechanical simulation are plotted in Appendix B.

5.6.3. ELECTRICAL CONDUCTIVITY OF THE COATING

In the last study of investigating different material parameter of a conductive cement-based composite, the electrical conductivity of the conductive coating was

changed, to see which impact the initial conductivity of the coating on the electro-mechanical behavior of the composite has. For the numerical simulation the volume fraction and coating thickness kept constant at 25 vol.% and 0.02 mm respectively. Also, the positions of the inclusions were fixed for all simulations to just investigate the impact of the coatings conductivity. The electrical conductivity was varied between 500 and 100000 S/m, whereas the initial conductivity of the coating, obtained from previous research, has a conductivity of 1000 S/m. Accordingly, the initial conductivity was halved, doubled and increased by 100. In Table 9 the initial values for the homogenized electrical resistivities of the setups are presented.

Table 9 Homogenized initial resistivity with different coating conductivities

Conductivity [S/m]	500	1000	2000	100000
Avg. Resistivity [Ωm]	200	194	188	185

Interpreting Table 9 it is realized, that the initial conductivity is just slightly variant between the different conductivities of the coating. Even, if the conductivity is increased with a factor of 100, the resistivity of the composite just slightly decreased, which is almost neglectable for a magnification factor of 100.

By considering the graph in Figure 41, which shows the FCR of the cement-based composite setup with different applied electrical conductivities of the coating, it is apparent, that this adjustment shows no significant change in resistivity between the different coating conductivities. An FCR is present between different stress states, which was expected, but it was not assumed, that a conductivity of 100000 S/m almost equally responds as a conductivity of 1000 S/m. Concludingly, the conductivity has not a significant impact on the sensing behavior in this simulation.

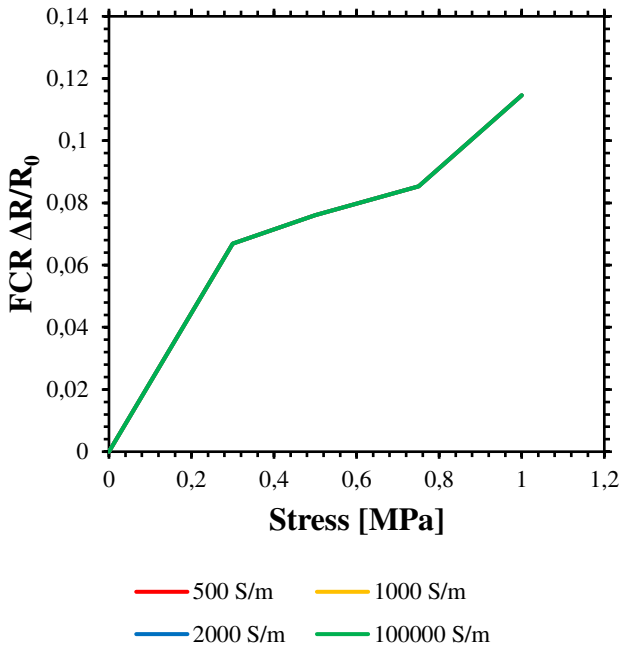

Figure 41 Comparison of FCR dependent on different coating conductivities

This phenomenon could be explained with the selected parameters for the generated microstructure. It is possible, that the selected volume fraction and coating thickness, which leads to a volume fraction of about 11 vol.% of the conductive phase, is well above the percolation threshold to form a conductive network, which results in a high piezoresistive behavior for strain sensing. In comparison, the percolation threshold of MWCNTs in a cement paste is around 0.7 vol.%. With a lower volume fraction of coated aggregates, also the amount of conductive material is reduced, which could lead to a more significant FCR by observing different material conductivities. Another reason could be the high conductivity of the coating compared to the cement matrix. Due to the high difference between these two conductivities of 1000 S/m and 0.002 S/m respectively, the maximum capability of the composite to increase the sensitivity might already reached at a significantly lower conductivity of the coating. This means, when the sensibility of the composite does not get further improved, the

conductivity of the conductive phase approaches to a threshold. It is assumed, that a visible jump in FCR between different coating conductivities is present, when the conductivity is much lower. But this could cause more noise in the sensing procedure.

6. CONCLUTIONS AND FUTURE WORK

In this thesis, the electro-mechanical behavior of cement-based composites containing latex CNTs thin film-coated cement aggregates was investigated by performing numerical simulations. After a review of the current state of the art of piezoresistive cementitious composites used in SHM of civil infrastructure, a method was developed to predict the strain-sensing behavior of cement mortar with numerical simulations. The basic idea was, to study the electro-mechanical behavior within an elastic range and detect a fractural change in resistivity by applying a tensile stress to a randomly generated microstructure.

It was observed, that by investigating microstructures, interfacial debonding between the coating and the cement matrix must be considered to predict the FCR upon different stress states. Debonding was achieved, by applying a cohesive zone model to the microstructure at the boundaries of the coatings and was considered in the electrical simulation part by generating a debonded perimeter around the coatings with averaged length dependent on the applied stress, since it was observed that the length of the debonded surface varied upon different stresses.

In a final step, the simulation was validated with experimental data and a parameter study was conducted, where different material parameters were changed to investigate their behavior on the piezoresistive effect of cement-based composites containing conductive coated cement aggregates. It was discovered, that the numerical simulation coincides very good with the obtained experimental data, which means that the developed analysis predicts the electro-mechanical analysis very precisely. Within the parameter study it was shown, that cement aggregates coated with a highly conductive

phase inherently improve the strain-sensing behavior, since the initial resistivity of plain mortar could be significantly reduced. With an applied stress, the FCR also showed considerable improvement, which is an indicator for a sensitive piezoresistive material. By varying several material parameters it was recognized, that the volume fraction of the coated aggregates and the thickness of the coating have a significant impact on the FCR. Variations in the conductivity of the coating did not lead to changes in FCR. This phenomenon was traced back to the fact, that the present conductivity of the coating was well above the maximum threshold. Concludingly, it can be summarized, that the developed method characterizes a way to accurately predict and optimize the piezoresistive behavior of these composites in the elastic range. Furthermore, it is worth mentioning, that cement-based composites containing nano-engineered latex CNTs thin film-coated cement aggregates are an effective way to homogeneously disperse CNTs inside of a cement matrix to achieve a self-sensing composite, that can be used for SHM in civil infrastructure.

This thesis presents a very fundamental part in the research field of piezoresistive cement-based composites enabled by conductive coated aggregates. In future research, the developed numerical simulation can be further improved, by discretizing the model more realistically. Instead of generating an RVE with a fixed inclusion size, the fine aggregates in a cement mortar could be modeled with a more accurate size distribution to achieve higher volume fractions and a denser aggregate packing. Moreover, instead of investigating the electro-mechanical behavior in the mortar scale, simulations in the scale of concrete could be computed by using coated coarse aggregates in addition to fine aggregates. Since, a conductive concrete would be the final product that is applied

to civil infrastructures, this would be a more useful and application-oriented way to perform this kind of simulations.

To understand the material and its effect on the electro-mechanical behavior much better, additional analysis, parameter studies and experiments could be conducted. Especially for the optimization it is important to know, at which volume fraction or electrical conductivity of the coating the composites resistivity percolates. Also, 3D analysis could be taken into consideration.

This thesis deals basically with simulations in the elastic zone of the cement mortar. Since, cementitious materials such as concrete are used in constructions where a plastic regime is present, and cracks appear, further investigations on this level should be conducted to model a more realistic behavior of the cementitious composites. Within this step of research, nonlinearities such as damage sensing or the impact of damage onto the piezoresistive behavior could also be taken under consideration.

One further and very important point of interest is the application of the investigated self-sensing composites to a real structure. The use of latex CNTs thin film-coated aggregates gives more opportunities to create a whole structure or thin layer out of conductive cementitious material. Accordingly, methods to achieve an accurate and reliable SHM of civil infrastructure must be carried out.

APPENDIX A VARIATION OF VOLUME FRACTION

A-1 RESULTS VARIATION OF VOLUME FRACTION 20 %

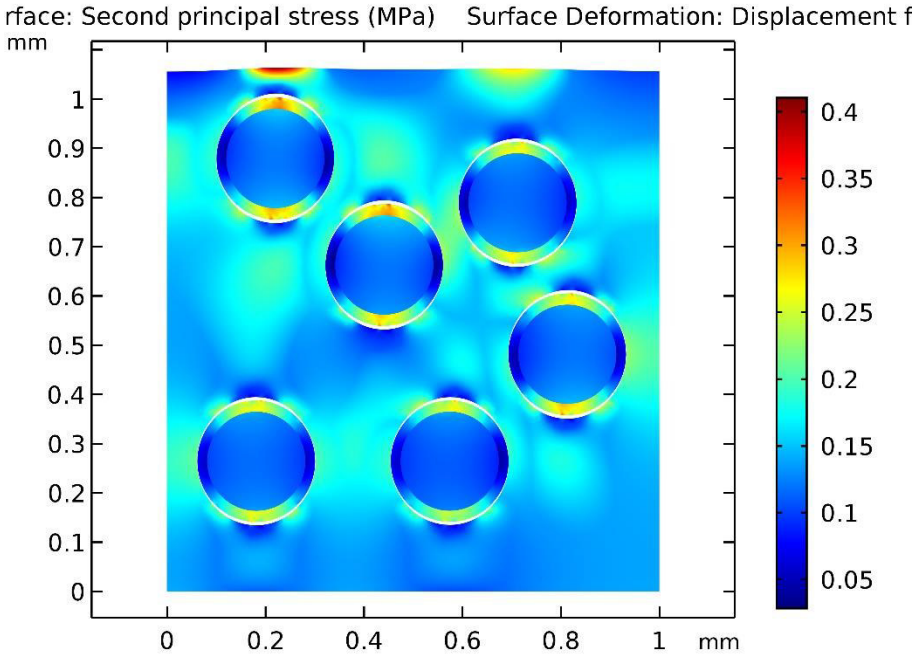

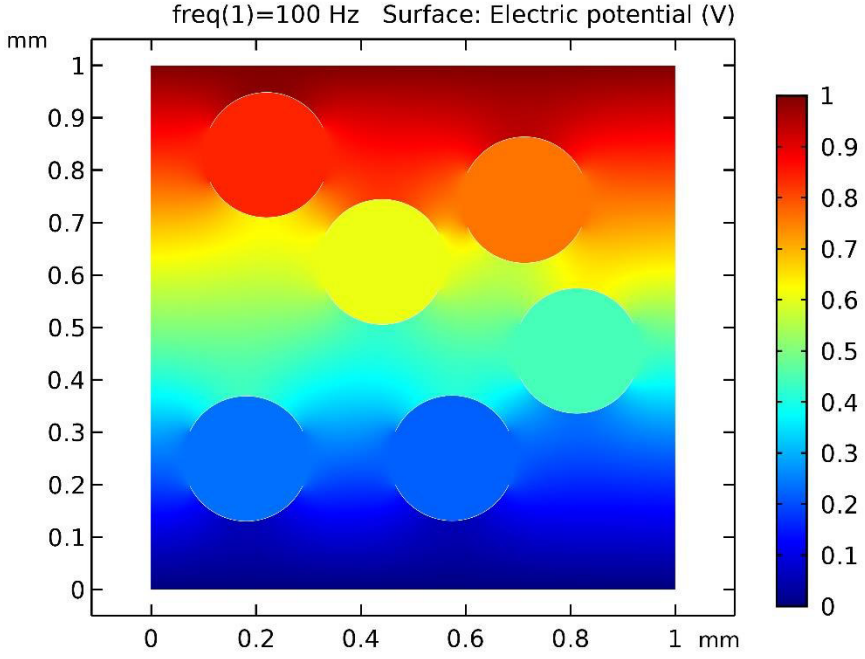

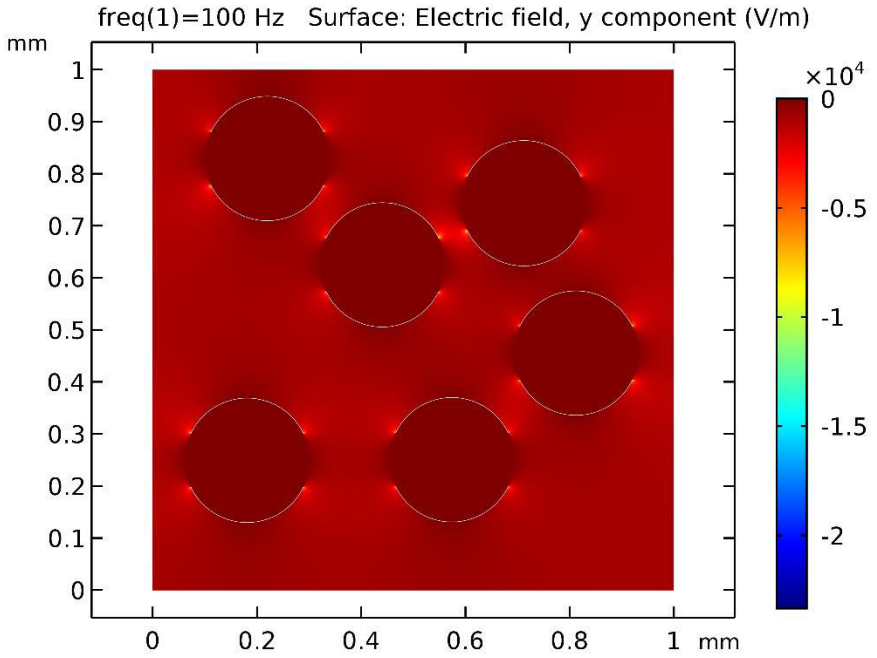
freq(1)=100 Hz Surface: Electric field, y component (V/m)
mm
1
0.9
0.8
0.7
0.6
0.5
0.4
0.3
0.2
0.1
0
0
0.2
0.4
0.6
0.8
1
mm
×10^4
0
-0.5
-1
-1.5
-2

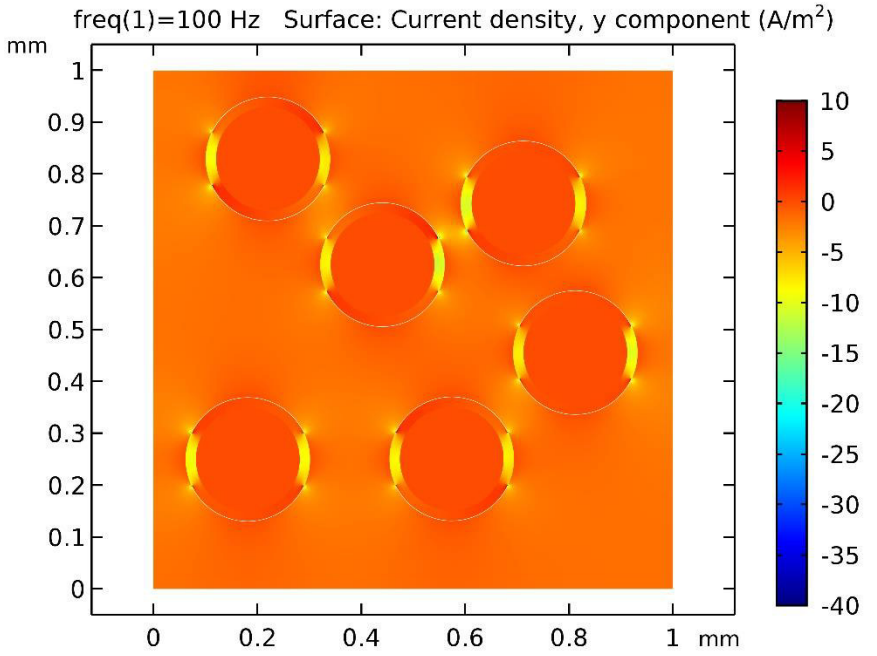
freq(1)=100 Hz Surface: Current density, y component (A/m^2)
mm
1
0.9
0.8
0.7
0.6
0.5
0.4
0.3
0.2
0.1
0
0
0.2
0.4
0.6
0.8
1
mm
10
5
0
-5
-10
-15
-20
-25
-30
-35
-40

A-2 RESULTS VARIATION OF VOLUME FRACTION 25 %

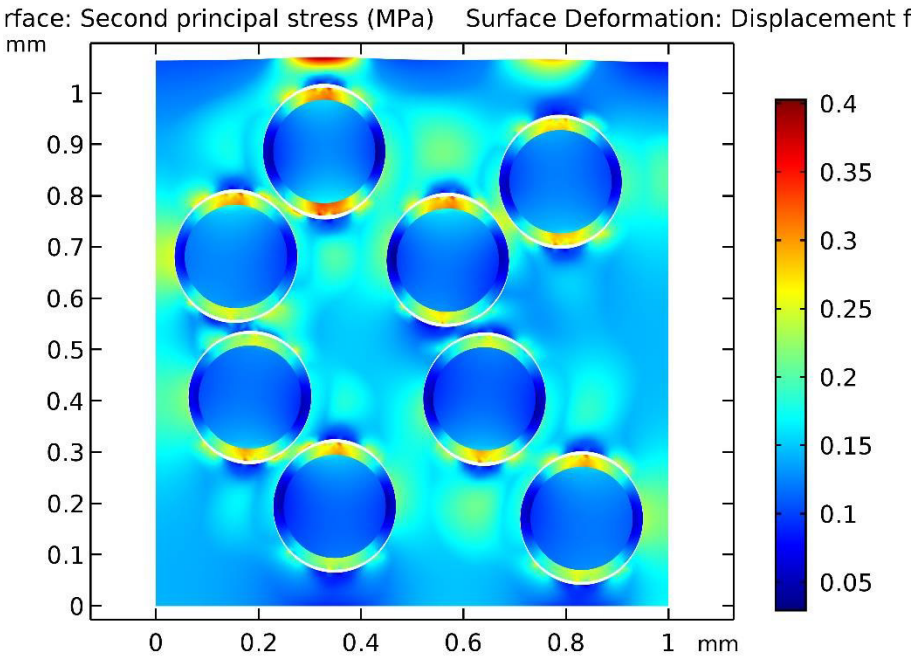

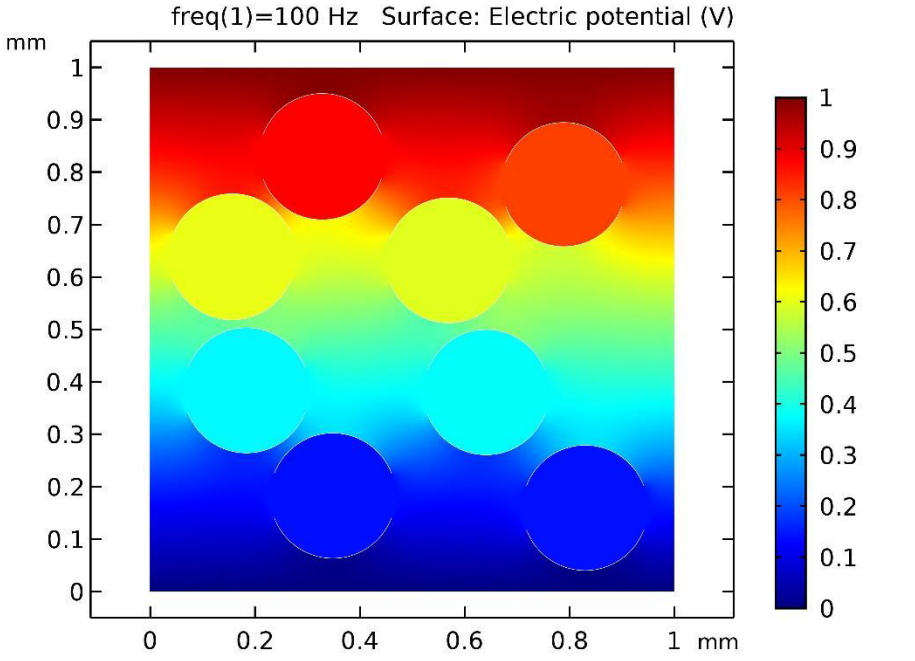

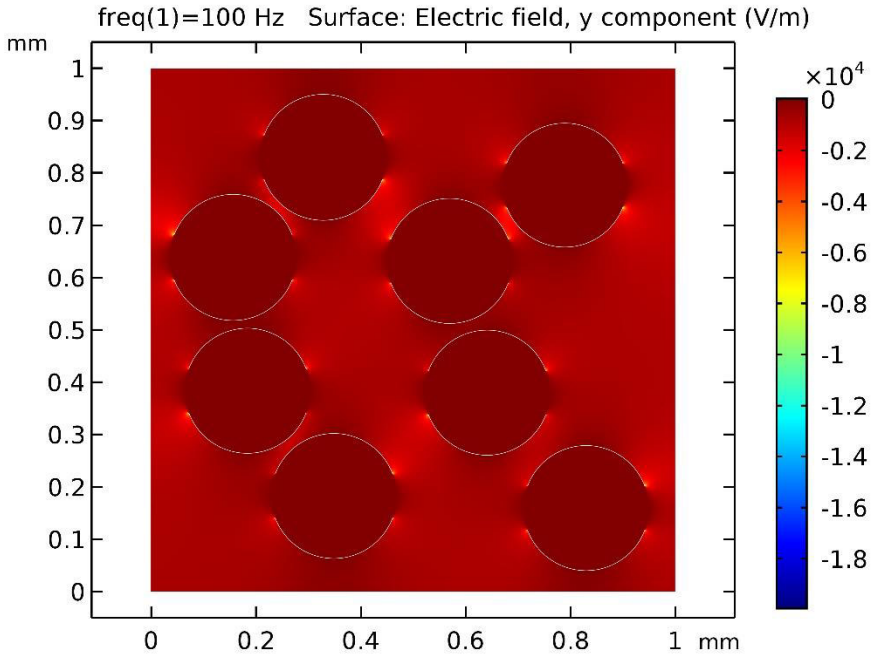
freq(1)=100 Hz Surface: Electric field, y component (V/m)
mm
1
0.9
0.8
0.7
0.6
0.5
0.4
0.3
0.2
0.1
0
0
0.2
0.4
0.6
0.8
1 mm
×10^4
0
-0.2
-0.4
-0.6
-0.8
-1
-1.2
-1.4
-1.6
-1.8

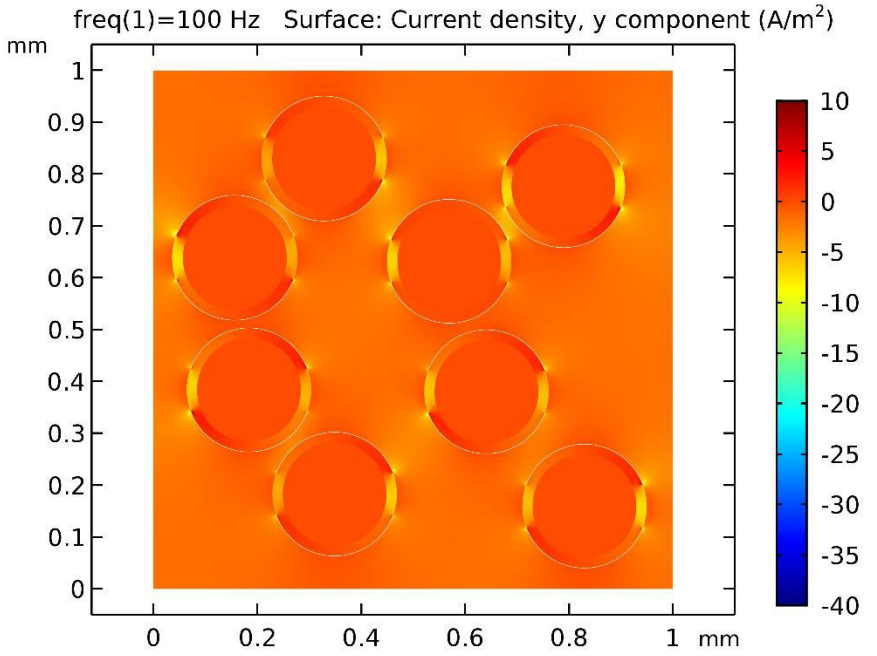
freq(1)=100 Hz Surface: Current density, y component (A/m^2)
mm
1
0.9
0.8
0.7
0.6
0.5
0.4
0.3
0.2
0.1
0
0
0.2
0.4
0.6
0.8
1 mm
10
5
0
-5
-10
-15
-20
-25
-30
-35
-40

A-3 RESULTS VARIATION OF VOLUME FRACTION 30 %

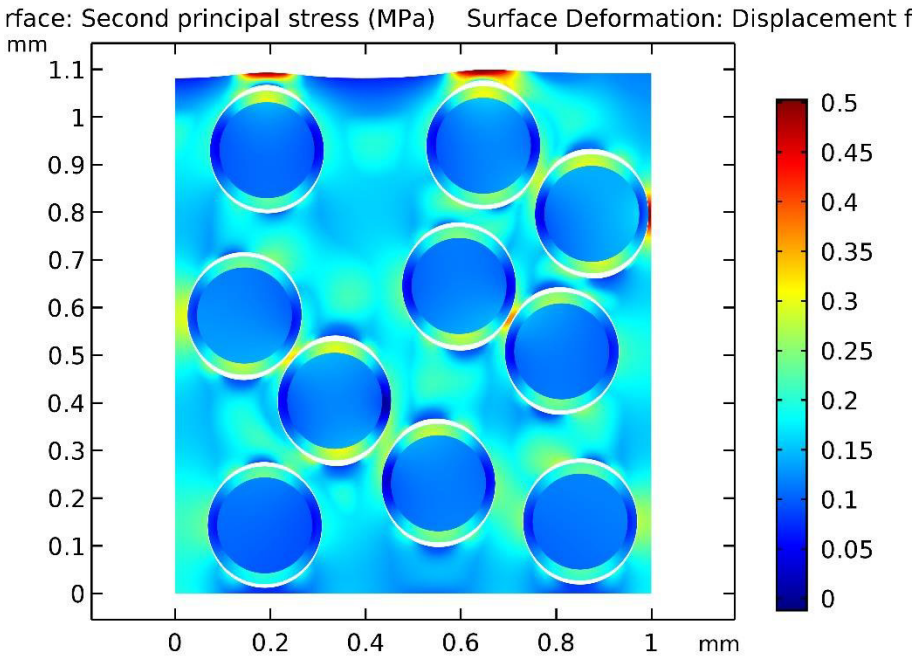

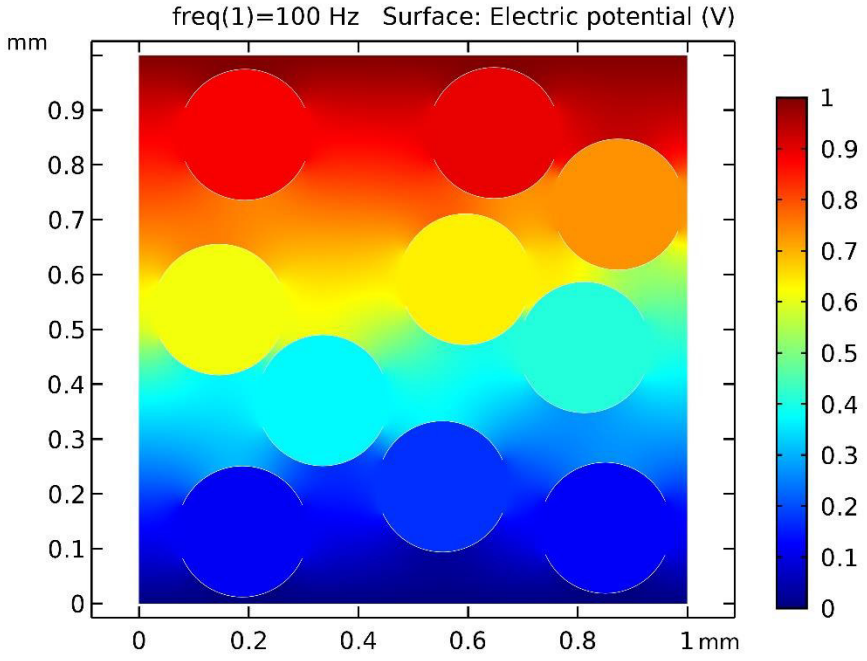

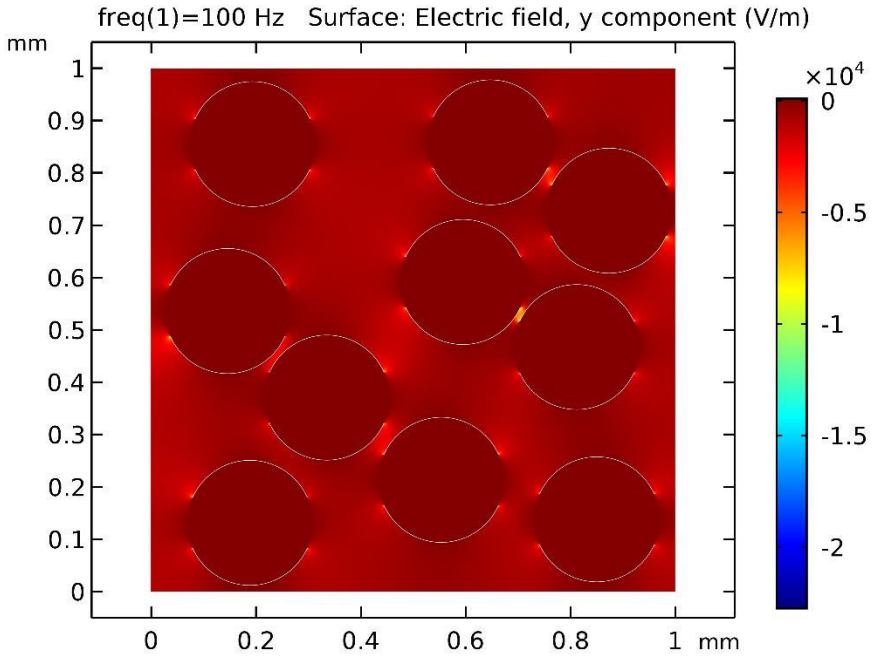
freq(1)=100 Hz Surface: Electric field, y component (V/m)
mm
1
0.9
0.8
0.7
0.6
0.5
0.4
0.3
0.2
0.1
0
0
0.2
0.4
0.6
0.8
1 mm
×10^4
0
-0.5
-1
-1.5
-2

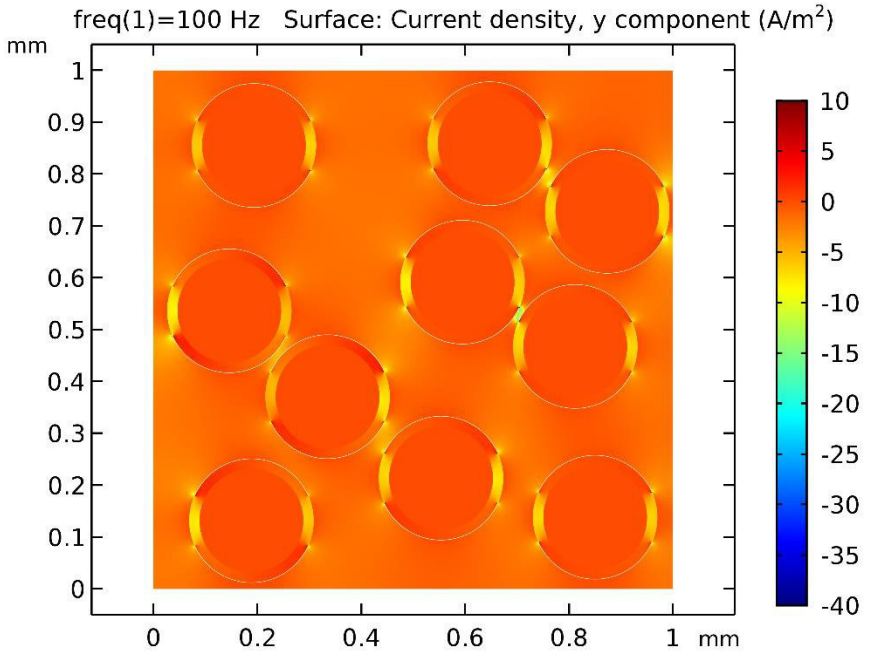
freq(1)=100 Hz Surface: Current density, y component (A/m^2)
mm
1
0.9
0.8
0.7
0.6
0.5
0.4
0.3
0.2
0.1
0
0
0.2
0.4
0.6
0.8
1 mm
10
5
0
-5
-10
-15
-20
-25
-30
-35
-40

APPENDIX B VARIATION OF COATING THICKNESS

B-1 RESULTS VARIATION OF COATING THICKNESS 0.01 MM

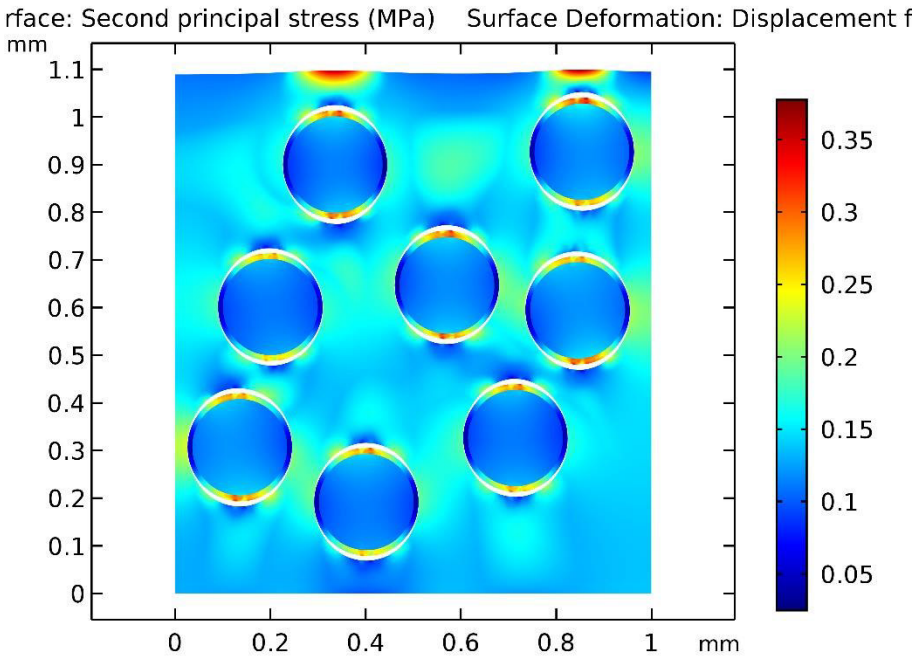

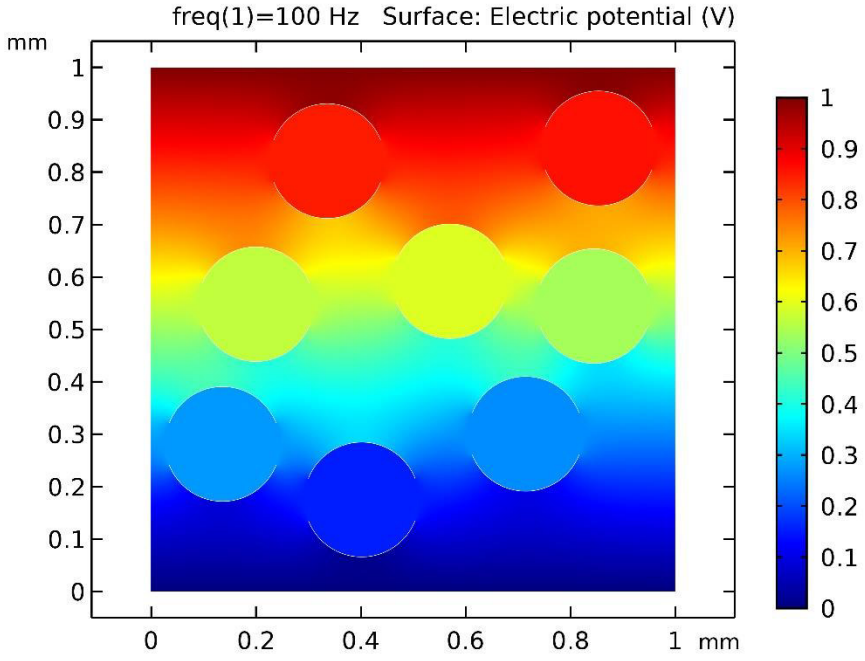

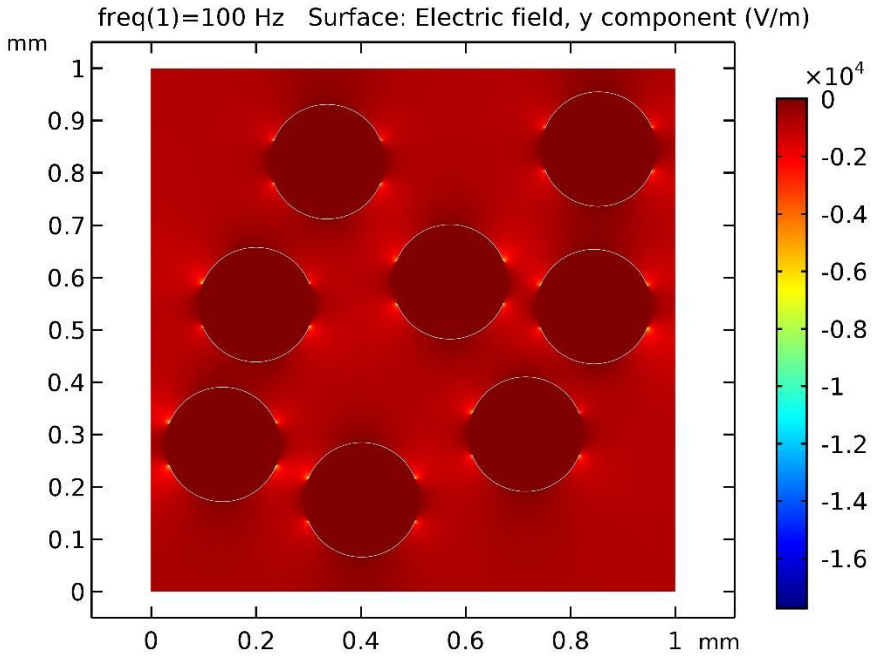
freq(1)=100 Hz Surface: Electric field, y component (V/m)
mm
1
0.9
0.8
0.7
0.6
0.5
0.4
0.3
0.2
0.1
0
0
0.2
0.4
0.6
0.8
1 mm
×10^4
0
-0.2
-0.4
-0.6
-0.8
-1
-1.2
-1.4
-1.6

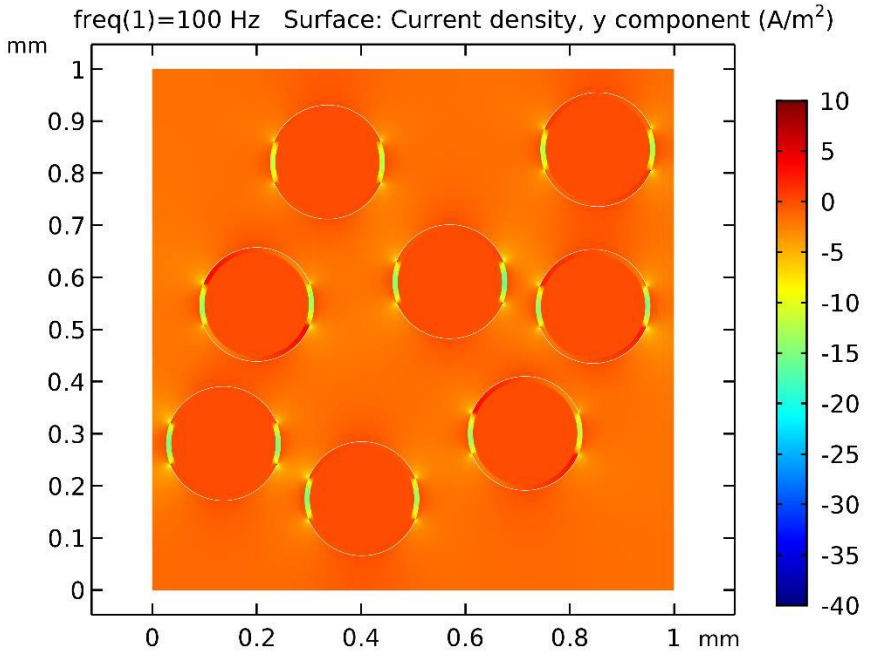
freq(1)=100 Hz Surface: Current density, y component (A/m^2)
mm
1
0.9
0.8
0.7
0.6
0.5
0.4
0.3
0.2
0.1
0
0
0.2
0.4
0.6
0.8
1 mm
10
5
0
-5
-10
-15
-20
-25
-30
-35
-40

B-2 RESULTS VARIATION OF COATING THICKNESS 0.02 MM

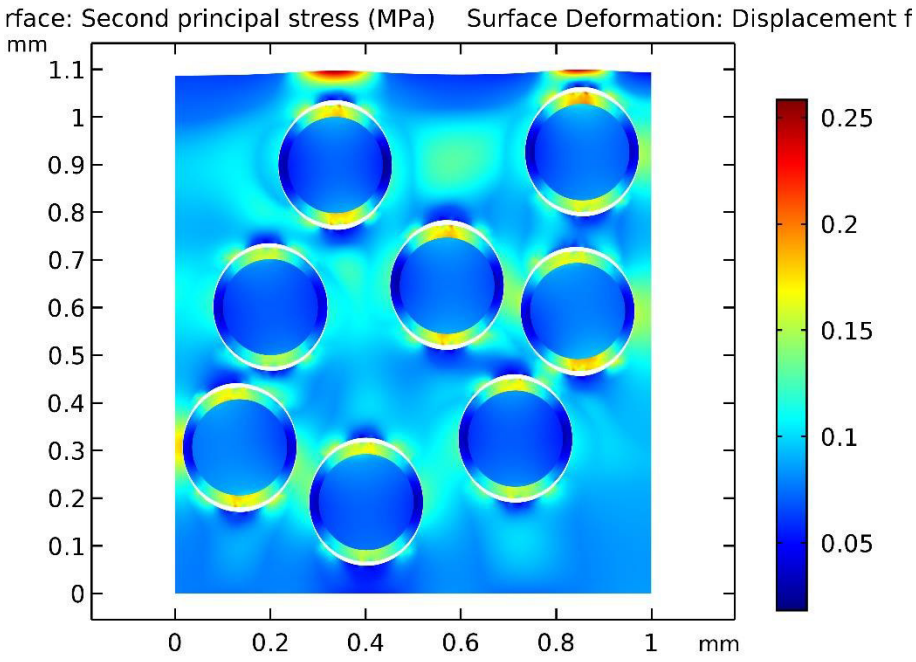

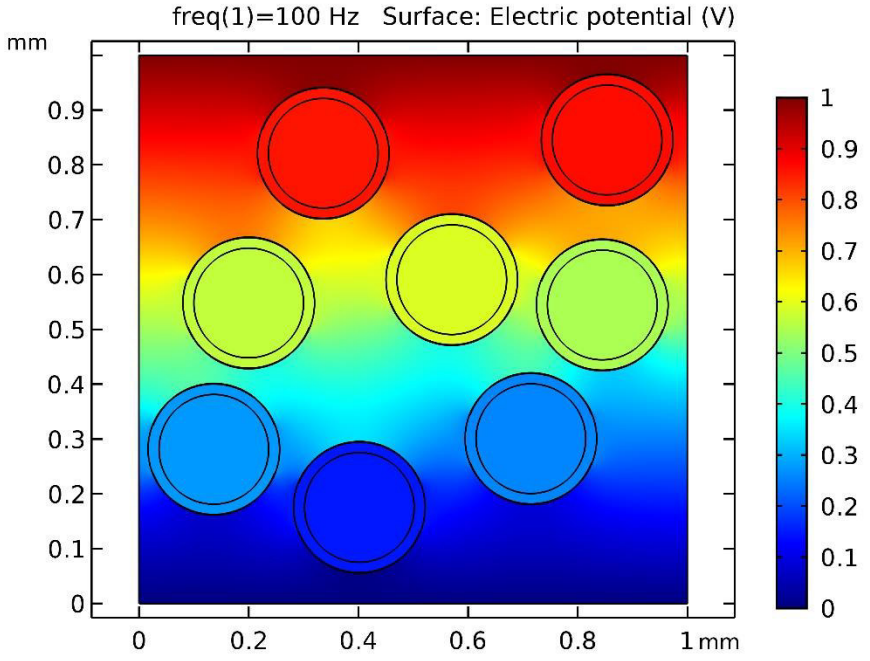

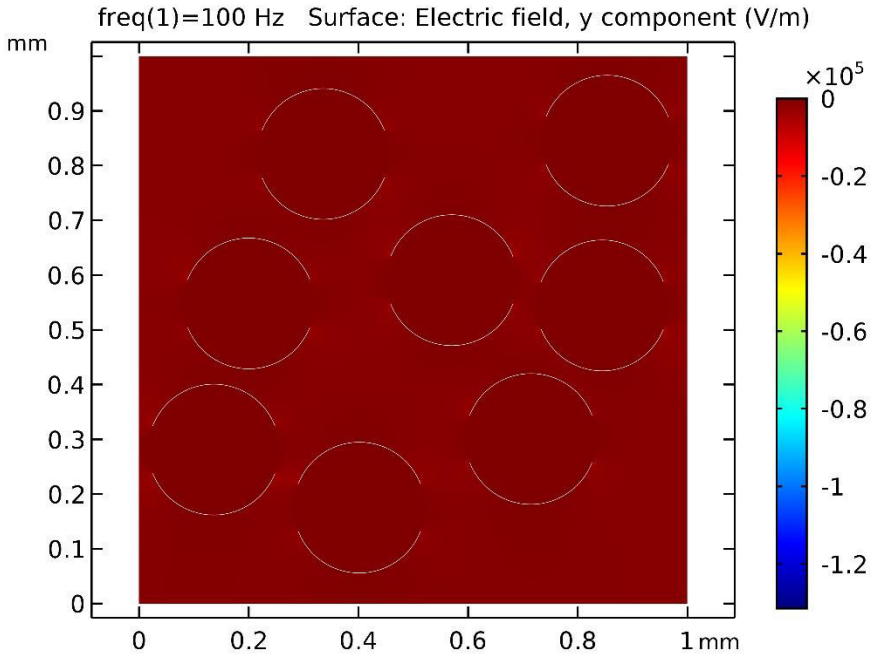
freq(1)=100 Hz Surface: Electric field, y component (V/m)
mm
0.9
0.8
0.7
0.6
0.5
0.4
0.3
0.2
0.1
0
0
0.2
0.4
0.6
0.8
1 mm
×10^5
0
-0.2
-0.4
-0.6
-0.8
-1
-1.2

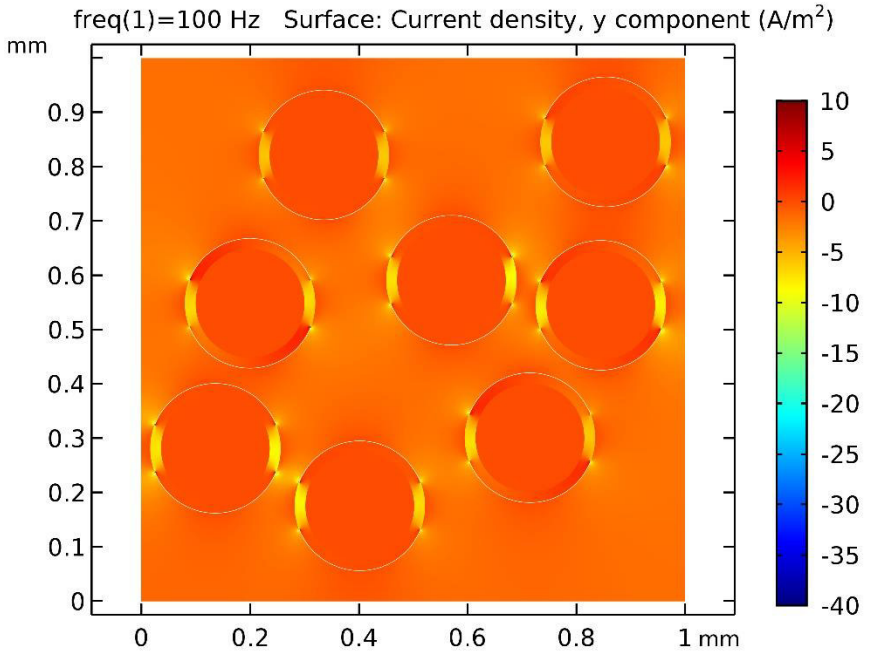
freq(1)=100 Hz Surface: Current density, y component (A/m^2)
mm
0.9
0.8
0.7
0.6
0.5
0.4
0.3
0.2
0.1
0
0
0.2
0.4
0.6
0.8
1 mm
10
5
0
-5
-10
-15
-20
-25
-30
-35
-40

B-3 RESULTS VARIATION OF COATING THICKNESS 0.03 MM

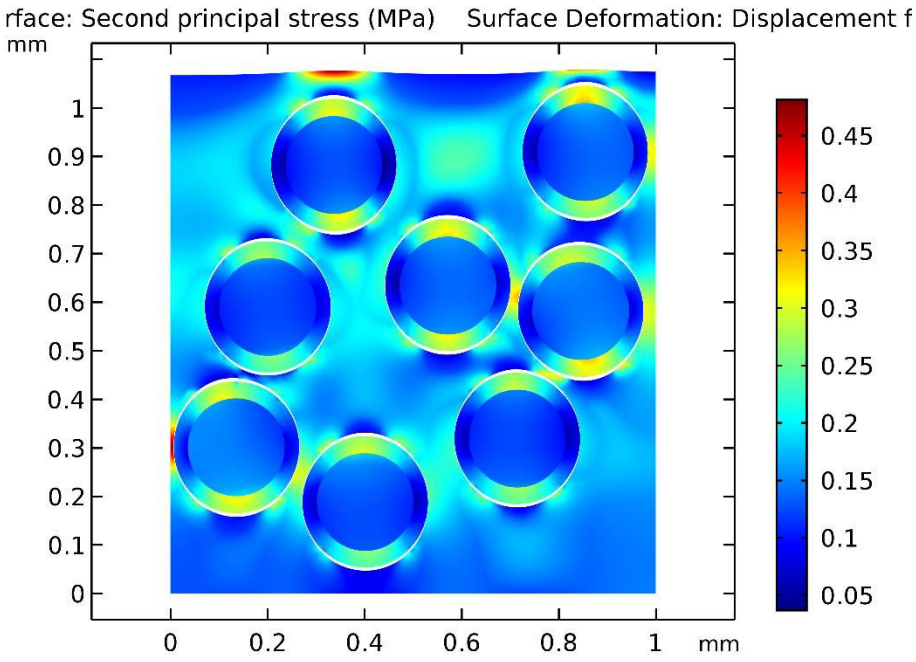

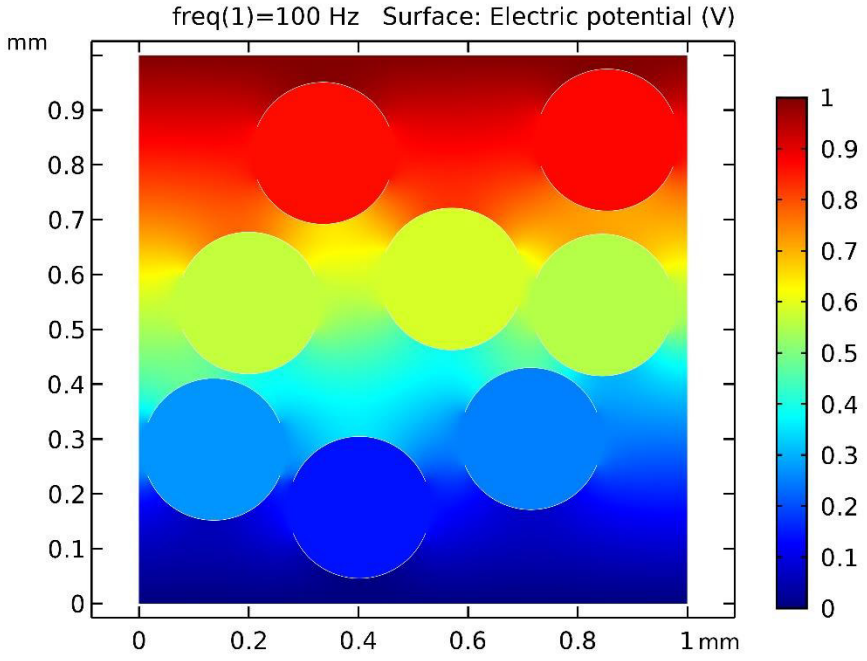

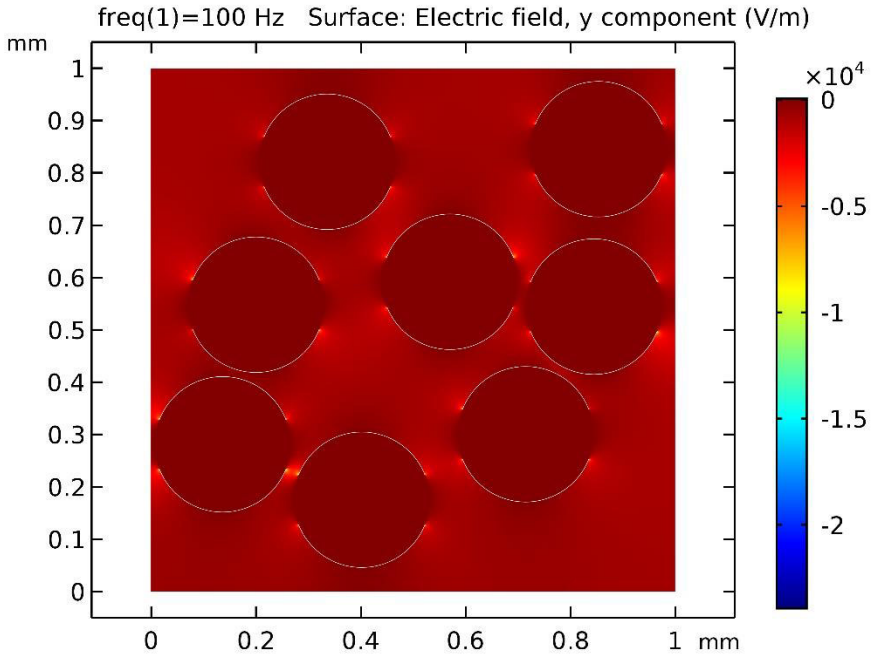
freq(1)=100 Hz Surface: Electric field, y component (V/m)
mm
1
0.9
0.8
0.7
0.6
0.5
0.4
0.3
0.2
0.1
0
0
0.2
0.4
0.6
0.8
1 mm
×10^4
0
-0.5
-1
-1.5
-2

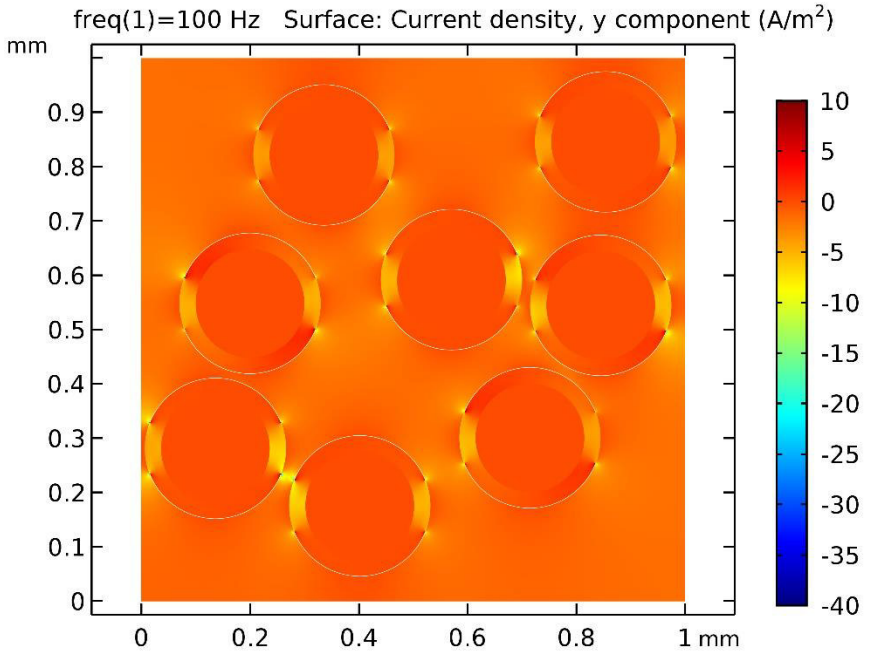
freq(1)=100 Hz Surface: Current density, y component (A/m^2)
mm
0.9
0.8
0.7
0.6
0.5
0.4
0.3
0.2
0.1
0
0
0.2
0.4
0.6
0.8
1 mm
10
5
0
-5
-10
-15
-20
-25
-30
-35
-40

BIBLIOGRAPHY

Al-Dahawi, A., Yıldırım, G., Öztürk, O., & Şahmaran, M. (2017). Assessment of self-sensing capability of Engineered Cementitious Composites within the elastic and plastic ranges of cyclic flexural loading. *Construction and Building Materials*, *145*, 1–10. https://doi.org/10.1016/j.conbuildmat.2017.03.236

Azhari, F. (2008). Cement-based sensors for structural health monitoring. University of British Columbia. Retrieved from https://open.library.ubc.ca/media/download/pdf/24/1.0063120/1

Azhari, F., & Banthia, N. (2012). Cement-based sensors with carbon fibers and carbon nanotubes for piezoresistive sensing. *Cement and Concrete Composites*, *34*(7), 866–873. https://doi.org/10.1016/j.cemconcomp.2012.04.007

Baeza, F. J., Galao, O., Zornoza, E., & Garcés, P. (2013). Multifunctional Cement Composites Strain and Damage Sensors Applied on Reinforced Concrete (RC) Structural Elements. *Materials (Basel, Switzerland)*, *6*(3), 841–855. https://doi.org/10.3390/ma6030841

Chen, P.-W., & Chung, D. D. L. (1995). Carbon-Fiber-Reinforced Concrete as an Intrinsically Smart Concrete for Damage Assessment during Dynamic Loading. *Journal of the American Ceramic Society*, *78*(3), 816–818. https://doi.org/10.1111/j.1151-2916.1995.tb08254.x

Chiarello, M., & Zinno, R. (2005). Electrical conductivity of self-monitoring CFRC. *Cement and Concrete Composites*, *27*(4), 463–469. https://doi.org/10.1016/j.cemconcomp.2004.09.001

Chowdhury, S. C., Haque, B. Z., Okabe, T., & Gillespie Jr., J. W. (2012). Modeling the effect of statistical variations in length and diameter of randomly oriented CNTs on the properties of CNT reinforced nanocomposites. *Composites Part B: Engineering*, *43*(4), 1756–1762. https://doi.org/10.1016/j.compositesb.2012.01.066

Chung, D. D. L. (2016). Piezoresistive Cement-Based Materials for Strain Sensing. *Journal of Intelligent Material Systems and Structures*, *13*(9), 599–609. https://doi.org/10.1106/104538902031861

Chung, D.D.L. (2000). Cement reinforced with short carbon fibers: A multifunctional material. *Composites Part B: Engineering*, *31*(6-7), 511–526. https://doi.org/10.1016/S1359-8368(99)00071-2

Coppola, L., Buoso, A., & Corazza, F. (2013). The influence of AC and DC electrical resistance and piezoresistivity measurements of CNTs/Cement composites. Retrieved from https://aisberg.unibg.it/bitstream/10446/30093/1/4_CNT_DCvsAC%20rev1.pdf

D'Alessandro, A., Ubertini, F., García-Macías, E., Castro-Triguero, R., Downey, A., Laflamme, S.,. . . Materazzi, A. L. (2017). Static and Dynamic Strain Monitoring of Reinforced Concrete Components through Embedded Carbon Nanotube Cement-Based Sensors. *Shock and Vibration*, *2017*(2), 1–11. https://doi.org/10.1155/2017/3648403

Daphalapurkar, N. P., Wang, F., Fu, B., Lu, H., & Komanduri, R. (2011). Determination of Mechanical Properties of Sand Grains by Nanoindentation. *Experimental Mechanics*, *51*(5), 719–728. https://doi.org/10.1007/s11340-010-9373-z

Das, S., Maroli, A., Singh, S. S., Stannard, T., Xiao, X., Chawla, N., & Neithalath, N. (2016). A microstructure-guided constitutive modeling approach for random heterogeneous materials: Application to structural binders. *Computational Materials Science*, *119*, 52–64. https://doi.org/10.1016/j.commatsci.2016.03.040

Elices, M., Guinea, G. V., Gómez, J., & Planas, J. (2002). The cohesive zone model: Advantages, limitations and challenges. *Engineering Fracture Mechanics*, *69*(2), 137–163. https://doi.org/10.1016/S0013-7944(01)00083-2

Fu, X., & Chung, D.D.L. (1996). Effect of polymer admixtures to cement on the bond strength and electrical contact resistivity between steel fiber and cement. *Cement and Concrete Research*, *26*(2), 189–194. https://doi.org/10.1016/0008-8846(95)00201-4

García-Macías, E., D'Alessandro, A., Castro-Triguero, R., Pérez-Mira, D., & Ubertini, F. (2017). Micromechanics modeling of the uniaxial strain-sensing property of carbon nanotube cement-matrix composites for SHM applications. *Composite Structures*, *163*, 195–215. https://doi.org/10.1016/j.compstruct.2016.12.014

Gupta, S., Gonzalez, J. G., & Loh, K. J. (2017). Self-sensing concrete enabled by nano-engineered cement-aggregate interfaces. *Structural Health Monitoring: An International Journal*, *16*(3), 309–323. https://doi.org/10.1177/1475921716643867

Han, B., Sun, S., Ding, S., Zhang, L., Yu, X., & Ou, J. (2015). Review of nanocarbon-engineered multifunctional cementitious composites. *Composites Part A: Applied Science and Manufacturing*, *70*, 69–81. https://doi.org/10.1016/j.compositesa.2014.12.002

Han, B., Wang, Y., Dong, S., Zhang, L., Ding, S., Yu, X., & Ou, J. (2015). Smart concretes and structures: A review. *Journal of Intelligent Material Systems and Structures*, *26*(11), 1303–1345. https://doi.org/10.1177/1045389X15586452

Han, B., Yu, X., & Ou, J. (2011). Multifunctional and Smart Carbon Nanotube Reinforced Cement-Based Materials. In K. Gopalakrishnan, B. Birgisson, P. Taylor, & N. O. Attoh-Okine (Eds.), *Nanotechnology in Civil Infrastructure: A Paradigm Shift* (pp. 1–47). Berlin, Heidelberg: Springer Berlin Heidelberg. https://doi.org/10.1007/978-3-642-16657-0_1

Hillerborg, A., Modéer, M., & Petersson, P.-E. (1976). Analysis of crack formation and crack growth in concrete by means of fracture mechanics and finite elements. *Cement and Concrete Research*, *6*(6), 773–781. https://doi.org/10.1016/0008-8846(76)90007-7

Kay Ackermann. (2016). Life-cycle analysis for mineralized foam and micro.reinforcement ultra-high-performance concrete (Bachelor Thesis). TU Darmstadt.

Konsta-Gdoutos, M. S., & Aza, C. A. (2014). Self sensing carbon nanotube (CNT) and nanofiber (CNF) cementitious composites for real time damage assessment in smart structures. *Cement and Concrete Composites*, *53*, 162–169. https://doi.org/10.1016/j.cemconcomp.2014.07.003

Konsta-Gdoutos, M. S., Metaxa, Z. S., & Shah, S. P. (2010). Multi-scale mechanical and fracture characteristics and early-age strain capacity of high performance carbon nanotube/cement nanocomposites. *Cement and Concrete Composites*, *32*(2), 110–115. https://doi.org/10.1016/j.cemconcomp.2009.10.007

Kuang, K. S. C., Quek, S. T., Koh, C. G., Cantwell, W. J., & Scully, P. J. (2009). Plastic Optical Fibre Sensors for Structural Health Monitoring: A Review of Recent Progress. *Journal of Sensors*, *2009*(3), 1–13. https://doi.org/10.1155/2009/312053

Lee, S.-J., You, I., Zi, G., & Yoo, D.-Y. (2017). Experimental Investigation of the Piezoresistive Properties of Cement Composites with Hybrid Carbon Fibers and Nanotubes. *Sensors (Basel, Switzerland)*, *17*(11). https://doi.org/10.3390/s17112516

Li, H., Xiao, H.-g., & Ou, J.-p. (2006). Effect of compressive strain on electrical resistivity of carbon black-filled cement-based composites. *Cement and Concrete Composites*, *28*(9), 824–828. https://doi.org/10.1016/j.cemconcomp.2006.05.004

Liew, K. M., Kai, M. F., & Zhang, L. W. (2016). Carbon nanotube reinforced cementitious composites: An overview. *Composites Part A: Applied Science and Manufacturing*, *91*, 301–323. https://doi.org/10.1016/j.compositesa.2016.10.020

Logan, D. L. (2002). *A first course in the finite element method* (3rd ed.). Pacific Grove, Calif.: Brooks/Cole. Retrieved from http://www.loc.gov/catdir/enhancements/fy1103/00067507-b.html

Loh, K. J., & Gonzalez, J. (2015). Cementitious Composites Engineered with Embedded Carbon Nanotube Thin Films for Enhanced Sensing Performance. *Journal of Physics: Conference Series*, *628*, 12042. https://doi.org/10.1088/1742-6596/628/1/012042

Lubachevsky, B. D., & Stillinger, F. H. (1990). Geometric properties of random disk packings. *Journal of Statistical Physics*, *60*(5-6), 561–583. https://doi.org/10.1007/BF01025983

Meier, H. A., Kuhl, E., & Steinmann, P. (2008). A note on the generation of periodic granular microstructures based on grain size distributions. *International Journal for Numerical and Analytical Methods in Geomechanics*, *32*(5), 509–522. https://doi.org/10.1002/nag.635

Miao, M., McDonnell, J., Vuckovic, L., & Hawkins, S. C. (2010). Poisson's ratio and porosity of carbon nanotube dry-spun yarns. *Carbon*, *48*(10), 2802–2811. https://doi.org/10.1016/j.carbon.2010.04.009

Muto, N., Arai, Y., Shin, S.G., Matsubara, H., Yanagida, H., Sugita, M., & Nakatsuji, T. (2001). Hybrid composites with self-diagnosing function for preventing fatal fracture. *Composites Science and Technology*, *61*(6), 875–883. https://doi.org/10.1016/S0266-3538(00)00165-2

Ou, J., & Han, B. (2008). Piezoresistive Cement-based Strain Sensors and Self-sensing Concrete Components. *Journal of Intelligent Material Systems and Structures*, *20*(3), 329–336. https://doi.org/10.1177/1045389X08094190

Pantea, D., Darmstadt, H., Kaliaguine, S., & Roy, C. (2003). Electrical conductivity of conductive carbon blacks: Influence of surface chemistry and topology. *Applied Surface Science*, *217*(1-4), 181–193. https://doi.org/10.1016/S0169-4332(03)00550-6

Roesler, J., Paulino, G. H., Park, K., & Gaedicke, C. (2007). Concrete fracture prediction using bilinear softening. *Cement and Concrete Composites*, *29*(4), 300–312. https://doi.org/10.1016/j.cemconcomp.2006.12.002

Safiuddin, M., Gonzalez, M., Cao, J., & Tighe, S. L. (2014). State-of-the-art report on use of nano-materials in concrete. *International Journal of Pavement Engineering*, *15*(10), 940–949. https://doi.org/10.1080/10298436.2014.893327

Schneider, J., Kuntsche, J. K., Schula, S., Schneider, F., & Wörner, J.-D. (2016). *Glasbau: Grundlagen, Berechnung, Konstruktion* (2. Auflage). *VDI-Buch*. Berlin, Heidelberg: Springer Vieweg. Retrieved from http://dx.doi.org/10.1007/978-3-540-68927-0

Spencer, B. F., Park, J.-W., Mechitov, K. A., Jo, H., & Agha, G. (2017). Next Generation Wireless Smart Sensors Toward Sustainable Civil Infrastructure. *Procedia Engineering*, *171*, 5–13. https://doi.org/10.1016/j.proeng.2017.01.304

State of Rhode Island: Rhode Island Department of Transportation. Retrieved from http://www.dot.ri.gov/rhodeworks/

Sun, M., Staszewski, W. J., & Swamy, R. N. (2010). Smart Sensing Technologies for Structural Health Monitoring of Civil Engineering Structures. *Advances in Civil Engineering*, *2010*(11), 1–13. https://doi.org/10.1155/2010/724962

Sun, M.-q., Li, J., Wang, Y.-j., & Zhang, X.-y. (2015). Preparation of carbon fiber reinforced cement-based composites using self-made carbon fiber mat. *Construction and Building Materials*, *79*, 283–289. https://doi.org/10.1016/j.conbuildmat.2015.01.060

Swaptik Chowdhury. (2017). Experimental Investigations and Modeling of the Strain Sensing Response of Matrices Containing Metallic Inclusions (Thesis Master of Science). Arizona State University.

Wen, S., & Chung, D.D.L. (2001). Effect of stress on the electric polarization in cement. *Cement and Concrete Research*, *31*(2), 291–295. https://doi.org/10.1016/S0008-8846(00)00412-9

Xiao, H., Li, H., & Ou, J. (2011). Strain sensing properties of cement-based sensors embedded at various stress zones in a bending concrete beam. *Sensors and Actuators A: Physical*, *167*(2), 581–587. https://doi.org/10.1016/j.sna.2011.03.012

Xie, P., Gu, P., & Beaudoin, J. J. (1996). Electrical percolation phenomena in cement composites containing conductive fibres. *Journal of Materials Science*, *31*(15), 4093–4097. https://doi.org/10.1007/BF00352673

Yang, P., Chowdhury, S., & Neithalath, N. (2018). Strain sensing ability of metallic particulate reinforced cementitious composites: Experiments and microstructure-guided finite element modeling. *Cement and Concrete Composites*, *90*, 225–234. https://doi.org/10.1016/j.cemconcomp.2018.04.004

Yu, J., Lu, K., Sourty, E., Grossiord, N., Koning, C. E., & Loos, J. (2007). Characterization of conductive multiwall carbon nanotube/polystyrene composites prepared by latex technology. *Carbon*, *45*(15), 2897–2903. https://doi.org/10.1016/j.carbon.2007.10.005

Zhu, S., & Chung, D. D. L. (2007). Theory of piezoresistivity for strain sensing in carbon fiber reinforced cement under flexure. *Journal of Materials Science*, *42*(15), 6222–6233. https://doi.org/10.1007/s10853-006-1131-3